STUDY OF COAGULATION OF DISPERSING AEROSOL SYSTEMS

By

S. ANAND
(PHYS01200704019)
Bhabha Atomic Research Centre, Mumbai

A thesis submitted to the

Board of Studies in Physical Sciences

In partial fulfillment of requirements

For the Degree of

DOCTOR OF PHILOSOPHY

of

HOMI BHABHA NATIONAL INSTITUTE

June, 2012

Homi Bhabha National Institute

Recommendations of the Viva Voce Board

As members of the Viva Voce Board, we certify that we have read the dissertation prepared by S. Anand entitled "Study of Coagulation of Dispersing Aerosol Systems" and recommend that it may be accepted as fulfilling the dissertation requirement for the Degree of Doctor of Philosophy.

Surender M Sharma

________________________________ **Date:** 05/11/2012

Chairman – Prof. S. M. Sharma

________________________________ **Date:** 05/11/2012

Guide / Convener – Prof. Y. S. Mayya

Sachida Nand

________________________________ **Date:** 05/11/2012

Examiner – Prof. S. N. Tripathi

________________________________ **Date:** 05/11/2012

Member – Prof. S. K. Gupta

D. M. Gaitonde

________________________________ **Date:** 05/11/2012

Member – Prof. D. M. Gaitonde

Final approval and acceptance of this dissertation is contingent upon the candidate's submission of the final copies of the dissertation to HBNI.

CERTIFICATE

I hereby certify that I have read this dissertation prepared under my direction and recommend that it may be accepted as fulfilling the dissertation requirement.

____ **Date:** 05/11/2012

Prof. Y. S. Mayya (Guide)

STATEMENT BY AUTHOR

This dissertation has been submitted in partial fulfillment of requirements for an advanced degree at Homi Bhabha National Institute (HBNI) and is deposited in the library to be made available to borrowers under rules of the HBNI.

Brief quotations from this dissertation are allowable without special permission, provided that accurate acknowledgement of source is made. Requests for permission for extended quotation from or reproduction of this manuscript in whole or in part may be granted by the Competent Authority of HBNI when in his or her judgment the proposed use of the material is in the interests of scholarship. In all other instances, however, permission must be obtained from the author.

S. Anand.

S. Anand

DECLARATION

I, hereby declare that the investigation presented in the thesis has been carried out by me. The work is original and has not been submitted earlier as a whole or in part for a degree / diploma at this or any other Institution / University.

S. Anand

To

Parents,

Aswatha Anand,

Nivedha, and

Kailaskumaran

ACKNOWLEDGEMENTS

First and foremost, I would like to express my deepest gratitude to my advisor, Prof. Y. S. Mayya, for his continuous guidance, encouragement, support, and valuable time throughout these years. I also extend thanks for the trust and freedom he gave me in my research. To work with him is both an honour and a great pleasure. My thanks can never be enough for the countless hours of discussion we have shared. He taught me how to approach complex research problems and the need to be persistent to accomplish any goal.

The following professors kindly served on my doctoral committee: S. M. Sharma, S. K. Gupta, and D. M. Gaitonde. I thank them for their valuable time and help through my course of study. I thank Dr. M. Yu, Dr. M. Seipenbusch, and Prof. G. Kasper for enlightening discussions on coagulation phenomena and for sharing several intricate details of experiments for comparing with the theoretical models. I take this opportunity to thank Dr. A. Prakash for his help in developing the numerical module of the coagulation equation.

I am grateful to Mr. V. K. Sharma for his support and understanding which helped me in continuing my research work. I would like to thank Dr. P.K. Sarkar for granting permission, and his continuous support throughout my study. I am also thankful to Dr. B.K. Sapra for her help, suggestions, and useful discussions throughout my study.

I am indebted to Mr. M. Joshi for the help and friendly support during the experiments, and by carefully going through the chapters during the preparation of this thesis. I gladly thank Mr. B. Sreekanth for his help, comments and discussions during this work. I cannot forget to thank my aerosol research group, Mr. Arshad, Ms. Rajni, and Mrs. Pallavi with whom I had constant interaction and discussions during the course of my study. I greatly appreciate all of

them. Last but not least, appreciation also goes to my friends and colleagues; of whom I wish to thank Mr. Kapil, Mr. Guneshwor, Mrs. Chitra, and Mrs. Arti for being wonderful officemates. I especially thank Mr. Pradeep for his continuous support during my study period.

I sincerely wish to dedicate this dissertation to my loving family whose care and devotion always encouraged me during my study. I am especially indebted to my wife, Aswatha Anand; this thesis would never have come out without her patience and encouragement. Also, the valuable time my loving wife and kids sacrificed for me. Their understanding during my many sleepless nights of study and research have been a great blessing to me. They have always been by my side and continue to be my treasures. I take this opportunity to thank my father and mother who are my first mentors for imbibing in me the discipline that I needed to pursue my goal. They set a live example for me to be a better person tomorrow.

CONTENTS

Synopsis xii

List of figures xxix

List of Tables xxxii

1. Introduction 1
   - 1.1. Background 1
   - 1.2. Literature Survey 8
   - 1.3. Scope of thesis 13
   - 1.4. Organization of this thesis 15
2. Theoretical framework 16
   - 2.1. Introduction 16
   - 2.2. Coagulation kernel 16
     - 2.2.1. Brownian coagulation 17
       - 2.2.1.1. Brownian coagulation in the free-molecular regime 17
       - 2.2.1.2. Brownian coagulation in the continuum regime 18
       - 2.2.1.3. Brownian coagulation in the transition regime 19
     - 2.2.2. Kinematic coagulation 21
       - 2.2.2.1. Gravitational coagulation 21
       - 2.2.2.2. Turbulent coagulation 22
       - 2.2.2.3. Electrostatic coagulation 23
   - 2.3. General coagulation equation 24
     - 2.3.1. Sectional method 27
       - 2.3.1.1. Nodal method 28
     - 2.3.2. Self-preserving theory 30
     - 2.3.3. Moment method 35
     - 2.3.4. Monte Carlo method 35
   - 2.4. Coagulation in dispersing aerosol systems 36
3. Survival fraction for instantaneous releases 40
   - 3.1. Introduction 40
   - 3.2. Survival fraction for burst releases 40
     - 3.2.1. Uniform expansion model 42

3.2.2. Formulation of problem 43

3.2.3. Results and Discussion 44

3.3. Survival fraction for puff releases 47

3.3.1. Diffusion approximation model 48

3.3.1.1. Formulation of problem 49

3.3.1.2. Method of solution 50

Analytical solution for constant kernel 50

Analytical solution for free-molecular kernel 61

Numerical solution 64

3.3.1.3. Results and Discussion 66

3.3.2. Diffusion approximation model with coagulation-induced flattening effect 73

3.3.2.1. Formulation of problem 74

3.3.2.2. The ultimate survival fraction: asymptotic limit for ψ 75

3.3.2.3. Transient analysis 78

3.3.2.4. Spatial variation of average particle mass inside puff 80

3.3.2.5. Application of the improved diffusion approximation model to vehicular emissions 81

3.4. Summary 83

4. Survival fraction for the plume releases 84

4.1. Introduction 84

4.2. Problem formulation 85

4.3. Survival fraction for constant diffusion coefficient 89

4.4. Survival fraction for the case of turbulent diffusion 91

4.5. Coagulation in a spatially inhomogeneous plume: Origin of bimodal size distribution 94

4.6. Applications of the model to forest fires 99

4.7. Summary 101

5. Coagulation of nanoparticle aerosols released continuously into a well stirred chamber 102

5.1. Introduction 102

5.2. Formulation of the problem 104
5.3. Two-group model 106
  5.3.1. Additive coagulation kernel 109
  5.3.2. Fuchs coagulation kernel 113
5.4. Numerical model 118
5.5. Results and Discussion 122
  5.5.1. Evolution of total particle number concentration 122
    5.5.1.1. Effect of particle fractal dimension on the total concentration 123
    5.5.1.2. Effect of source strength on the total concentration 126
    5.5.1.3. Effect of initial particle size on the total concentration 130
    5.5.1.4. Effect of removal rate due to ventilation on the total concentration 131
  5.5.2. Evolution of particle size 133
    5.5.2.1. Evolution of particle size distribution 133
    5.5.2.2. Evolution of the mean particle size 137
    5.5.2.3. Evolution of the surface area concentration 139
  5.5.3. Comparison with experimental results 140
    5.5.3.1. Experiment carried out by Seipenbusch et al (2008) 140
    5.5.3.2. Experiments carried out using nichrome hot wire generator 141
5.6. Summary 148
6. Summary and Conclusions 150
6.1. Summary 150
6.2. Conclusions 154
6.3. Future work 156
References 158
A Expressions for equation of state parameters of TNT explosion products 173
B Volume expansion rate of a diffusing puff 176
C Similarity formulation of diffusion-coagulation equation 178
D Equation for total number concentration in the case of $K(u,v)=\alpha(u+v)$ kernel 182
E List of publications 183

SYNOPSIS

1. Introduction

Aerosols in the atmosphere affect climate and human health. Changes in the atmospheric concentrations of aerosols alter the energy balance of the climate system. They affect the absorption, scattering and emission of radiation within the atmosphere and at the Earth's surface. The resulting positive or negative changes in energy balance due to these factors are expressed as radiative forcing, which is used to compare warming or cooling influences on global climate. Aerosols also influence cloud life time and precipitation. Anthropogenic contributions to aerosols (primarily sulphate, organic carbon, black carbon, nitrate and dust) together produce a cooling effect, with a total direct radiative forcing of -0.5 [-0.9 to -0.1] W/m^2 (due to reflection of sunlight that reaches earth's surface back into space by aerosols) and an indirect cloud albedo forcing of -0.7 [-1.8 to -0.3] W/m^2 (due to the change in the cloud properties by aerosols). Both effects increase the amount of sunlight that is reflected to space without reaching the surface (IPCC, AR4 SYR, 2007). Aerosols from volcanic eruptions contribute an additional episodic cooling term for a few years following an eruption. These same particles that affect climate also impact the quality of the air that we breathe and the health of all living organisms, both outdoor and indoor environments. Common examples of the adverse health effects of aerosols among humans are the higher incidence of bronchial infections during periods of high aerosol loading, and short- and long-term adverse reactions to the toxicity of pollution particles. Hence, quantifying natural and human-induced (anthropogenic) emissions, transport, atmospheric processing, and aerosol sinks is crucial.

The key to predicting the effects of aerosols on air quality and climate change, and health effects lies in improving our understanding of key processes, in long-term monitoring, and in improved predictive capabilities through models. Aerosol effects are complicated because of variation in sources, particle sizes, chemical compositions, and dynamic evolutionary characteristics. In view of these, considerable interest has grown in understanding the evolution of particle size, number and composition of aerosol particles from various natural and anthropogenic sources in recent years. Usually aerosol emissions from multiple sources occur in a highly inhomogeneous manner being distributed randomly in time and space. Freshly emitted aerosols near the emission source undergo evolution due to various aerosol microphysical processes and their number concentrations are reduced to background levels rapidly in the atmosphere due to large atmospheric dilution. The near source characteristics, be it number or mass emission factors, provide only indices of potential for effects, and the actual effects are more closely related to the characteristics of emitted particles which ultimately persist in the atmosphere and their subsequent interaction with background aerosols. Thus, along with near source characterization, it is equally important to estimate its far field consequence, namely, contribution to particle number loading factors to aerosol background. Since direct measurements of far field contributions from a given source are hugely difficult due to enormous atmospheric dilutions, it should essentially rely on model estimates. Furthermore, the problem of understanding the evolution lies in the fact that one cannot easily perform experiments with real-world conditions in order to understand how it behaves if certain parameters of the system are changed. Hence, approximate analytical solutions and numerical computer simulations are needed to quantify the effective contribution of emission sources to background aerosols. These solutions (simple formulae) are proposed as modifiers of the emission factors, and hence they are called as ‘source term modifiers’. They provide an important analysis tool in the study of coagulation of dispersing aerosols in the atmosphere at early time scale or near the emission sources.

The present work aims at developing analytical and numerical models, and their solutions to estimate the fraction of particles that persist in the atmosphere to form background aerosols. Coagulation is an important growth process for the aerosol particles in a high-concentration system. It occurs when two particles collide and stick together, reducing the number concentration but conserving the mass concentration of particles in the atmosphere. Simulating coagulation in a model is important, since if coagulation is neglected, erroneously large aerosol number concentrations will be predicted. Even if the total aerosol mass concentration in a model is correct, the mass concentration will be spread among too many particles. The condensation/evaporation processes, being number conserving, are beyond the scope of this study. Hence, in the present study, the combined action of coagulation and dispersion is investigated through suitable microphysical models.

2. Scope of the work

The combined action of coagulation and dispersion reduces the total particle number concentration significantly in a high concentrated release of aerosol particles near the source. The fraction of particles surviving the coagulation in the puff or plume is termed as ‘survival fraction’. The survival fraction for various release scenarios is obtained in this study by solving the coagulation-dispersion equation using analytical and numerical techniques. The goal has been broken into two specific objectives:

1. Obtaining simpler expressions or approximations for the survival fraction for puff and plume releases, and

2. Estimation of important metrics like total number concentration, average particle size, etc., in the case of continuous volumetric releases.

Although a large number of studies are available on aerosol coagulation as well as dispersion/diffusion taken separately, the joint problem has received far less attention. Furthermore, most of the work on the Smoluchowski coagulation equation has been concerned with the time dependent spatially homogeneous situation. The present study, however, introduces the spatial heterogeneity in the system to account for the dispersion/diffusion process. This renders the problem difficult for obtaining the solutions both numerically and analytically. The primary processes considered in the present study are (i) coagulation, and (ii) atmospheric dispersion.

The study problem is formulated by considering simultaneous action of these two processes by constructing coagulation-dispersion equation which is a second order non-linear integro-differential equation. To overcome the difficulty of handling dispersion along with coagulation, due to the non-linearity introduced by the latter process in the model, certain approximations are made either at the level of formulating the equation itself or at the level of developing solutions. However, the numerical solutions to these models are obtained without any approximations, and hence they are considered as the exact solutions for these models.

Using these models, analytical approximate formulae for the survival fraction are obtained for the puff and plume releases. In some cases where the analytical approximations are difficult, the numerical solutions are fitted to obtain the survival fraction formula. In the case of continuous volumetric release, asymptotic analytical solutions for the total number concentration and average particle size are obtained using the two-species coagulation model. The temporal evolution of the particle number concentration and its size distribution are obtained from the numerical solutions.

3. Description of the research work

The formulations of the problem, different analytical and numerical models to solve the coagulation-dispersion equation, their solutions are explained in this section. The problem is formulated by considering the two important processes coagulation and dispersion responsible for the aerosol evolution in the early release phase as mentioned in the previous sections.

3.1. Puff releases

Two different analytical approaches are used for estimating the number survival fraction of an aerosol puff released instantaneously. They are,

1. Uniformly mixed-expansion model, and
2. Diffusion approximation model.

3.1.1. Uniformly mixed-expansion model

The uniformly mixed-expansion model (Nathans et al, 1970, and Turco & Yu 1997, 1998) treats the dispersion process through a relatively simple model which assumes a uniformly mixed volume element expanding under a prescribed rate in time. In this model, the approximation is made at the level of formulation of the equation. The simplifying feature of this model is that it altogether replaces the space dependent nature of the dispersion process by a purely time dependent term which, for the case of constant and homogeneous coagulation kernels, renders it exactly solvable by analytical techniques. However, one has to employ numerical techniques to solve this model for complex problems.

Numerical methods are developed as a part of this study to solve the coagulation-dispersion equation. The most important part of this numerical model is obtaining the solution to the coagulation equation. Several approaches to solve the coagulation equation numerically have been developed over the years. The most employed general method and its variants for simulating aerosol dynamics is based on dividing the particle size domain into sections as developed by Gelbard et al (1980). The model used in the present work, Nodal method (Prakash et al, 2003), is a modification of the sectional method developed by Gelbard et al (1980) and an extension of a coagulation nodal method by Lehtinen and Zachariah (2001). In this method, the finite-sized sections of the sectional model have been reduced to discrete points called 'nodes' on the size domain. It is assumed that particles exist only at these nodes, which are evenly spaced on a logarithmic size scale. This assumption simplifies the computation by limiting the number of parameters. If the new particle volume falls between two nodes, then it is split into adjacent nodes by a size-splitting operator under the constraint of mass conservation. This model can handle the following Brownian coagulation kernels:

1. Free-molecular kernel,
2. Continuum kernel,
3. Fuchs kernel.

The numerical code has the options to include the effect of fractal nature of the aerosol particles also. This coagulation module forms the core part of the numerical code. By combining this coagulation numerical module with any other numerical module of the physical processes, the general dynamic equation for the evolution of aerosols can be solved.

To solve the uniformly mixed-expansion model, the numerical code is appropriately modified to account for the puff dispersion. The puff dispersion part is handled by using equivalent volume expansion rate for a particular system, and the numerical solutions are then obtained by combining these numerical models appropriately. A case study is carried out for an energetic aerosol puff release with high temperature and pressure. This study is carried out to simulate the early phase of the evolution of aerosol particle characteristics in an expanding cloud due to the aerial detonation of a solid explosive with radioactive material. The puff volume increases due to adiabatic expansion, and the required volume expansion rate and the temperature transient are obtained from the relationships between the equation of state parameters. With these inputs, the numerical code is run for a problem time of 234 microseconds. The volume of the puff reaches to 1.39 m^3 (diameter = 1.385 m) at the end of the adiabatic expansion.

The initial total number concentration in the puff is 1.66×10^{26} particles/m^3; at the end of the simulation period (t = 234 μsec), the particle number concentration reaches to $\sim 2.9 \times 10^{16}$ particles/m^3. The average particle diameter of the aerosol cloud reaches the value of ~239 nm in this case. The code also outputs other important particle characteristics such as particle size distribution of the aerosol cloud. The study shows that if the local population of aerosols in a puff is subject to dilution by mixing with ambient air, the particle concentration decreases more rapidly and coagulation is quenched. Hence, the dispersion or dilution acts to increase the total number of particles that survive coagulation, and dispersion determines the fraction of the particles initially present that is likely to survive after a fixed time.

3.1.2. Diffusion approximation model

The second approach, diffusion approximation model, explicitly postulates diffusion as the mechanistic basis of dispersion and allows for spatial gradients. The diffusion term then replaces the purely time dependent term in the volume expansion model, and it is called as diffusion-coagulation model. Since it is difficult to solve this diffusion-coagulation model exactly even for constant coagulation kernels, approximation at the level of solutions is developed. The approximation implicitly assumes that spatial distribution function is essentially given by pure diffusion laws, and the coagulation alters the spectral function and the total number concentration. The scope of this model is limited to constant and free-molecular coagulation kernels, and the aim is to obtain simple and practically useful analytical formulae for various aerosol characteristics like survival fraction or source term modifier (defined as the fraction of space and volume integrated number of original particles surviving in the puff at any time), average particle size, and particle size distribution.

To this end, a diffusion–coagulation model is formulated for the evolution of a spatially inhomogeneous aerosol puff with an assumption of initially Gaussian distributed particle number concentration having spatially homogeneous size spectrum. The analytical solutions have been obtained for constant and free-molecular coagulation kernels by combining prescribed diffusion approximation with Laplace transforms and scaling theory, respectively. These yield a simple formula for survival fraction ($F(t)$) which combines the variables of the problem in to a single parameter A as shown below:

$$F(t) = \frac{1}{[1+A\,\mu(t)]^{(1/(1-\alpha))}}$$

where, $\mu(t) = 1 - \frac{1}{\sqrt{1+4Dt/b_0^2}}$, and $A = \frac{R\phi_0^\alpha N_0^{1-\alpha}(1-\alpha)}{2(2\pi)^{3/2}Db_0}$. For constant coagulation kernel, $\alpha = 0$, and $R = K/2$; for free-molecular kernel, $\alpha = 1/6$, and $R = 6\sqrt{kT/\rho}$. D is the particle diffusion coefficient, b_0 is the initial puff width, N_0 is the initial total number concentration, and K is the constant coagulation coefficient. It may be noted that the quantity A captures all the basic parameters of the problem in a single expression.

The diffusion-coagulation equation is also solved by the comprehensive numerical model based upon the nodal method (described above in section 3.1.1) capable of simulating the simultaneous processes of aerosol coagulation and atmospheric dispersion. In this model, the diffusion part is solved by appropriate finite difference methods. The exact numerical results are compared with the approximate analytical formulae for the survival fraction, size spectrum, and effective size of particles. In the case of free-molecular kernel, scaling theory is used to convert the integro-differential equation into a set of coupled ordinary differential equations. The ODE for the total number concentration is then solved by finite difference methods. Although the analytical results for the temporal variations of the survival fractions follow similar trends as numerical predictions, they show systematic deviations up to about 25% under strong coagulation (larger values of A). This calls for improvement in the analytical approach beyond prescribed diffusion approximation. Nevertheless, the analytical solutions yield simple formulae for quickly estimating the survival fractions for the number concentrations of particles injected into the open environment from puff releases.

A special case of the above mentioned problem is to have its size spectrum varying in space in a complex fashion. The combination of analytical approximation method proposed above and numerical techniques can in principle be used for obtaining essential results even when the spectrum is spatially inhomogeneous. This is demonstrated by taking the case of a distribution, in which bigger particles are scattered to farther distances in a centro-symmetric spherical cloud, as if they are formed by an explosive process. The total number concentration is assumed to be a Gaussian distribution in space. With these assumptions, the diffusion-coagulation model is solved by using prescribed diffusion approximation theory. Although tedious, the resulting nonlinear equation for survival fraction can be integrated to a quadrature using Mathematica (Wolfram Research, Inc., 2005). The final formula for the Laplace transformed spectral function is very complex and the actual size distribution needs to be obtained by Laplace inversion. This cannot be easily done analytically over the entire spectrum. A simple numerical Laplace inversion algorithm in Mathematica is used to obtain the inversion of Laplace transformed particle size spectrum using a 15 point Legendre polynomial expansion technique by Bellman et al. (1966) and Narayanan and Ramadurai (1992).

3.1.3. Diffusion approximation model with coagulation-induced flattening effect

As mentioned in the previous section (3.1.2), the analytical approximation is further improved by taking a closer look at the formulation and the solution procedure. For puff releases, the study is restricted to the case of a constant, representative, diffusion coefficient chiefly because it renders itself amenable to exact analytical solution that is useful for benchmarking the functional form of solutions in more complex situations. A comparison of the previous approximate analytical solution with the accurate numerical solutions of the diffusion-coagulation equation indicated that the simple formula always yielded lower survival fractions than the numerical values. This is mainly because of the restrictive assumption on the evolution of the variance. In reality, there will be a rapid depression of concentration at the centre of the puff due to higher particle concentrations there. This would appear as a distribution, flattened at the top. When this distribution is expressed as a renormalized Gaussian it would result in an apparently enhanced variance of the distribution. It is called as the ‘coagulation-induced flattening effect’. This effect is accounted in the new approximation scheme for puff and plume situations by a systematic mathematical procedure based on Fourier space analysis.

The solution approach consists of constructing moment equations from the Fourier transformed equation for the evolution of number concentration and variance of the spatial extension of puff in terms of either time or downstream distance. The original diffusion-coagulation equation is then reduced to a simpler coupled set of ordinary differential equations. These equations capture the essential elements of the coagulation-dispersion problem and carry information on the important variables such as the particle number concentrations and puff dimensions. Although still nonlinear, these equations are solved relatively more easily since redundant space and size variables have already been eliminated. Analytical solutions are obtained for special cases; when this is not feasible, numerical solutions are generated in terms of the relevant combination of dimensionless parameters.

The puff model, applicable to instantaneous releases is solved within a 3-D, spherically symmetric framework. An asymptotic analytical formula is obtained for the number survival fraction $\left(\psi(\infty)\right)$ for a puff of initial width (b_0) consisting of (N_0) particles as,

$$\psi(\infty) = \frac{1}{[1+(5A/4)]^{4/5}}$$

where, A is the parameter defined for the constant coagulation coefficient in the section 3.1.2. The present solution (4/5th law) is seen to agree closely with the exact numerical solution of the diffusion-coagulation equation even for large values of A.

3.2. Plume releases

Unlike the situation in respect of pure dispersion problems, the extension from puff to plume for continuous releases is far from simple when nonlinear reactions such as coagulation are considered. The diffusion approximation with coagulation-induced flattening effect described in the section 3.1.3 is utilized to study an important class of problem, i.e., plume releases. The plume case, corresponding to continuous releases, is discussed within a 2-D framework under the assumptions of constant advection velocity (U) and space dependent diffusion coefficient expressed in terms of turbulent energy dissipation rate (ε). In general, the diffusion coefficients of the particles follow the atmospheric eddy diffusion coefficients, which in turn are expressed either as space dependent functions ($r^{4/3}$ formula, Richardson, 1926), or time dependent functions (t^2 formula, Batchelor,1952). But, invoking space varying diffusion coefficients is essential for continuous 2-D plume releases, since these do not admit of non-zero ultimate survival fractions for any assumed constant diffusion coefficient. Hence for plume releases, the case of a diffusion coefficient that varies as a function of the downstream distance analogous to the t^2 law above is considered.

A steady-state dispersion-coagulation equation for the evolution of the number concentration is set-up under the assumptions of constant coagulation kernel and cylindrical symmetry of the plume. The dispersion-coagulation equation is then converted to a set of coupled ordinary differential equations using the diffusion approximation mentioned above. These coupled ODEs are solved by numerical methods using Mathematica. For plume of initial width (σ_0) emitting S_0 particles per unit time, the survival fraction formula is obtained by fitting the numerical solutions. The asymptotic survival fraction $\left(\psi(\infty)\right)$ in this case (fitted formula for the plume model) is then given by,

$$\psi(\infty) = \frac{1}{[1 + 1.32B]^{0.76}}$$

where, $B = \frac{KS_0}{6\sqrt{3}U\sigma_0^{4/3}(C\varepsilon)^{1/3}}$, and C is a constant.

The survival fraction obtained using the above formula is compared with the formula obtained for the case of weak coagulation ($\psi(\infty) = (1 + B)^{-1}$) which includes turbulent diffusion. The formula for the weak coagulation is obtained (B <<1, small B limit) which does not involve the coagulation-induced flattening effect. From the comparison, one can observe that these two formulae are agreeing in the limit of small B values. However, the fitted formula from the numerical solutions which accounts for the coagulation-induced flattening effect can be used for the entire range of the parameter B from very low to high. That is, from weakly coagulating system to strongly coagulating system.

The implication of these results such as robustness with respect to uncertainties in the choice of the initial data and applications for a few practically important problems such as vehicular emissions, forest fires, etc are also discussed in this study. While there is no alternative to full numerical computations for detailed information on aerosol distributions, the summary formulae presented here could still serve as useful guidelines for establishing the relative importance of processes in implementing these models. The main advantage of these simple formulae is the quick computation of the survival fraction in comparison to the numerical solutions which it takes few hours. In the case of plume model, the results demonstrate a certain level of robustness of the ultimate particle loading rates with respect to the initial data on the initial number emission rates and atmospheric turbulence energy dissipation rates, which is reassuring in view of the practical difficulties in obtaining these data accurately.

3.3. Continuous volumetric releases

For instantaneous and homogeneous aerosol releases, the problem gets simplified because the particle concentration is uniform within the volume of interest. However, obtaining analytical solutions is not an easy task when a continuous source term is added to the coagulation equation. Analytical solutions are available in the literature only for simple and homogenous kernels like constant, gelation, free-molecular, ($u + v$) kernels, etc but there are no analytical solutions for the non-homogeneous kernels like Fuchs kernel. Adding complexity to this problem is the inclusion of the fractal nature of the particles. This study is being carried out to understand the evolution of important metrics such as total number concentration and size distribution of nanoparticles undergoing Brownian coagulation in a continuous source injection mode in an indoor environment.

Exact numerical solutions for this case are obtained through suitable modification to the numerical code used for the previous studies, and the simulations are based on the general dynamic equation for the aerosol coagulation process along with a continuous source term. A source term is added to the coagulation equation to account for the continuous particle injection. The numerical model is then suitably modified to take into account the appropriate definitions of the mobility and the area equivalent radii required for the Fuchs kernel for fractal agglomerates. Other aerosol processes like removal by ventilation and deposition are also added in this model. The simulations are carried out with various options like, i) coagulation kernel, ii) source injection rates, iii) fractal nature of the particles, and iv) ventilation removal rates. From these studies, it is found that the rate of coagulation process along with the source injection rate plays important role in determining the aerosol particle characteristics, and the following interesting observations are made. The total particle number concentration reaches a peak value in a short time and then it gradually decreases, even though the source is continuously emitting the particles. The size spectrum at the source is lognormal with single mode, but it evolves to bimodal distribution from a single mode in the injected volume. Numerous possible release conditions are simulated by varying few input parameters like source injection rates, count median diameter, fractal dimension etc.

Since classical similarity formulations do not work for the case of continuous injection and exact numerical methods are computationally quite intensive, there is a fundamental need to look for alternative computational simpler formulations, which may not be as rigorous as the classical coagulation equation, but which captures the essential features of the processes. For this purpose a simplified two-species model which entails the essential features of coagulation process under continuous injection by formulating differential equations for the number concentrations in the primary (injected particle) mode and the secondary mode nonlinearly coupled through overall mass conservation law is formulated. The simplified model considers coagulation of two species in the system, the first species (A) is the primary nanoparticles emitted continuously by a source and the second one (B) is all the particles other than the first species. In essence, two size groups are assigned, the first is the injected source size and the second is the effective size that constantly evolves in time, of the previously injected particles. The species A and B in the system undergoes both heterogeneous and homogeneous coagulation. In this model, time dependent coagulation coefficient for the heterogeneous coagulation between the two size groups is introduced. The set of equations in this model with the given initial conditions are solved easily using the differential equation solver of the Mathematica. Further, the simplified equation is amenable to asymptotic analysis to obtain large time results. The main advantage of this two-species model is the computation time. The numerical approach of integration of the coagulation equation using realistic kernels is computationally quite intensive and requires considerable investment of time to obtain long time results under different parametric scenarios. To obtain asymptotic results, the numerical code has to be run for few hours (>2 hours) in a single core desktop computer whereas it takes less than a minute to obtain the same results using the simplified two-species model.

Further, a comprehensive numerical study of the coagulation process in a well-mixed aerosol chamber with a constant source term of nanoparticles has been carried out to analyze and place into perspective the experimental observations made by Seipenbusch et al. (2008) related to the accidental release of nanoparticles into workplace air. When allowing for a fractal nature of particles, the numerical simulation reproduces the salient features of the experimental observations of Seipenbusch et al. (2008) such as the peaking effect in the time variation of the total number concentration and formation of a bimodal distribution. The model results are further discussed from the point of view of the aerosol metrics required for toxicological assessment. Furthermore, an experimental system is designed and assembled for carrying out studies in the case of continuous volumetric releases. The experimental results are then compared with the numerical and two-species model results.

4. Conclusions

- A key question for assessing the impact of anthropogenic aerosols on the environment pertains to the estimation of the fraction of particles that persist in the atmosphere to form background aerosols. Among the various factors that contribute to this, coagulation is an important and numerically the most difficult issue to handle. The study addresses this question by combining coagulation with dispersion and different emissions scenarios to understand the long time and far field behaviour of aerosol size spectra and number concentrations. To this end, numerical and analytical models have been developed for modeling aerosol evolution in the atmosphere, emitted from localized sources under the combined action of coagulation and dispersion. In particular, the study introduces the concept of survival fractions as a means of predicting the atmospheric number loading factors of particles released from localized sources.

- For puff emissions, an approximate analytical formula, termed as 4/5th law, is obtained for the survival fraction which is in close agreement with accurate numerical solutions. This formula combines the coagulation and diffusion variables into a single parameter and provides a simple estimator of modifier for the source emission factor.
- The study addresses the question of plume emissions from localized sources in the presence of atmospheric turbulence. It provides simple scaling relations for the survival fractions and the number loading factors. When the source is intense, it is shown that the atmospheric ultimate number loading factor ($S(\infty)$) is relatively insensitive to the original number emission rate ($\sim S_0^{1/4}$), and the turbulent energy dissipation rate ($\sim \varepsilon^{1/4}$).
- The detailed numerical study for the volumetric releases brings forth several important features of coagulation of particles injected continuously into an air space. Fractal dimension, initial particle size, injection rate, and ventilation are identified as key variables that influence the evolution of particle characteristics. An asymptotic law ($t \to \infty$) for the decay of number concentration is derived using a simple analytical model. Simulations combined with analytical results using simplified model indicate an asymptotic decay of number concentration in the form $N^*(t^*) \sim t^{*-0.4}$ which is in marked contrast with the well known t^{-1} behavior for systems with a one-time aerosol injection. The above results have implications for an assessment of toxicological risk as well as in planning of safety measures in the context of industrial processing and applications of nanoparticles.

List of Figures

2.1 Coagulation process - Schematic diagram 26

2.2 Illustration of node spacing on a logarithmic volume space where q is the geometric spacing factor. The heights of the nodes correspond to the volume of the node (not drawn to scale). 30

2.3 Schematic classification of coagulation kernels (Van Dongen & Ernst, 1985) 34

3.1 Temperature and volume of the cloud during adiabatic expansion (Explosive mass considered in this case is 2000 g of T.N.T with a loading density of 1.5 g/cm^3) 45

3.2 Temporal evolution of total number concentration and average particle diameter in a burst release 46

3.3 Final aerosol particle size distribution in the cloud at t = 243 μsec 47

3.4 Illustration of number survival fraction of aerosol particles in a puff due to coagulation with and without diffusion. 67

3.5 Analytical and numerical solutions for the variation of survival fraction with time for various values of A (constant kernel, homogeneous size spectrum, initial size distribution - monodisperse) 68

3.6 Analytical and Numerical solutions for the variation of survival fraction with time for various values of A (free-molecular kernel, homogeneous size spectrum, initial size distribution - monodisperse) 69

3.7 Aerosol particle size distribution for monodisperse, spatially homogeneous size spectrum at scaled time, $t^* = D\, t/b_0^2$ =10. (A =1.0, constant kernel) 70

3.8 Aerosol particle size distribution for polydisperse, spatially homogeneous size spectrum at scaled time, $t^* = D\, t/b_0^2$ =10. (A =1.0, constant kernel) 71

3.9 Evolution of average particle size with time for A=1.0 (constant kernel) 72

3.10 Evolution of average particle size with time for A=3.0 (free-molecular kernel) 73

3.11 Comparison of various solutions for the ultimate survival fraction of particles in a spherical puff as a function of the parameter A. The present solution (4/5th law) is seen to agree closely with the exact numerical solution of the coagulation-diffusion equation. 77

3.12 Temporal variations of the survival fraction for a 3-D spherical puff ($A = 10$) 78

3.13 Effect of coagulation-induced flattening on the temporal evolution of variance $\xi(\tau)$ of the spatial distribution of a spherical aerosol puff ($A = 10$) 79

3.14 Evolution of average particle size segregation of particles in a Gaussian puff ($A = 10$) 81

4.1 Comparisons of different approaches for the temporal variations of the survival fraction for a cylindrical column ($d = 2$) for the case with B =10. 91

4.2 Survival fraction in the plume as a function of μ (turbulent diffusion case) 94

4.3 Evolution of bimodal size distribution in a spatially inhomogeneous plume 98

5.1 Temporal evolution of the scaled concentration ($N^*(t^*)$) for various removal rates (λ^*) 112

5.2 Steady-state number concentration vs. removal rate in the case of (u + v) type kernel 113

5.3 Effect of particle fractal dimension on the total number concentration. The ventilation rate is zero. 124

5.4 Effect source injection rate on the total number concentration of particles with d_f=1.75. The ventilation rate is zero. 127

5.5 Non-dimensionalized representation of total concentration $N^*(t^*)$ vs. time for various source injection rates. The ventilation rate is zero. 128

5.6 Effect of source particle size on the total number concentration. Source strength and fractal dimension are constant at $S = 1.67x10^9$ m^{-3} s^{-1} and d_f =1.75. 131

5.7 Effect of ventilation rate on the total number concentration. S = $2x10^8$ $m^{-3}s^{-1}$; d_f = 1.75. 132

5.8 Evolution of particle size spectrum for compact particles with d_f = 3.0 (S = $2x10^9$ $m^{-3}s^{-1}$, CMD=15 nm; zero ventilation rate) 134

5.9 Evolution of particle size spectrum for fractal particles with d_f = 1.75. (S = $2x10^9$ $m^{-3}s^{-1}$, CMD=15 nm; zero ventilation rate) 135

5.10 Evolution of particle size spectrum for fractal particles at a higher injection rate of S = 2 x 10^{10} $m^{-3}s^{-1}$. (d_f – 1.75, CMD=15 nm; zero ventilation rate) 136

5.11 Evolution of particle size spectrum for a larger initial particle size CMD=30 nm. (S = 2 x 10^9 $m^{-3}s^{-1}$, d_f – 1.75, zero ventilation rate) 137

5.12 Evolution of mean particle diameter with time for various combinations of parameters. 138

5.13 Experimental setup to study the aerosol evolution in a well-stirred chamber 142

5.14 Temporal evolution of particle size spectrum (Each curve was obtained at an interval of ~8 minutes) 145

5.15 Evolution of total number concentration in the 0.5 m^3 chamber - comparison of experimental results with numerical simulation 146

5.16 Temporal evolution of particle diameter (geometric mean) in the 0.5 m^3 chamber 147

List of Tables

1.1 Guideline values for particulate matter (PM) 3

2.1 Examples of scaling solutions for various coagulation kernels 32

2.2 Some commonly used coagulation kernels 33

Chapter 1. Introduction

1.1. Background

Aerosols have profound effect on the nature of the atmospheric environment. The visibility, the colour of the sky, electrical conductivity of the atmosphere and cloud formation are some of the day-to-day phenomena that are governed by aerosols. In recent times, large concern has arisen due to their potential role in inducing global warming or cooling and climate change as well as in affecting human health. Although aerosols existed in the atmosphere for times immemorial due to natural sources such as sea sprays, windblown dust, volcanic eruptions and large-scale forest fires, the human activity related with the use of fossil/renewable fuels to meet the increased energy needs of the large population has led to a voluminous increase in the anthropogenic aerosol contribution into the atmosphere. Power plant plumes, biomass burning, industrial emissions, vehicular exhausts, aircraft emissions, and intense fireworks during festive seasons are the important anthropogenic sources that contribute to the atmospheric aerosols. The effects of these particles depend not only on their concentrations and regional distributions, but also on the chemical compositions, and particle sizes. These parameters in turn depend on the mode of emissions. For example, aerosol produced by direct ejection into the atmosphere, called as primary aerosols are inorganic and are generally large in sizes. On the other hand, those produced by physico-chemical processes within the atmosphere called as secondary aerosols are extremely fine. The global production rates of primary and secondary aerosols are estimated to be in the range of (3000-6000) and (100-300) Tg/yr respectively (Seinfeld & Pandis, 2006).

The increasing importance of atmospheric aerosol studies stems from the fact their spatial and temporal variations alter the energy balance of the climate system at both regional and global levels. This is by way of altering absorption, scattering and emission of solar radiation in the Earth-atmosphere system depending on the size distribution and chemical composition of the aerosols. These changes are expressed in terms of "radiative forcing" which is a measure of the influence attributable to a given factor in altering the balance of incoming and outgoing energy in the Earth-atmosphere system. Positive forcing tends to warm the system while negative forcing tends to cool it. It has been estimated that anthropogenic contributions (primarily sulphate, organic carbon, black carbon, nitrate and dust) to atmospheric aerosols together produce a cooling effect, with a total direct radiative forcing of -0.5 W/m^2 (range: -0.1 W/m^2 to -0.9 W/m^2). This is due to reflection of sunlight that reaches Earth's atmosphere back into space by aerosols. Furthermore, an indirect cloud albedo forcing of -0.7 W/m^2 (range: -0.3 W/m^2 to -1.8 W/m^2) from the change in the cloud properties by aerosols contribute an additional cooling term. Both these effects increase the amount of sunlight that is reflected to space without reaching the surface (IPCC, AR4 SYR, 2007). It has also been noted that the estimates of aerosol contributions have the largest uncertainty among the various factors which contribute to global warming/cooling. These uncertainties, in part, are due to our inadequate knowledge of the source terms, mixing state and compositions of emitted particles.

These same particles that affect climate also impact the quality of the air that we breathe and the health of all living organisms, both outdoor and indoor environments. Common examples of the adverse health effects of aerosols among humans are the higher incidence of bronchial infections, reduced lung functions, increased respiratory symptoms, and cardiovascular diseases during periods of high aerosol loading. In addition to natural and anthropogenic sources of ultrafine particles in the ambient air, certain workplace conditions also generate nanoparticles (particles in the size range of <100 nm) that can reach much higher exposure concentrations, up to several hundred micrograms per cubic meter, than is typically found at ambient levels. Recent workplace environment studies show that the occupational exposure to the engineered nanoparticles results in higher health risk to the personnel working in this environment (Oberdorster et al, 2005). These workplace exposures can occur during production, handling, and waste disposal of nanomaterials.

The aerosol pollution in the atmosphere is generally monitored, for the purposes of air quality assessments, by mass concentration measurement using devices such as grab samplers and cascade impactors. Various regulatory agencies specify air qualities based on this mass concentration. The particles are identified according to their aerodynamic diameter, as either PM_{10} (particles with an aerodynamic diameter smaller than 10 µm) or $PM_{2.5}$ (aerodynamic diameter smaller than 2.5 µm). World Health Organization (WHO) specifies the following guideline values for the air pollution levels based on particulate mass,

	Annual mean ($\mu g/m^3$)	24-hour mean ($\mu g/m^3$)
$PM_{2.5}$	10	25
PM_{10}	20	50

Table 1.1: Guideline values for particulate matter (PM)

However, there is emerging evidence that additional quantification by number, size and surface area is needed to better characterise health relevant exposure as well as optical effects in the context of climate change (Oberdorster et al, 2000; Lighty et al, 2000; Ramachandran & Rajesh, 2007). Even very low mass concentrations of nanosized materials in the air represent very high particle number concentrations, as is well known from measurements of ambient ultrafine particles (Hughes et al, 1998). For example, a low concentration of 10 $\mu g/m^3$ of unit density 20-nm particles translates into $> 1 \times 10^6$ particles/cm^3. In an average urban aerosol size distribution, most of the particles are in the nuclei mode (5-100 nm) by count but most of their mass is split between accumulation (0.1-2 μm) and coarse (> 2 μm) particle modes. As a result, mass based measurements direct greater focus on coarser particles, thereby missing the significance of the nanoparticles. To strike a right balance, increasing attention is being paid to characterize air pollution sources in terms of their particle number emission characteristics in the nanoparticle size range <100 nm (nuclei mode) by using advanced instrumentation such as mobility analysers (Lighty et al, 2000).

Nanoparticles are produced copiously near the sources. These particles are rapidly dispersed in the atmosphere as a result of which their number concentrations are reduced to background levels due to large atmospheric dilution. However, in the course of the dispersal between source and receptor, aerosols undergo evolution due to condensation of water vapour and coagulation, and their ambient concentrations are not necessarily proportional to those measured at the sources. Hence, source and ambient measurements must be paired in time to establish reasonable estimates of source/receptor relationships. However, it is next to impossible to actually measure the contribution of the given source to the persisting contribution to the background aerosols. Since direct measurements of far-field contributions from a given source are hugely difficult due to enormous atmospheric dilutions, it should essentially rely on model estimates. Additionally, there is a need to understand persisting aerosols changes if certain atmospheric and source characteristics are changed. Hence, mathematical models have an irreplaceable role to play in source impact characterizations and it is important to examine these models and their solutions more closely.

Most generally, atmospheric aerosol evolution models combine dilution effects due to advection and dispersion mechanisms with physical transformation processes. The dominant aerosol microphysical processes are nucleation, coagulation, vapour condensation/evaporation, and plate out/wash out mechanisms (Jacobson & Seinfeld, 2004; Aloyan, 2009; Albriet, 2010). Nucleation is the process of forming new particles from a purely gaseous precursor phase. Coagulation occurs when two particles collide and stick together. During this process, the particles may undergo coalescence or aggregation depending on whether they are liquid droplets or solid particles. Both these processes reduce the number concentration but conserve the mass concentration of particles in the atmosphere. It also changes the particle size distribution due to the formation of larger particles thereby affecting their residence times in the atmosphere. Condensation is the process by which an aerosol particle grows with the accretion of monomers or individual vapour molecules to an already existing particle. Condensation/evaporation processes are essentially number conserving processes, which mainly affect the size spectrum, but do not create or destroy particles. These processes can be split into two, near-source and far-source phenomena based on the spatial domain from the source to ultimate background. In the far-source domain, condensation and dispersion will dominate the other particle processes, and they influence the particle properties in the atmosphere. The significance of coagulation process reduces drastically in regions far away from the sources as the aerosols are diluted in the atmosphere. In the near-source domain, coagulation is primarily responsible for depletion of number concentration and evolution of size distribution.

In few cases like vehicular emissions, there has been a certain debate as to whether it is worthwhile to include coagulation at all (Zhang & Wexler, 2002; Zhu et al, 2002; Jacobson & Seinfeld, 2004). This is because the number concentrations at these emission points are low due to the removal of particles in the exhaust pipe, and large atmospheric dilution. However, it is realised that coagulation is very important in the cases of large scale emission sources like forest fires, biomass burning, volcanic releases, aircraft emissions, explosive releases, where very high number concentration is seen at the emission points (Radke et al, 1995; Fiebig et al, 2003; Hobbs et al, 2003; Turco & Yu, 1997; Nathans et al, 1970). There exist several other topical sources on which systematic studies are only beginning to emerge: mosquito coils, candles and incense sticks used extensively in Asian homes (Li et al, 1992; Zai et al, 2006) and large scale display of fire-works during community celebrations (Mönkkönen et al, 2004) are some examples that may be mentioned in this context. To quantify the process of transformation of these aerosols from source to environment, it is necessary to combine the dispersion process with coagulation mechanism.

A natural question that arises in this context is: what fraction of the number of particles emitted at the source point eventually form a part of the background aerosols, subsequent to the joint action of dispersion and coagulation?. For this purpose, we introduce the concept of 'survival fraction', which is closely related to the concept of 'survival probability' introduced by Pierce et al (2009). The survival fraction is defined as the fraction of particles emitted from a source ultimately surviving coagulation and dispersing into background. This fraction will be a function of original emission rate, size, and atmospheric turbulence and dilution factors. This quantity also captures the relative importance of the coagulation vis-a-vis atmospheric dispersion. The survival fraction can be viewed as environmental "source modifier" function for particle releases from localised sources. While the survival fraction estimates the fraction of particles ultimately surviving in a puff or a plume, the concept of the source modifier function provides an effective factor by which the source term has to be reduced while modeling its "persisting" contribution to the background aerosols. Another important quantity useful in this context is the "number loading factor", which provides a measure of the effective injection rate of persisting particles in the atmosphere. It is obtained by multiplying the source modifier with the source number emission rate. Also, one can make use of the available mass emission rates (Rodriguez & Cuevas, 2007; Ichoku et al., 2008; Garcia-Nieto, 2006; Gramotneva et al, 2003; Janhall et al, 2010) of the sources to estimate the initial number emission rates and there from obtain the final number loading factors using the source modifier function. The ultimate survival of the emitted particles is fundamentally a result of competing effects of dilution that tends to preserve total number of particles, vis-a-vis coagulation, which tends to reduce the number of particles. While each of these effects has been well studied individually, there exists very little treatment of the combined action. Hence, it is endeavored in this thesis to develop predictive models to estimate the impact of sources on aerosol concentrations in the ambient environment.

The mathematical treatment of the combined problem of coagulation and dispersion necessarily brings in the question of spatial heterogeneity in aerosol systems, especially at the emission points of localized sources. The extent of this heterogeneity will depend upon several source related and local atmospheric factors and need to be addressed on a case to case basis. Even if one sets up detailed equations involving all the factors, such an equation will be highly data intensive and the results will once again be approximate depending upon the lacunae in the necessary data inputs. In this connection, simpler generic models based only on the most significant parameters, will be far more fruitful as they will have the capability to provide analytical expressions for the source modifiers. With this view, the present study addresses the issue by treating coagulation and atmospheric dispersion in their simplest forms, to derive the essential results. The condensation/evaporation processes is excluded as being not central to the theory of number evolution since these processes are basically number conserving.

1.2. Literature Survey

Most of the classical work on the aerosol coagulation phenomena has been concerned with the time dependent, spatially homogeneous situation. Similarly, classical literature on dispersion does not generally take coagulation into account (Holmes & Morawska, 2006). However, in recent times several models have been developed to delineate air pollution effects of sources and sinks in the atmosphere by taking the combined effect of dispersion, coagulation and removal into account. Aloyan et al (1997) discussed in detail a coagulation-dispersion model to handle transport of coagulating particles in the atmosphere. This work addresses complex distribution of aerosols at various atmospheric layers and develops an adjoint formalism to identify sources from aerosol distributions. Wexler et al (1994) developed numerical methods to solve the aerosol dynamic equation for modeling urban and regional particle transport in conjunction with the Eulerian gas-phase dispersion model. This study shows that the coagulation is only significant in locations with higher aerosol loading. Sheih (1977) used a finite difference model that incorporated the mechanisms of coagulation and gravitational sedimentation in the equation of diffusion to predict the particulate size distribution downstream from an urban area source. He found that coagulation effects dominate in the near source region. Hudischewskyj and Seigneur (1989) developed a comprehensive numerical model that takes into account gas phase and aerosol phase pollutant concentration in a plume, especially to address the scattering of light by sulphate aerosols. Kerminen and Wexler (1995) studied the interdependence of the basic aerosol phenomena and mixing in plumes generated by industrial point sources through numerical modeling. Brock et al (2002) measured the evolution of sub-micron particle size distribution in the plumes downwind of coal-fired power generation plants, and found that there was a significant particle growth in these plumes. Based on these measurements, they performed two analyses: one to calculate the apparent fraction of plume sulfur incorporated into the particles and the other to examine the size dependence of particle growth.

The large scale numerical studies cited above are computationally intensive, with considerable numerical difficulties for obtaining solutions. Also, these studies do not specifically address the question of particle survival fractions and do not throw specific insight on the sensitivity of the resulting aerosol distributions on the source- and environment-related input parameters. To address these issues, one is required to introduce somewhat idealized models that maintain the essential elements of the processes, yet that can be traced analytically. To understand the structure of solutions in such systems, Slemrod (1990) proved the existence of solutions of the coagulation-diffusion equation for the case of constant coagulation kernel and diffusion coefficient. Explicit exact solutions are possible only for a few specific cases (Herrero & Rodrigo, 2005, Simons, 1987) that too in one dimension. Simons (1987, 1992, 1996) conducted a series of studies on the solution of one-dimensional steady state coagulation-diffusion equation. He obtained solutions for the above-mentioned system with size dependent diffusion coefficient and coagulation kernel by invoking the validity of self-preserving distribution for sufficiently large times (Simons, 1987, 1996). For the case of constant diffusion coefficient and constant coagulation kernel, he solved the coagulation-diffusion equation without assuming a similarity solution (Simons, 1992). Simons and Simpson (Simons & Simpson, 1988) combined scaling theory with moment method to reduce the coagulation-diffusion equation in 3-dimensions to simpler nonlinear form of recombination-diffusion equation, which, however, cannot be solved analytically.

Being non-linear, coagulation-diffusion equation does not have exact analytical solutions. Hence, to elicit functional forms of the solutions, certain approximations have been made either at the level of formulating the equation itself or at the level of developing solutions. In the former category, one sometimes encounters what may be termed as "Uniform expansion models" (Nathans et al, 1970; Turco & Yu, 1997). This model assumes a uniformly mixed volume element expanding under a prescribed rate in time. The prescription for the expansion rate may be arrived at either from deeper mechanistic considerations (as in the case of explosive releases) or from heuristic correlations based on broad physical considerations (as in the case of diffusive processes). The simplifying feature of this model is that, it altogether replaces the space dependent nature of the dispersion process by a purely time dependent term, which is exactly solvable for the case of constant kernel. However, for complex kernels like Fuchs kernel, one has to use numerical techniques. Nathans et al (1970) used this uniformly mixed volume expansion model to simulate the evolution of particle size distribution in an expanding cloud formed due to nuclear air burst. The volume and temperature transients of the expanding cloud for this case were obtained from the literature (Glasstone, 1962; Nathans et al, 1970). Brownian motion of the particles with and without slip correction was considered for the coagulation in this study. A study by Turco and Yu (1997, 1998) dealing with the coagulation and dispersion of aerosols emitted by high-altitude aircraft plumes also belongs to this category. Similarly, in the case of forest fire models, many researchers consider coagulation as an important process and used this uniformly mixed volume expansion model to estimate the final average particle size and the size spectrum which finally becomes a part of the background aerosols (Radke et al, 1995; Fiebig et al, 2003; Hobbs et al, 2003).

In spite of great analytical advantages, uniform expansion models have certain drawbacks. First, of course, concerns the choice for the law of expansion, which remains essentially empirical, when coagulation is brought in since the expansion rates of the air parcels may not be the same as that of particles. More important disadvantage of this model is the limitation in respect of its applicability of steady sources. While one can formulate an expanding volume for an instantaneous release, it is difficult to extend it for a standing plume existing in a steady state. It may be possible in principle to develop an equivalent form in steady-state but it is not available at present and is unlikely to be simple.

In the simplest case of constant coagulation kernel, the coagulation-diffusion equation for the total particle number concentration can be shown to reduce to a form that is often known in the literature as reaction-diffusion equation. These are still nonlinear and arise in the study of kinetics of evolution of two interacting species simultaneously undergoing diffusion and recombination (Rosen, 1984; Thomas & Imel, 1987; Cheng et al, 1989; Byakov & Stepanov, 2006). In recent times, several new applications viz., (i) remote detection of alpha radiations using ion transportation technology (Naito et al, 2007), (ii) atmospheric ion balance dynamics (Mayya & Hollander, 1995), (iii) primary biological effects of ionizing radiations (Byakov & Stepanov, 2006), and (iv) aerosol coagulation and dispersion in the atmosphere from localized sources (Turco & Yu, 1997), have renewed the interest in the study of reaction/recombination-diffusion equation. Variants of recombination-diffusion equation have also been used for describing multiple species free-radical recombination (Wojcik & Tachiya, 2004), and pattern formation (Lee et al, 1994).

The reaction-diffusion or recombination-diffusion equation were solved by many researchers in the past by assuming approximate analytical solutions. By applying prescribed diffusion approximation at the level of developing solutions, a simple solution to the recombination-diffusion equation was provided about 100 years ago by George Jaffe (Jaffe, 1913, 1940). Jaffe approximation assumes that the spatial dispersion of the species is controlled by diffusion laws at all times while the recombination term influences essentially the survival fraction, defined as the number of ions/particles that survive recombination/coagulation. Subsequently, alternative approaches were attempted with a view to provide better solutions (Ganguly & Magee, 1956; Wilhelm, 1967). Kramers (1952) obtained exact solution to the problem of ion survival in the presence of external electric field by neglecting diffusion altogether. However, when electric fields are absent or very weak, diffusion cannot be neglected nor can it be taken as perturbative since it is the most dominating dispersal mechanism. Rosen (1984) provided a Brownian dynamics description of the reaction-diffusion equation and obtained bounds for the survival fraction. His formulation is not readily useful for practical applications. Wilhelm (1967) attempted a hybrid approach of combining diffusion with recombination, which have been employed by some authors (Byakov & Stepanov, 2006) recently. However, Wilhelm's solutions are not reliable in view of a major anomaly in his mathematical transformation and physically unacceptable asymptotic results. In view of these, Jaffe solution still remains the most useful analytical solution to the field-free reaction-diffusion problem.

In the case of continuous volumetric releases, several analytical and numerical studies have been carried out for a variety of aerosol systems with continuous source injection. Barrett & Mills (2002) studied the evolution of an aerosol system undergoing coagulation with constant kernel, removal, and continuous source injection by obtaining approximate analytical solutions under the assumption that the size distribution is always unimodal and lognormal. Schneider & Jensen (2009) discussed the importance of the coagulation process on the basis of a steady-state solution of the coagulation model. Numerical simulations were also carried out in the past to estimate the particle size and its distribution during continuous release of nanoparticles in different systems. Landgrebe & Pratsinis (1989) studied the interplay of reaction rate (source release rate) and aerosol coagulation rate in the free-molecular regime using a numerical model. They observed the formation of bimodal size distribution depending on the ratio of primary particle formation and particle removal by coagulation. Kim et al. (2003) investigated particle growth specific to a plasma reactor by using a discrete-monodisperse model for various process conditions related to the production of monodisperse particles. This study also showed the formation of a bimodal distribution under specific conditions when including the effect of a particle charge distribution.

In fact, there is a certain paucity of knowledge regarding the asymptotic and steady-state behaviour of solutions to the coagulation equation with a continuous source term. Some theoretical studies (White, 1981; Crump & Seinfeld, 1982; Davies et al, 1999, Lushnikov, 2010) have generally focused on the question of boundedness of solutions to the coagulation equation for certain types of idealized kernels, but have not addressed the interesting question as to the conditions for sustaining a finite (non-zero) asymptotic concentration by a steady source.

1.3. Scope of thesis

While there exist many studies, both analytical and numerical, dealing with coagulation and dispersion in the context of air pollution, the basic issue of quantifying the impact of the emissions from sources in contributing to the persisting aerosol concentrations in the environment has remained unaddressed. This thesis addresses this issue precisely from a theoretical perspective. The framework adopted is based on solving the combined coagulation and dispersion equation to predict number concentrations in a concentrated release of aerosol particles from sources. To provide generic solution to the problem, the concept of survival fraction is formulated and various relationships are derived using a combination of analytical and numerical techniques for various release scenarios. The goal has been broken into two specific objectives:

1. Obtaining correlations for the survival fraction as a function of source strength, spatial expansion of the source, dispersion parameter and coagulation coefficient for instantaneous, explosive and plume releases, and
2. Estimation of important metrics like total number concentration, average particle size, etc., in the case of continuous volumetric releases.

Numerical programs have been developed for solving the second order differential equation for diffusion in space coupled with the non-linear integro-differential formulation of coagulation in particle size variables. The analytical solutions have been compared with numerical solutions. In some cases where the analytical approximations are found to be difficult, asymptotic analysis is carried out to assess the possible functional forms of the survival fraction and the parameters of these forms are determined by fitting the numerical solutions. In the case of continuous volumetric release, the temporal evolution of the particle number concentration and its size distribution are obtained from the numerical solutions. Numerical methods are unable to throw insight into long time behaviour for which asymptotic analytical solutions are obtained by proposing a two-group model. An experimental study is also carried out to validate some of the models by injecting nanoparticle aerosols continuously into a closed chamber. In this case, aerosols are generated inside the chamber using nichrome hot wire generator and their kinetics is studied using a Condensation Particle Counter (CPC), and Scanning Mobility Particle Sizer (SMPS). Upon combining the theoretical methods with observations, a method of estimating the near source number emission rates and particle sizes have been devised.

1.4. Organization of this thesis

The outline of this work is described as follows. Chapter II (theoretical framework) starts with a discussion on the aerosol coagulation process. It introduces various types of coagulation kernels, and methods of obtaining solution to the coagulation equation. It also briefly describes the coagulation of dispersing aerosol systems. Chapter III describes about the formulation of different models to obtain the survival fraction for the instantaneous releases. Further, it shows how the analytical and numerical approximation formulae are obtained using different models, their applications, results and summary. Chapter IV describes the methodology to obtain survival fraction for the steady-state plume releases using improved diffusion approximation model. It further shows the application of the survival fractions to obtain the ultimate number loading factor for practical cases. Chapter V deals with continuous volumetric releases. It demonstrates the ability of numerical model to predict the important metrics that control the evolution of aerosol characteristics in this case. A simplified analytical model is formulated to estimate the asymptotic behavior of the total number concentration, and compared with the numerical results. This chapter includes the experimental study of continuous releases in a closed chamber, and comparison of its results with the simulations. Chapter VI summarizes the results and also discusses the conclusions obtained from the study.

Chapter 2. Theoretical framework

2.1. Introduction

Many important physical properties of natural or manmade aerosol particles such as light scattering, electrostatic charges, and toxicity, as well as their behavior involving physical processes such as diffusion, condensation, and thermophoresis, depend strongly on their size distribution. An important aerosol behavior mechanism affecting the size distribution of aerosol particles is coagulation. Aerosol particles suspended in a fluid may come into contact because of their Brownian motion, or as a result of their relative motion produced by external forces (e.g., gravity, hydrodynamic forces, electrical forces, etc.). The result is a continuous decrease in number concentration and an increase in particle size. In the case of solid particles, the process is called agglomeration or coagulation, and the resulting particle clusters are known as agglomerates. The theory of coagulation was originally devised for colloids (particles in liquids) and was later extended to aerosols (Smoluchowski, 1916). In many basic and applied fields (e.g., synthesis of nanostructured material via gas-phase synthesis, atmospheric aerosols), the evolution of the particle size distribution because of coagulation is of fundamental importance and interest. The coagulation process is described in detail in this chapter.

2.2. Coagulation Kernel

Aerosol coagulation is caused by relative motion among particles. A basic quantity governing the coagulation process is the coagulation kernel ($K(u, u')$), which describes the rate at which particles of size u coagulate with particles of size u'. These kernels are symmetric in nature, i.e. $K(u, u') = K(u', u)$. The coagulation kernel is defined as the ratio between the flux of particles of size u' on the surface of a stationary particle size u and the total number concentration at very large distance. The kernels incorporate the kinetic mechanisms and interparticle forces that are responsible for the coagulation process. Depending on these parameters and the physics of collisions, several forms of coagulation coefficients have been derived. When the relative motion is because of Brownian motion, the process is called Brownian coagulation. When the relative motion arises from external forces such as gravity or electrical forces, or from aerodynamic effects, the process is called kinematic coagulation. Kinematic coagulation includes gravitational coagulation, turbulent coagulation, electrostatic coagulation, etc. Some of the well-known coagulation kernels are discussed in this section.

2.2.1. Brownian Coagulation

The Brownian coagulation kernel can be derived either by the kinetic theory of gases, or by the continuum diffusion theory according to the particle size. Generally, the Knudsen number ($Kn = \lambda/r$), with λ as the mean free path length of the surrounding gas molecules and r as the particle radius, is used to define the particle size regime. Particles much smaller than the mean free path length of the gas molecules behave like molecules ($Kn > 50$), and the kinetic theory of gases must be used to derive the collision kernel. In the meanwhile, for the particles much larger than the mean free path of the gas molecules ($Kn < 1$), the continuum diffusion theory should be used.

2.2.1.1. Brownian coagulation in the free-molecular regime

In the free-molecular regime, the drag force exerted by fluid on suspended particles is small and hence these particles are decelerated very slowly. In effect, particles move along rectilinear trajectories between collisions, which occur at distances much larger than their size similar to the case of gas molecules. As a result, the aerosol particle behaviour in the fluid can be treated using the classical kinetic theory of gases. The coagulation kernel in this free-molecular regime is obtained by multiplying the collision cross-section with the relative velocity of the colliding fragments. Considering a particle of volume *u* surrounded by particle volume *u'*, the relative thermal RMS velocity between the two particles is given by $\sqrt{\overline{\boldsymbol{v}}_{\boldsymbol{i}}^{2}+\overline{\boldsymbol{v}}_{\boldsymbol{j}}^{2}}$, where, $\boldsymbol{v_i} = \sqrt{\boldsymbol{8k_bT/\pi m_i}}$ is the thermal velocity of particle of size *i* in air, k_b is the Boltzmann constant, *T* is the temperature, and m_i is the mass of the particle. In this regime, the collision cross-section of the particles of radii r_i and r_j is the actual geometric cross-section given by, $\boldsymbol{\pi(r_i+r_j)^2}$. Then, the coagulation kernel in this regime can be written as, $\boldsymbol{K_{fm}(r_i,r_j)} = \boldsymbol{\pi(r_i+r_j)^2}\sqrt{\overline{\boldsymbol{v}}_{\boldsymbol{i}}^{2}+\overline{\boldsymbol{v}}_{\boldsymbol{j}}^{2}}$. In terms of volume variable, this coagulation kernel ($K_{fm}(u, u')$) is written as:

$$\boldsymbol{K_{fm}(u,u')} = \left(\frac{3}{4\pi}\right)^{1/6}\sqrt{\frac{6kT}{\rho}}\left(\boldsymbol{u}^{1/3}+u'^{1/3}\right)^{2}\sqrt{\frac{1}{u}+\frac{1}{u'}} \qquad (2.1)$$

where, u_i is the volume of the particle of radius r_i, and ρ is the particle density.

2.2.1.2. Brownian coagulation in the continuum regime

In the continuum regime, particles move in the fluid through the process of Brownian motion. In this case, the kernel in this regime is found by solving the time-dependent diffusion equation around a stationary spherical absorber in an infinite medium with suspended particles. The direction of particle motion changes over a length scale that is a small fraction of the particle size. This leads to particle transport and collisions through random walk that is characteristic for the continuum diffusion process. In the continuum regime, where the Knudsen number is smaller than about 1, $K_{co}(u, u')$ is derived by the continuum diffusion theory as follows:

$$\boldsymbol{K_{co}(u,u')} = \frac{2kT}{3\mu}\left(\boldsymbol{u}^{1/3}+\boldsymbol{u}'^{1/3}\right)\left(\frac{C_c(u)}{u^{1/3}}+\frac{C_c(u')}{u'^{1/3}}\right) \qquad (2.2)$$

where, $Cc(u) = 1+Kn(u)\{1.142+0.558 \exp[-0.999/Kn(u)]\}$ is the gas slip correction factor (Allen & Raabe, 1982).

2.2.1.3. Brownian coagulation in the transition regime

The entire transition regime is characterized by Knudsen numbers in the range of ~1<Kn<50. In the transition regime, the coagulation rate is described neither by the continuum diffusion theory nor by the simple kinetic theory. The coagulation kernel in this regime can be obtained by either one of the following:

1. flux matching method,
2. solution of the Fokker-Planck equation.

The flux matching method is first used by Fuchs to obtain the coagulation kernel for the entire size regime. Fuchs (1964) found a semi-empirical solution of the collision kernel by assuming that outside of a certain distance, namely, an average mean free path of an aerosol particle, the transport of particles is described by the continuum diffusion theory including the slip correction, and that inside the distance, the particles behave like in a vacuum and the transport is described by the kinetic theory. The two theories were brought together by matching the fluxes at the radius of the absorbing sphere. This so-called flux matching was the basis for most of the following theories because of its phenomenological approach and the guarantee that the collision kernel is valid over the entire size regime. All theories dealing with an absorbing sphere use a correction function first calculated by Fuchs. This function is mainly expressed as an enhancement of the collision kernel for the continuum regime including the slip correction:

$$\boldsymbol{K_{tr}}(\boldsymbol{u}, u') = \frac{\boldsymbol{K_{co}}(\boldsymbol{u}, u')}{\frac{\boldsymbol{r_u} + \boldsymbol{r_{u'}}}{\boldsymbol{r_u} + \boldsymbol{r_{u'}} + \boldsymbol{\delta_{uu'}}} + \frac{\boldsymbol{K_{co}}(\boldsymbol{u}, u')}{\boldsymbol{K_{fm}}(\boldsymbol{u}, u')}} \qquad (2.3)$$

where, r_u and $r_{u'}$ are the radii of the particles with volume u and u' respectively, and $\delta_{uu'}$ is the distance between the collision surface and the regime dividing surface. Fuchs (1964) proposed, for a single particle,

$$\boldsymbol{\delta_u} = \frac{\left[(d_u+\lambda_u)^3-(d_u^2+\lambda_u^2)^{3/2}\right]}{3d_u\lambda_u} - d_u \tag{2.4}$$

where, d_u is the particle diameter and λ_u is the mean free path of the particle, and for a pair of particles,

$$\delta_{uu'} = \sqrt{\delta_u^2 + \delta_{u'}^2} \tag{2.5}$$

Many efforts were made to substitute the extremely complicated integral nature of the Fuchs kernel using simpler form of the flux-matching type kernels (Otto et al, 1999). The simplest choice is $\delta_{uu'} = 0$, i.e., to perform flux matching directly at the collision surface, which leads to the harmonic mean coagulation kernel:

$$K_{hm}(u,u') = \left(\frac{1}{K_{co}(u,u')} + \frac{1}{K_{fm}(u,u')}\right)^{-1} \tag{2.6}$$

Dahneke (1983) described the diffusion process as a mean free path phenomenon. To obtain the coagulation coefficient, Dahneke also matched the two fluxes but at a distance which is the mean free path of the particles, and proposed

$$\delta_{uu'} = \frac{2D_{uu'}}{\overline{v_{uu'}}} \tag{2.7}$$

where, $\overline{v_{uu'}}$ is the average velocity. By comparing various theories on the collision kernel in the transition regime, Otto et al (1999) recommended Dahneke's theory to be used partially for its simplicity and partially for its accuracy.

Flux matching method is a simplification. In reality, the character of particle motion does not change from ballistic to random walk abruptly, but rather gradually. A theoretically more sound approach to calculate the coagulation kernel in the transition regime is to solve Fokker-Planck equation. One of the solutions is given by Sahni (1983a, b):

$$K_{tr,FP}(u,u') = \frac{K_{co}(u,u')}{1+\kappa+\frac{\kappa}{2}\left[\frac{\pi}{\kappa^2}-\left(1+\frac{\pi}{\kappa^2}\right)erf\left(\frac{\sqrt{\pi}}{\kappa}\right)\right]} \tag{2.8}$$

where, $\kappa = \frac{K_{co}(\boldsymbol{u},\boldsymbol{u}\prime)}{K_{fm}(\boldsymbol{u},\boldsymbol{u}\prime)}$.

In the present study, we employ Fuchs kernel, one of the most widely used coagulation kernel for the entire particle size regime.

2.2.2.Kinematic Coagulation

Kinematic coagulation occurs because of relative particle motion caused by mechanisms other than Brownian motion. The following three important kinematic coagulation processes, gravitational, turbulent, and electrostatic coagulation, are presented in this section.

2.2.2.1. Gravitational Coagulation

Particles of different sizes will settle at different rates under the influence of gravity and thereby create relative motion between them, which leads to collision and coagulation. This mechanism is called gravitational coagulation. The collision kernel by gravitational coagulation is expressed as the following equation when the slip correction factor is neglected:

$$\boldsymbol{K_G(u,u') = \frac{2\pi g\rho}{9\mu}\varepsilon(u,u')(r_u + r_{u'})^2\left|r_u^2 - r_{u'}^2\right|} \tag{2.9}$$

where, $\boldsymbol{\varepsilon(u,u')}$ is the collision efficiency defined as the ratio of actual collision cross-section to the geometrical cross-section which can be expressed as follows:

$$\boldsymbol{\varepsilon(u,u') = \frac{3y^2}{2(r_u+r_{u'})^2}} \tag{2.10}$$

if $\boldsymbol{r_u \leq r_{u'},\ y = r_u}$ and if $\boldsymbol{r_u > r_{u'},\ y = r_{u'}}$.

When both the Brownian and gravitational coagulations are significant, the two collision kernels $K_B(u, u')$ and $K_G(u, u')$ are commonly added to predict the behavior of the aerosol system. This simple addition is due to the assumption that these two processes are independent of each other. However, Simons et al (1986) obtained a combined kernel and showed that these two processes are not independent. Their study showed that the combined effect of Brownian and gravitational coagulations increases the rate of coagulation compared with the sum kernel in the size range of 0.1-1 μm. On the contrary, Qiao et al (1998) reported that weak Brownian diffusion, the effect of which is nonlinearly coupled with gravity, can act to decrease the coagulation rate.

2.2.2.2. Turbulent Coagulation

In many physical situations, the flow field in a fluid is turbulent. There are two ways in which turbulence causes collisions between neighboring particles. First, there are spatial variations of the turbulent motion. Because of this process, collision mechanism is conventionally called "shear mechanism". Second, each particle moves relative to the air surrounding it, owing to the fact that the inertia of a particle is different from that of an equal volume of air. Because the inertia of a particle depends on its size, neighboring particles of unequal size will have different velocities and this will also lead to collisions. This mechanism is called "accelerative or inertial mechanism". Saffman and Turner (1956) derived the following collision kernel by combining the shear mechanism (w_s) and the accelerative mechanism (w_a):

$$\boldsymbol{K_T(u,u') = \left(\frac{8\pi}{3}\right)^{1/2} (r_u + r_{u'})^2 (w_s^2 + w_a^2)^{1/2}}$$

$$= \boldsymbol{\left(\frac{8\pi}{3}\right)^{1/2} (r_u + r_{u'})^2 \left[\frac{1}{5}(r_u + r_{u'})^2 \frac{\epsilon}{\nu} + 3\left(1 - \frac{\rho_f}{\rho_p}\right)^2 (\tau_u - \tau_{u'})^2 \overline{\left(\frac{D\, v_f}{Dt}\right)^2}\right]^{1/2}} \tag{2.11}$$

where, r_u is the radius of particle volume u, ρ_f is the fluid density, ρ_p is the particle density, ε is the turbulent energy dissipation rate, v_f is the root mean square (rms) fluid velocity, and ν is the kinematic viscosity of the fluid. w is the relative particle velocity where, the suffices a and s indicates the accelerative and shear mechanisms. The particle relaxation time (τ_u) for a particle volume u is defined as:

$$\boldsymbol{\tau_u} = \frac{Cc_u(2\rho_p+\rho_f)r_u^2}{9\mu} \tag{2.12}$$

where, μ is the dynamic viscosity of the fluid, and Cc_u is the Cunningham slip correction factor for a particle of volume u. The average acceleration of eddies in the dissipation range $\overline{\left(\frac{D\,v_f}{Dt}\right)^2}$ is defined as (Hinze, 1975):

$$\overline{\left(\frac{D\,v_f}{Dt}\right)^2} = \mathbf{1.16}\boldsymbol{\varepsilon}^{3/2}\boldsymbol{\nu}^{-1/2} \tag{2.13}$$

The first and second terms in the square root term on the right-hand side of Eq. (2.11) represent the shear mechanism and accelerative mechanism, respectively. However, under more vigorous turbulence or with larger particles, the approaching particles may no longer be entrained completely by the smallest eddies, so they will have less correlated velocities. Recently, Kruis and Kusters (1997) analyzed this problem using a turbulence spectrum, which describes both the viscous sub range and the inertial sub range.

2.2.2.3. Electrostatic Coagulation

Charged particles may experience either enhanced or retarded coagulation rates depending on their charges. For a unipolar aerosol, it is necessary to consider electrostatic dispersion (i.e., the tendency of charged particles of the same sign to move away from each other). This dispersion tends to reduce the concentration of an aerosol, for example, by causing particles to deposit on the walls of any containing vessel or nearby surface. In the presence of particle charging, the collision kernel of particles must be corrected by:

$$K_e(u,u') = \frac{K_n(u,u')}{W} \tag{2.14}$$

where, the subscript 'n' designates neutral particles. The Fuchs stability function W is given by (Fuchs, 1964):

$$W = \frac{exp(\kappa)-1}{\kappa};\ \kappa = \frac{z_1 z_2 e^2}{(r_1+r_2)k_B T} \tag{2.15}$$

where, z_1 and z_2 are the numbers of unit charges contained in particles, and e is the electron charge. For $\kappa > 0$ (like charge), $W > 1$ and coagulation is retarded from that for neutral particles. Conversely, for $\kappa < 0$ (unlike charge), $W < 1$ and coagulation is enhanced.

2.3. General Coagulation Equation

Let us consider a system of polydisperse aerosols where a wide range of particle sizes is present. Particles of various sizes collide with each other results in the alteration of particle size distribution as shown in Fig. 2.1. Since the coagulation kernel ($K_{j,k\text{-}j}$) describes the rate at which particles of size *j* coagulate with particles of size (*k-j*), the rate of formation of size *k* is given by, $\boldsymbol{K_{j,k-j} n_j\, n_{k-j}}$. For the formation of particles of size *k*, various combinations of sizes *j* and (*k-j*) are possible, where the value of *k* may vary between 1 and (*k*-1). Then, the rate of formation of particles of size *k* is the summation of all agglomerations resulting in particle size *k* and is given by, $\boldsymbol{\frac{1}{2}\sum_{j=1}^{k-1} K_{j,k-j}\, n_j n_{k-j}}$. The factor 1/2 is introduced because each collision is counted twice in the summation. The rate of loss of particles of size *k* by collision with all other particles is, $\boldsymbol{n_k \sum_{j=1}^{\infty} K_{k,j}\, n_j}$. Hence, the net rate of generation of particles of size *k* is given by,

$$\boldsymbol{\frac{dn_k(t)}{dt} = \frac{1}{2}\sum_{j=1}^{k-1} K_{j,k-j}\, n_j n_{k-j} - n_k \sum_{j=1}^{\infty} K_{k,j}\, n_j, \qquad k \geq 2} \tag{2.16}$$

where, *n* is the number concentration at time *t*, the suffices *j* and *k* indicate the particle sizes, and $K_{k,j}$ is the coagulation kernel between particle sizes *k* and *j*. The resultant equation (Eq.(2.16)) is called as discrete coagulation equation.

Eq.(2.16) cannot be solved analytically in its most general form, solutions can be obtained assuming constant coagulation coefficients. This approximation is applicable to the early stages of coagulation of a monodisperse aerosol system (or rapidly coagulating system).

Although polydispersity is an inherent consequence of coagulation process, one often considers a situation for pedagogical point of view involving the evolution of monodisperse aerosols. Smoluchowski (1916) derived the discrete coagulation equation for an initially monodisperse aerosol system by solving the diffusion equation around a single particle, and by obtaining the flux of other particles toward it. The key assumptions in this problem formulation are that i) particles adhere at every collision (due to binary collisions) and that particle size changes slowly, and ii) initially particles of equal size are present in a unit volume of the medium. Assuming $K_{k,j} = K$, and summing the entire equation (Eq.(2.16)) over the entire range of particle size k, the rate equation for the total number concentration is given by,

$$\frac{dN}{dt} = -\frac{1}{2}KN^2 \tag{2.17}$$

where, $N(t)\left(= \sum_1^\infty n_k\,(t)\right)$ is the total number concentration of the particles, K (= $8\pi d_p D$) is the Brownian coagulation coefficient in the continuum regime for equal sized particles, D is the diffusion coefficient of the particles, and d_p is the particle diameter. By integrating Eq. (2.17), the total number concentration is determined as a function of time as follows:

$$\frac{N}{N_0} = \frac{1}{1+(K_{co}N_0 t/2)} \tag{2.18}$$

where, N_0 is the particle number concentration of size k (k = 1, monodisperse) at time t = 0. The particle size distribution at any time t is then obtained by solving the discrete coagulation equation (Eq.(2.16)),

$$\frac{n_k}{N_0} = (t/\tau)^{k-1}(1 + t/\tau)^{-k-1} \tag{2.19}$$

where, n_k is the number concentration of particle size k at time t, and $\tau = 2/KN_0$ is the characteristic coagulation time. From this expression, it is shown that the original monodisperse system will evolve necessarily into polydisperse system. Seen in this sense, coagulation is a fundamental mechanism that creates polydispersity from initially monodisperse particles, say critical nuclei formed from the vapour phase.

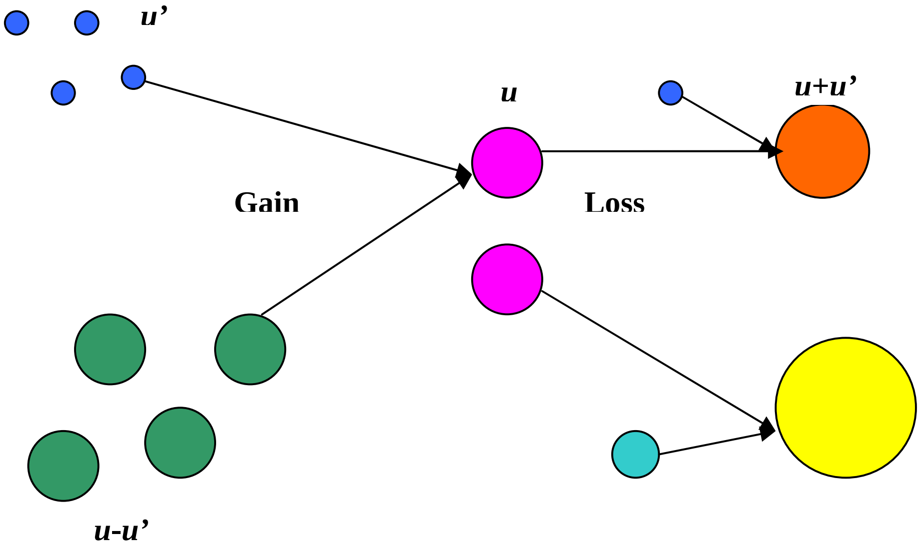

Fig.2.1: Coagulation process - Schematic diagram

The discrete coagulation equation (Eq.(2.16)) can be written in the following continuous form by considering the quantity $n(u, t)$ as the continuous particle size distribution function at time t,

$$\frac{dn(u,t)}{dt} = \frac{1}{2}\int_0^u K(u', u-u')n(u',t)n(u-u',t)\,du' - n(u,t)\int_0^\infty K(u',u)n(u',t)\,du' \quad (2.20)$$

where, $K(u, u')$ is the coagulation kernel for two particles of volume u' and u. In this formulation, $K(u, u')$ contains all the physics of the problem as it is calculated by taking the cluster structure (fractal or compact), the bulk forces (gravitational, hydrodynamic, etc.,) as well as the inter-cluster interactions (Van der waal-Hamaker, electrostatic, etc.,) into account. The first term in the right-hand side of Eq.(2.20) represents the increase in particles with volumes between u and $(u+du)$ from the combination of particles of volume u-u' and u'. The second term in the right-hand side of this equation represents the loss of particles with volumes between *u* and (*u*+*du*) resulting from the coagulation of particles of volume *u* and *u'*. Thus this equation gives an expression for the net rate of change of particles whose volumes lie between *u* and (*u*+*du*). The coagulation process is schematically shown in Fig. 2.1.

Methods of solving a coagulation equation were summarized by Hidy and Brock (1972), and Williams and Loyalka (1991). These methods range from the discrete (computationally intensive) and sectional models in which Eq. (2.20) is transformed into a number of differential equations, to the less accurate monodisperse models described in the previous sub-section. Approximate solutions can be found using the method of moments. Exact solutions for asymptotic limiting cases can be obtained with the self-preserving theory. Stochastic methods like Monte Carlo techniques are also used to solve the coagulation equation.

2.3.1. Sectional Method

Because solving the coagulation equation with a direct numerical method is impractical owing to its time-consuming property, several approximate methods have been developed. The most employed general method and its variants for simulating aerosol dynamics is based on dividing the particle size domain into sections as developed by Gelbard et al (1980). This model solves a one-dimensional form of the aerosol general dynamic equation by dividing the particle size domain into a finite number of sections by particle volume, and by calculating the addition and subtraction of particle mass to each section. The model assumed that particles kept their spherical shape during growth; therefore the volume sections corresponded to sections of particle size. However, substantial progress has been made in developing models that account for irregular particle shape through fractal dimensions. The volume and surface area of irregularly shaped particles are chosen as the two particle size dimensions. Then the two-dimensional aerosol dynamic equations are solved by extending a one-dimensional sectional technique to the two-dimensional space (Xiong and Pratsinis, 1993). A two-dimensional particle size distribution function is defined as $n(u, a, t)$, where, $n(u, a, t)\, du\, da$ is the number density of particles having a volume between u and $u+du$ and a surface area between a and $a+da$ at time t. The rate of change in $n\ (u, a, t)$ due to coagulation can be obtained by extending the classical coagulation theory to the two-dimensional space u, a as:

$$\frac{\partial n(u,a,t)}{\partial t} =$$

$$\frac{1}{2}\int_0^u \theta\left(a > \left(\frac{u'}{u_0}\right)^{2/3} a_0 + \left(\frac{u-u'}{u_0}\right)^{2/3} a_0\right) \int_{\left(\frac{u}{u_0}\right)^{2/3} a_0}^{\frac{u}{u_0} a_0} K_{u',u-u'}(a', a-a')\, n(u',a',t) n(u-u', a-a', t) da' du'$$

$$-n(u,a,t) \int_0^\infty \int_{\left(\frac{u}{u_0}\right)^{2/3} a_0}^{\frac{u}{u_0} a_0} K_{u,u'}(a,a') n(u',a',t) da' du' \qquad (2.21)$$

where, v_0 and a_0 are the volume and surface area, respectively, of the primary particle, which is the smallest possible particle (e.g., a molecule or a monomer). Eq.(2.21) is a two-dimensional partial integro-differential equation that needs to be solved numerically. The sectional method proves to be both computationally efficient and numerically robust, especially in dealing with aerosols having an extremely large size spectrum.

2.3.1.1. Nodal Method

Based on the sectional model approach, a nodal form of the size distribution has been assumed wherein the total volume range for the aerosol is divided into nodes as opposed to discrete sections. This method is termed as nodal method (Prakash et al, 2003), a modification of the sectional method developed by Gelbard et al (1980) and an extension of a coagulation nodal method by Lehtinen and Zachariah (2001). In other words, the bins of finite width in the sectional model have been squeezed to zero width nodes in the nodal method (the finite-sized sections of the sectional model have been reduced to discrete points called 'nodes' on the size domain), with the constraint that particles reside only at the nodes. The nodes are evenly spaced on a logarithmic size scale, and this assumption simplifies the computation by limiting the number of parameters.

Within each node, the integral average of the aerosol property is assumed constant. A collision leads to 'scattering into' a higher size node and 'scattering out' from the initial size node. Coagulation is assumed here to be a binary collision, which introduces transfer of particles from one size node into another. No fragmentation is considered, therefore no "up-scattering" (transfer into smaller nodes) is allowed. Because of the assumption of homogeneous aerosol concentration over the spatial domain, it can be modeled without considering spatial discretization. This nodal method is implemented by using an efficient, stable, and accurate semi-implicit algorithm (Prakash et al, 2003). The advantage of using a semi-implicit equation instead of a fully-implicit method is that it allows immediate (fast), and volume conserving solutions. As described by Prakash et al (2003), it is an efficient numerical model for the solution of nucleation, surface growth, and coagulation problems.

Generally, in an aerosol system the particle sizes range from ~1 nm to about 10 μm. On the volume scale this size range corresponds to ~10^{-27} m^3 to ~10^{-15} m^3. To cover the 12 orders of magnitude for the volume range, the nodes are spaced linearly (with equal spacing) on a logarithmic scale. The particles exist only at these nodes evenly spaced on a logarithmic size scale at all times (Fig. 2.2). Geometry spacing factor (q) is defined as the spacing between the nodes, and it is given by, $q = \frac{u_{i+1}}{u_i}$. Using a geometric spacing factor of less than 2 would increase the accuracy; however, computational requirements increase substantially, with only a small increase in accuracy. With the geometric factor of 2, there are 10 size nodes per order of magnitude in the particle diameter space. In order to cover the above particle size range, 40 size nodes are required. Figure 2.2 illustrates the division of nodes on a logarithmic scale. If the new particle volume falls between two nodes, then it is split into adjacent nodes by a size-splitting operator under the constraint of mass conservation. At every coagulation step, the size-splitting operator redistributes the particles back to nodes. By combining this coagulation numerical module with any other numerical module of the physical processes, the general dynamic equation for the evolution of aerosols can be solved.

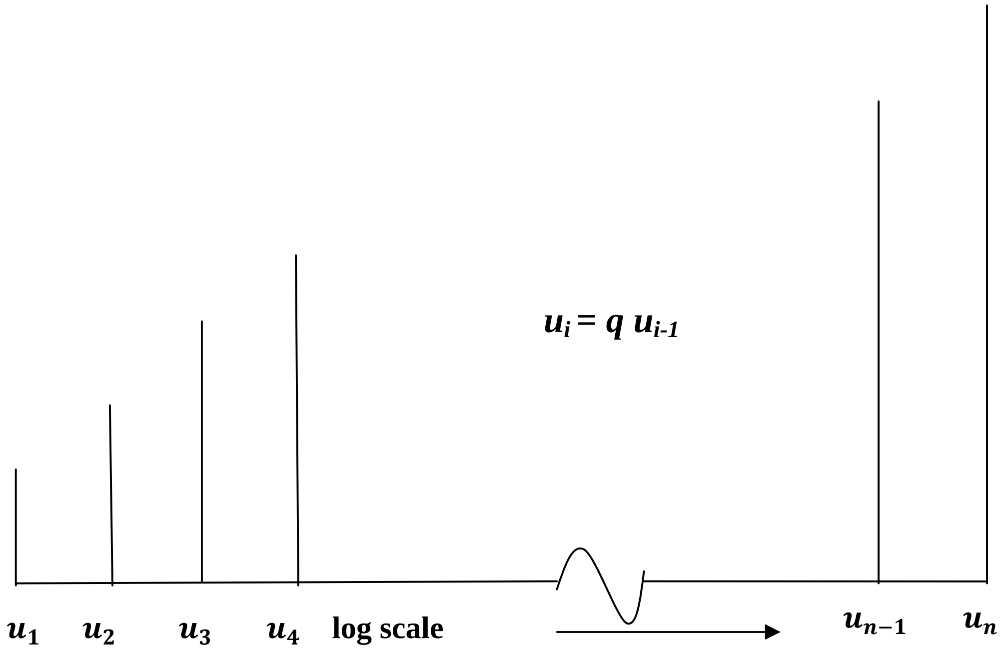

Fig. 2.2: Illustration of node spacing on a logarithmic volume space where q is the geometric spacing factor. The heights of the nodes correspond to the volume of the node (not drawn to scale).

2.3.2. Self-Preserving Theory

One of the interesting features of coagulation known to date is that the shape of the size distribution of suspended particles undergoing coagulation often does not change after a long time and the distribution becomes self-preserving. Friedlander (2000) proposed the theory of self-preserving spectra based on the method of similarity transformations, which in essence seeks scaling solutions to Eq.(2.20) for the case of homogeneous kernels. The idea of scaling assumes that the number concentration, which is a function of two variables, can be expressed as a function of single variable at large times, providing one scales the cluster sizes in terms of a characteristic size such as the mean size of the evolving spectrum. Conventionally, in the self-preserving formulation, the dimensionless particle volume is defined as:

$$\eta = \frac{N(t)u}{\phi(t)} \tag{2.22}$$

and the dimensionless size distribution density function is defined as:

$$\psi(\eta) = \frac{n(u,t)\phi(t)}{N^2(t)} \tag{2.23}$$

Friedlander and Wang (1966) obtained the following equation for the Brownian coagulation in the continuum regime:

$$(1+ab)\eta\frac{\partial\psi(\eta)}{\partial\eta} + \left(2ab - b\eta^{1/3} - a\eta^{-1/3}\right)\psi(\eta) + \int_0^{\eta}\psi(\eta-\bar{\eta})\psi(\bar{\eta})\left\{1+\left(\frac{\eta-\bar{\eta}}{\bar{\eta}}\right)^{1/3}\right\}d\bar{\eta} = 0 \tag{2.24}$$

where, $a = \int_0^{\infty}\eta^{1/3}\,\psi(\eta)d\eta$ and $b = \int_0^{\infty}\eta^{-1/3}\,\psi(\eta)d\eta$.

Friedlander and Wang (1966) derived analytical solutions of Eq. (2.24), shown in Eqs. (2.25) and (2.26), for small η regime and for large η regime, respectively:

$$\psi(\eta) = \frac{0.5086}{\eta^{1.06}}exp\left(1.758\eta^{1/3} - 1.275\eta^{-1/3}\right) \tag{2.25}$$

$$\psi(\eta) = 0.915exp(-0.95\eta) \tag{2.26}$$

Eq.(2.24) can be solved numerically for the entire η range. The results obtained by Friedlander and Wang (1966) are in good agreement with the results of numerical simulations by Vemury et al (1994), who solved the coagulation equation (Eq. 2.16) using the sectional method of Landgrebe and Pratsinis (1990). Lai et al (1972) used the above technique to derive the self-preserving size distribution for the free molecule regime. Wang and Friedlander (1967) applied the same method to the Brownian coagulation either with slip correction or with simultaneous shear flow.

Existence of scaling solution does not necessarily guarantee that a system with arbitrary initial distribution will attain it. In fact, if the initial distribution has power law tails (Mulholland & Baum, 1980), it is found that the asymptotic spectrum will not approach the scaling regime for certain types of kernels. However, for narrower initial distributions, scaling is supposed to be valid. Table 2.1 gives some examples of scaling solutions for various types of kernels.

$\boldsymbol{K(u, u')}$	$\boldsymbol{\bar{u}(t)}$	$\boldsymbol{\psi(\eta)}$	**Remarks**
1	t	$exp(-\eta)$	-
uu'	$(1-u_0t)^{-1}$	$\eta^{-5/2}exp(-\eta)$	$t < t_c = 1/u_0$
$\left(\boldsymbol{u}^{1/3}+\boldsymbol{u}'^{1/3}\right)\left(\boldsymbol{u}^{-1/3}+\boldsymbol{u}'^{-1/3}\right)$	t	$\eta^{-1.06}exp\left(-\eta^{-1/3}\right)$	-

Table 2.1: Examples of scaling solutions for various coagulation kernels

The coagulation equation is well studied (Ernst, 1986) using scaling theory for homogeneous kernels of the following type,

$$K(\lambda u, \lambda u') = \lambda^{\alpha} K(u, u') \tag{2.27}$$

Eq.(2.27) implies that $K(u, u') = (uu')^{\alpha/2} f(u/u')$, where, $f(u/u')$ is an arbitrary function and α is the degree of homogeneity. α is a measure of the coagulation rate of two equal, large clusters. When one of the coagulating clusters is much larger, $K(u, u')$ is assumed to have the form

$$\boldsymbol{K(u, u')} \sim \boldsymbol{u}^{\mu} u'^{\tau}, \tag{2.28}$$

with $\boldsymbol{\mu}+\boldsymbol{\tau}=\boldsymbol{\alpha}$, $u' >> u$. The indices $\boldsymbol{\alpha}, \boldsymbol{\mu}$, and $\boldsymbol{\tau} \equiv \boldsymbol{\alpha}-\boldsymbol{\mu}$ are sufficient to characterize the coagulation equation for homogeneous kernels. Van Dongen and Ernst (1985) provide upper bounds viz., $\boldsymbol{\alpha} \leq \mathbf{2}$ and $\boldsymbol{\tau} \leq \mathbf{1}$, by setting constraint on the maximum cross-section for the coagulation of large-large and large-small clusters, respectively. The index $\boldsymbol{\mu}$ can take up any value. When $\boldsymbol{\mu} > 0$, large-large interactions dominate (Class I systems, Fig.2.3). When $\boldsymbol{\mu} < 0$, large-small interactions dominate (Class III systems, Fig.2.3). When $\boldsymbol{\mu} = \mathbf{0}$, the interations of a large cluster is insensitive to the size of its partner and a marginal-type behavior occurs (Class II systems, Fig.2.3). Some of the commonly used kernels in coagulation theory are presented in Table 2.2.

S. No.	***K*(*u*, *u'*)**	**Remarks**
1	$\left(\boldsymbol{u}^{1/3} + \boldsymbol{u}'^{1/3}\right)\left(\boldsymbol{u}^{-1/3} + \boldsymbol{u}'^{-1/3}\right)$	Smoluchowski kernel for Brownian coagulation (μ = -1/3; α = 0)
2	$\left(\boldsymbol{u}^{1/3} + \boldsymbol{u}'^{1/3}\right)^2\left(\boldsymbol{u}^{-1} + \boldsymbol{u}'^{-1}\right)^{1/2}$	Brownian coagulation in free-molecular regime (μ = -1/2; α = 1/6)
3	$\left\lvert\boldsymbol{u}^{2/3} - \boldsymbol{u}'^{2/3}\right\rvert\left(\boldsymbol{u}^{1/3} + \boldsymbol{u}'^{1/3}\right)^2$	Coagulation by gravitational settling (μ = 0; α = 4/3)
4	$\left(\boldsymbol{u}^{1/3} + \boldsymbol{u}'^{1/3}\right)^3$	Coagulation in shear flow (μ = 0; α = 1)
5	$\boldsymbol{u}\boldsymbol{u}'$	Polymerization (μ = 1; α = 2)

Table 2.2: Some commonly used coagulation kernels

An important property of the coagulation equation is that it shows a discontinuous transition at a finite time for kernels with $\boldsymbol{\alpha} > 1$. This arises because when $\boldsymbol{\alpha} > 1$, interactions between large clusters dominate to such an extent that a single infinite sized cluster gets formed in a finite time. The transition is known as gelation transition and occurs in polymers. This is not relevant for aerosols because of their low density. Aerosol kernels generally belong to Class II and Class III domains. Figure 2.3 shows the different classifications, including the domain of gelation transition, in μ, τ space.

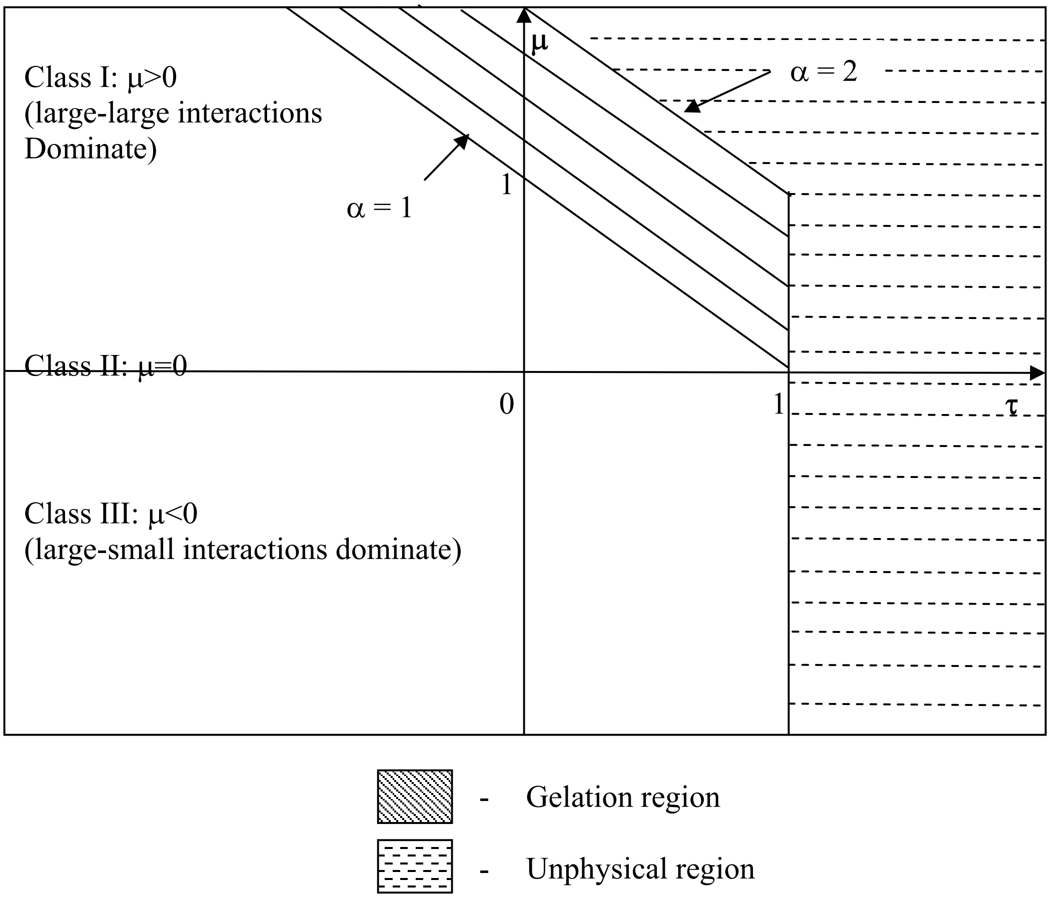

Fig. 2.3: Schematic classification of coagulation kernels (Van Dongen & Ernst, 1985)

The sol-gel transition is commonly observed in colloidal systems but the aerosol-aerogel transition is very rare and the first experimental observations were reported by Lushnikov et al (1990). The dynamics of aerosol gelation with $K(u, u') \sim uu'$ was studied by many researchers in the past (Ernst & Pratsinis, 2006; Ziff, 1980), and exact analytical solutions are available for the sol-gel transition systems (Lushnikov, 2004). Apart from this gelation kernel, shear-induced coagulation in the viscous regime (commonly used in aerosol dynamic simulations) also leads to gelation. Shear-induced coagulation for $\alpha = 1$ is a limiting case for which a more precise analysis is undertaken, and Lushnikov and Kulmala (2002) investigated analytically coagulation rates of the form $K(u, u') \sim u^a u'^b + u^b u'^a$, where, $a+b=\alpha$ and $a>=b$.

2.3.3. Moment Method

Although the self-preserving size distribution theory played a very important role for researchers in understanding the coagulation mechanism, one shortcoming of the theory is its inability to resolve the size distribution for the time period before an aerosol attains the self-preserving size distribution. Therefore, it was still necessary to resort to numerical calculations. However, during coagulation, the size distribution of particles changes by the interaction of particles in so many size classes at each time step that the computing time becomes excessive for the calculation of the change of size distribution of particles. To overcome this problem and to accelerate the computations, much effort has been made. Cohen and Vaughan (1971) succeeded in reducing the coagulation equation to a set of ODEs for the moments of size distribution. By choosing a specific functional form for the distribution of the particle size, they were able to calculate the parameters of the size distribution as a function of the three leading moments. This method, known as the moment method, has the advantage of simplicity while providing important information on the change of the size distribution of aerosol. Therefore, the moment method has been widely applied in the simulation of aerosol coagulation.

2.3.4. Monte Carlo Method

In this method, coagulation process is considered as a stochastic process, and modeled by keeping track of all particles in the system or through a probabilistic simulation. It considers the system as a statistical ensemble where each event has a known probability described by the collision frequency function. The Monte Carlo simulation of coagulation is based on a

Markovian model where the physical and velocity space is omitted and instead the collisions are modeled as transitions in a Markov chain. It is broadly classified into two types,

1. Time-driven Monte Carlo: here the time step (Δt) is chosen before the simulation event, and the simulation technique is used to decide which events will be realized within this time.
2. Event-driven Monte Carlo: the time between the events is calculated based on the known event probability, and then a single event is selected to occur and the time is advanced.

Many algorithms are available to implement this method. Constant Volume Monte Carlo (CVMC) simulation (Shah et al, 1977) and Constant Number Monte Carlo (CNMC) simulation (Zhao et al, 2007) are the two simulation algorithms widely used. The advantage of this method is that it is easy to implement numerically for problems with complex kernels. However, the computation time is one of the limitation to this method.

2.4. Coagulation in dispersing aerosol systems

Aerosol dispersion modelling is concerned with predicting the concentration distributions of source particles introduced into the atmosphere and its subsequent dispersion downwind. Most generally, atmospheric aerosol particle evolution models combine dilution effects due to advection and diffusion mechanisms with physical transformation processes such as nucleation, coagulation, vapour condensation/evaporation, and plate out/wash out mechanisms (Jacobson & Seinfeld, 2004; Aloyan, 2009; Albriet et al., 2010). Many of these models use two separate modules, one for atmospheric transport (ex. Gaussian plume model) and another for aerosol dynamic processes, and these models are solved together, in step-wise manner, by numerical methods. In the present study, we consider the two most significant mechanisms governing the near-source aerosol behaviour, viz. coagulation and dispersion.

The general evolution equation for a coagulation-dispersion system is then given by,

$$\frac{\partial n(u,r,t)}{\partial t} = \left.\frac{\partial n(u,r,t)}{\partial t}\right|_{dispersion} + \left.\frac{\partial n(u,r,t)}{\partial t}\right|_{coagulation} - \left.\frac{\partial n(u,r,t)}{\partial t}\right|_{removal} + S(u,r,t) \qquad (2.29)$$

where, $n(u,r,t)\,du$ be the number of particles with volumes lying between u and $u+du$ per unit volume of the fluid at position r and time t. The first term on the RHS represents the dispersion process that includes advection and diffusion. Two basic approaches are in use to describe dispersion in a turbulent fluid: Eulerian and Lagrangian. The Eulerian approach refers to dispersion in which the behaviour of species is described relative to a fixed coordinate system. When the motion of the fluid is turbulent, there is usually a significant augmentation of mass transfer from regions of high to low mass fraction of a particular component. The influence of this mechanism is usually referred as turbulent dispersion, and is entirely dominant over molecular diffusion in the atmospheric boundary layer. Dispersion of pollutants in the atmosphere is a random process, it is impossible to predict the instantaneous concentration due to highly irregular three-dimensional turbulent motions of the atmosphere. Ensemble averaging the instantaneous diffusion equation makes it possible to find solutions to turbulent diffusion problem. Eq.(2.30) is the basic diffusion equation for non-reactive contaminants, ignoring molecular diffusion:

$$\frac{\partial \bar{n}(u,r,t)}{\partial t} + \bar{v}\nabla\left[\bar{n}(u,r,t)\right] = -\nabla\left[\overline{v'n'}(u,r,t)\right] \qquad (2.30)$$

where, $\bar{n}(u,r,t)$ is the ensemble-averaged number concentration, $\bar{v}$ is the average wind velocity, and variables with primes represent their turbulent parts. The correlation $\overline{v'n'}(u,r,t)$ is ensemble-averaged turbulent advection term, and is called turbulent mass flux, caused by wind fluctuations, analogous to the molecular mass flux. These turbulent components dominate the diffusion of the pollutant particles in the atmosphere.

The diffusion equation of Eq.(2.30) for mean concentration is not closed. To solve Eq.(2.30) to get mean concentration, $\overline{n}(u,r,t)$, an equation for the turbulent diffusion term needs to be added. The simplest and probably the most widely used closure approach in turbulent diffusion is first-order closure, based on the gradient transport hypothesis. According to this hypothesis, turbulent mass fluxes are proportional to the gradient of the mean concentration. This is true for most situations in the surface layer, with several exceptions, such as in convective conditions (Arya, 1999). Thus, $\overline{v'n'} = -K\,\nabla\overline{n}(u,r,t)$,where, K is turbulent diffusivity. Turbulent diffusivities have to be specified for the complete closure and solutions of Eq.(2.30) can be obtained for any desired initial, boundary, and source conditions.

In stationary and homogeneous turbulent atmospheric flow, eddy diffusivities are not expected to be dependent on time and space. In Cartesian co-ordinate system, for the specified constants, K_x, K_y, and K_z, and for an instantaneous point release, the solution of Eq.(2.30) is expressed as

$$n(u,x,y,z,,t) = \frac{n_0}{(2\pi)^{3/2}\sigma_x\sigma_y\sigma_z}\exp\left(-\frac{x^2}{2\sigma_x^2}-\frac{y^2}{2\sigma_y^2}-\frac{z^2}{2\sigma_z^2}\right) \qquad (2.31)$$

where $\sigma_x^2 = 2K_x t$, $\sigma_y^2 = 2K_y t$, and $\sigma_z^2 = 2K_z t$ are called dispersion coefficients in the x, y, z directions, and are functions of dispersion time. Eq.(2.31) shows that the concentration distributions in the x , y , z directions are Gaussian in shape.

The second and third term on the RHS of Eq.(2.29) represents coagulation and removal processes respectively. The last term, $S\,(u,r,t)$, is the source term defined as the mean number of particles injected per unit volume of space per unit time per unit particle volumes around u, and the following basic parameters affect the source release scenario,

i) source type (instantaneous or plume release),

ii) spatial distribution of the source particles (homogeneous or heterogeneous), and

iii) particle size distribution (either monodisperse or polydisperse).

The variations in the above parameters lead to different release scenarios and models. Given the above considerations, the focus of this work is to provide simple, albeit approximate, approaches for estimating the fraction of particles formed at the source that eventually survive coagulation to persist in the atmosphere as background aerosols. For homogeneous and instantaneous, burst release conditions, the dispersion process is modeled using volume expansion model. In the case of inhomogeneous puff and plume releases at ambient conditions, diffusion model is used to obtain analytical and numerical solutions. For the case of continuous and homogeneous releases, approximate and asymptotic analytical solutions are obtained using a simplified two-group model; accurate solutions are obtained using numerical models.

Chapter 3. Survival fraction for instantaneous releases

3.1. Introduction

Among the dispersion processes, instantaneous releases occupy a fundamental position. When the dispersion and transformations are linear, one can develop solutions by the method of Green's functions. However, when nonlinear processes are present, each release scenario needs to be addressed separately. The instantaneous releases can be further classified as,

i) Burst releases with initial rapid expansion, and

ii) Puff releases with gradual diffusion.

In this chapter, analytical and numerical techniques to obtain survival fraction formulae for these instantaneous release conditions are presented.

3.2. Survival fraction for burst releases

In recent times, the possibility of deployment of radiological dispersal devices (RDDs) by malevolent groups or the accidental release of radionuclides has raised considerable concerns among the public. A radiological dispersal device is a device that spreads radioactive material in the environment with malicious intent. It is the combination of a conventional explosive device (for example, TNT) with radioactive materials that can be obtained from industrial, commercial, medical and research applications. Aerosol particles (both radioactive and non-radioactive) are generated from the detonation of these radiological dispersal devices. In order to predict certain important parameters at the receptor location (such as surface contamination, time-integrated air concentrations, and dose rates) due to these releases, it is necessary to model the transformation of particle size distributions during their dispersion in the atmosphere. International Atomic Energy Agency (IAEA) launched a programme called EMRAS (Environmental Modelling for

Radiation Safety) to focus on the predictive capability of environmental models used in assessment of radioactive contamination in urban settings, including dispersion and deposition events, short- and long-term contaminant redistribution following deposition events, and potential countermeasures or remediation efforts for reducing human exposures and doses. Although, gross calculation suggests that actual doses to the public are negligible, the psychological effects are considerable. Many experimental studies were also attempted out in the past in a closed aerosolization chamber, and outdoor simulation test to investigate the aerosol particle formation and their atmospheric transport from the RDDs (Harper et al, 2007; Lee et al, 2010). Study of estimating the health hazards resulting from RDDs has been carried out by Andersson et al (2008). A brief description of aerosol particles formation and its evolution due to a RDD is given below.

A RDD essentially contains conventional explosive, radioactive, and structural materials. The detonation of the explosive material will result in a rapid increase in volume and release of energy usually at high temperature and pressure. A detonation wave is caused by rapid compression of the substance in a shock wave, which rapidly compresses and heats the substance so the reaction can proceed at a high rate. Detonation involves a supersonic exothermic front (shock wave) accelerating through a medium that eventually drives a shock front propagating directly in front of it. Following the detonation wave-front, the products of detonation (C, CH_4, N_2, CO_2, CO, etc., obtained due to the chemical reactions) form a cloud and expand isotropically. The gaseous products formed during the explosion undergo chemical reaction at high temperature, which leads to overall change in the chemical composition within the cloud. The condensable gaseous products in the cloud nucleate to form primary multi-component aerosol particles due to the reduction in the cloud temperature. This cloud containing aerosols expands at a rate determined by the equation of state of the detonation products. Aerosols released in such high concentrations into the atmosphere from low yield conventional explosives undergo simultaneous coagulation and volume expansion before influenced by the other atmospheric transport processes such as advection and turbulent diffusion. In the present study, a simplified approach (uniformly mixed volume expansion model) is used to simulate the combined effect of these two processes on the evolution of aerosol number concentration and size distribution in the puff.

3.2.1. Uniform expansion model

Uniform expansion model was introduced by Nathans et al (1970) to estimate the particle size distribution in clouds from nuclear airbursts. This model treats the dispersion process through dilution model, which assumes a uniformly mixed volume element expanding under a prescribed rate in time. It has been used in the context of estimating the properties of particulates emitted by high-altitude aircrafts, volcanoes (Turco & Yu, 1997), and large-scale forest fires (Radke et al, 1995; Fiebig et al, 2003). Turco and Yu (1997) demonstrated that the total number of particles in an evolving aerosol plume or cloud is limited in a predictable way by the competing rates of coagulation and atmospheric dispersion, and is generally independent of the details of particle nucleation or growth. These studies show that the particle characteristics are independent of the initial total number, and depend on the average coagulation kernel and plume dispersion rate. Using this simplified phenomenological model, the temporal evolution of the total number of aerosols generated by localized sources can be calculated, as well as their size distribution and local concentrations.

3.2.2. Formulation of problem

Let us consider an instantaneous burst release of aerosol particles from an aerial detonation of conventional explosive like TNT. The aerosol particles are assumed to be homogeneously distributed in the puff volume. Further, it is assumed that the removal rates are negligible in the near-time and -space domain of this system. Inserting in Eq.(2.29) a term that represents dispersion as entrainment and mixing of ambient air into a puff, and assuming uniform mixing of the aerosols within the local puff volume, the aerosol continuity equation (2.29) can be written

$$\frac{\partial n(u,t)}{\partial t}=\frac{1}{2}\int_0^u K(u',u-u')\,n(u',t)\,n(u-u',t)\,du'-n(u,t)\int_0^\infty K(u,u')\,n(u',t)\,du'-n(u,t)\frac{d\log V(t)}{dt} \tag{3.1}$$

where, $n(u, t)$ is the number of particles of volumes lying between u and $u+du$ at time t, $V(t)$ is the volume of the system at time t. The simplifying feature of the volume expansion model is that, it altogether replaces the space dependent nature of the dispersion process by a purely time dependent term. The first and second term on RHS represents the growth and loss terms due to coagulation process. The third term on RHS represents the dispersion process governed by the dilution term ($d\log V(t)/dt$). In the case of constant and homogeneous coagulation kernels, Eq.(3.1) is exactly solvable, and the solutions for the total number concentration are given by Nathans et al (1970) and Turco and Yu (1997, 1998). However, Eq.(3.1) is not analytically solvable if a complex coagulation kernel like Fuchs kernel is used in the model. This kernel is used in the present study to account for the transition regime effects, and hence numerical techniques (nodal method described in Section 2.3.1.1) are employed to solve the aerosol dynamics model.

For the case of constant kernel, Eq.(3.1) is easily solvable and the total number concentration at time *t* is given by (Nathans et al, 1970),

$$N(t) = \frac{\exp[-g(t)]}{[(1/N_0) + h(t)]} \tag{3.2}$$

where, $N(t) = \int_0^\infty n(u,t)du$, $g(t) = \int_0^t p(x)dx$, $h(t) = \frac{1}{2}\frac{8kT}{3\mu}\int_0^t \exp[-g(x)]dx$, $p(t) = \frac{d\log V(t)}{dt}$, and N_0 is the initial total number concentration.

3.2.3. Results and Discussion

The present study refers to an airburst scenario, i.e., assuming that the TNT explosion takes place at a height well above the ground so that the influence of the ground dust particles is negligible. When the explosive is detonated, the initial volume of the cloud is just equal to the volume of the explosive material. The temporal variation of the temperature and volume due to the adiabatic expansion of the cloud are obtained using the numerical model for the equation of state variables (Sreekanth, 2011; See Appendix – A for details). The numerical solutions are obtained until the cloud temperature and pressure reaches the ambient values. Figure 3.1 shows that the temperature of the cloud reaches to the ambient temperature (300 K) in 243 μsec. At this point of time, the cloud expands to a volume of 1.39 m^3; assuming spherical geometry, the corresponding diameter of the cloud is estimated as, 1.385 m. During this period, the cloud pressure rapidly reduces from 1.5 x 10^5 atm to 1 atm. Expressions are obtained for the temporal evolution of volume and temperature by fitting the numerical values using the polynomial curve fitting routine of Mathematica (Wolfram Research Inc., 2005). The expression obtained for the temperature evolution is one of the inputs required to calculate the Fuchs coagulation kernel. The other one for volume is an important input to the volume expansion model to estimate the dilution rate.

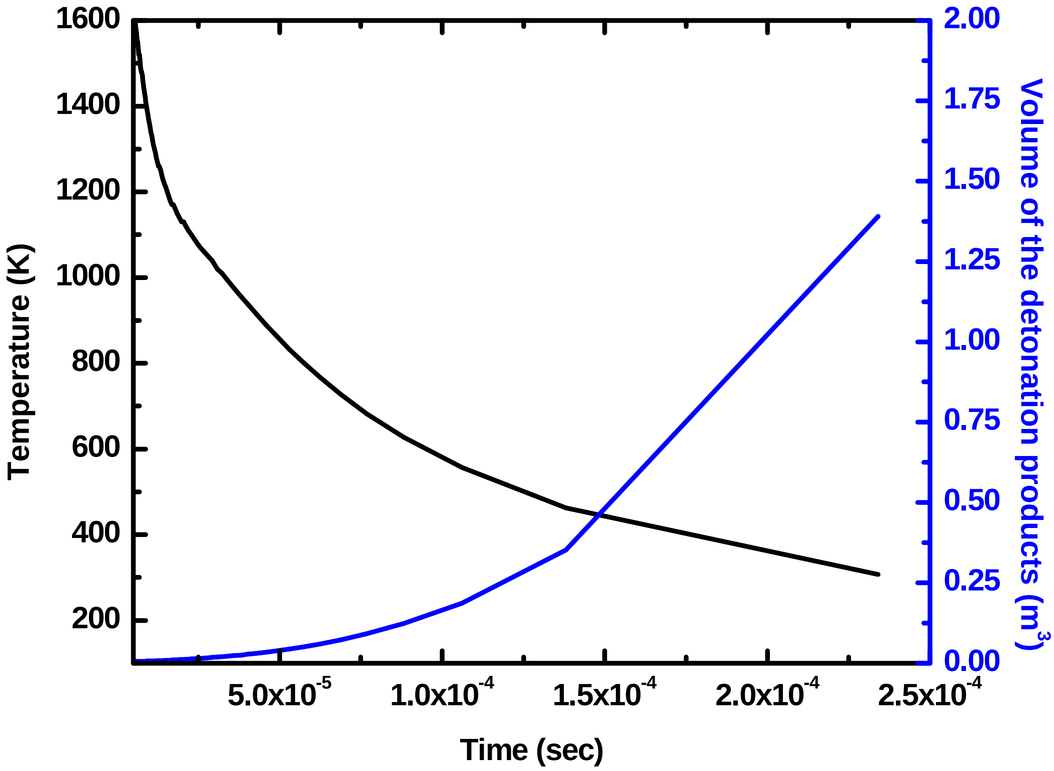

Fig. 3.1: Temperature and volume of the cloud during adiabatic expansion (Explosive mass considered in this case is 2000 g of T.N.T with a loading density of 1.5 g/cm^3)

The temporal evolution of the total particle number concentration and average particle diameter in the puff due to adiabatic expansion are shown in Fig. 3.2. The aerosol particles are initially formed by homogeneous nucleation of the condensable gaseous species of the device material in a very short span of time (Nathans et al, 1970). Thus, the initial total number concentration in the puff is estimated to be 1.66 x 10^{26} particles/m^3 from the condensable mass fraction, assuming an average initial particle diameter of 1 nm. At the end of the simulation period (t = 243 μsec), the particle number concentration and the average particle diameter of the aerosol cloud reaches to ~2.9 x 10^{16} particles/m^3 and ~239 nm respectively. The final particle size distribution of the aerosol cloud at t = 243 μsec is shown in figure 3.3. It shows that an initially monodisperse system evolves to a peaked polydisperse size distribution with a peak value at ~200 nm. All these particle characteristics together will serve as very important inputs for the atmospheric aerosol transport models, which estimate the atmospheric particle concentration and its ground deposition.

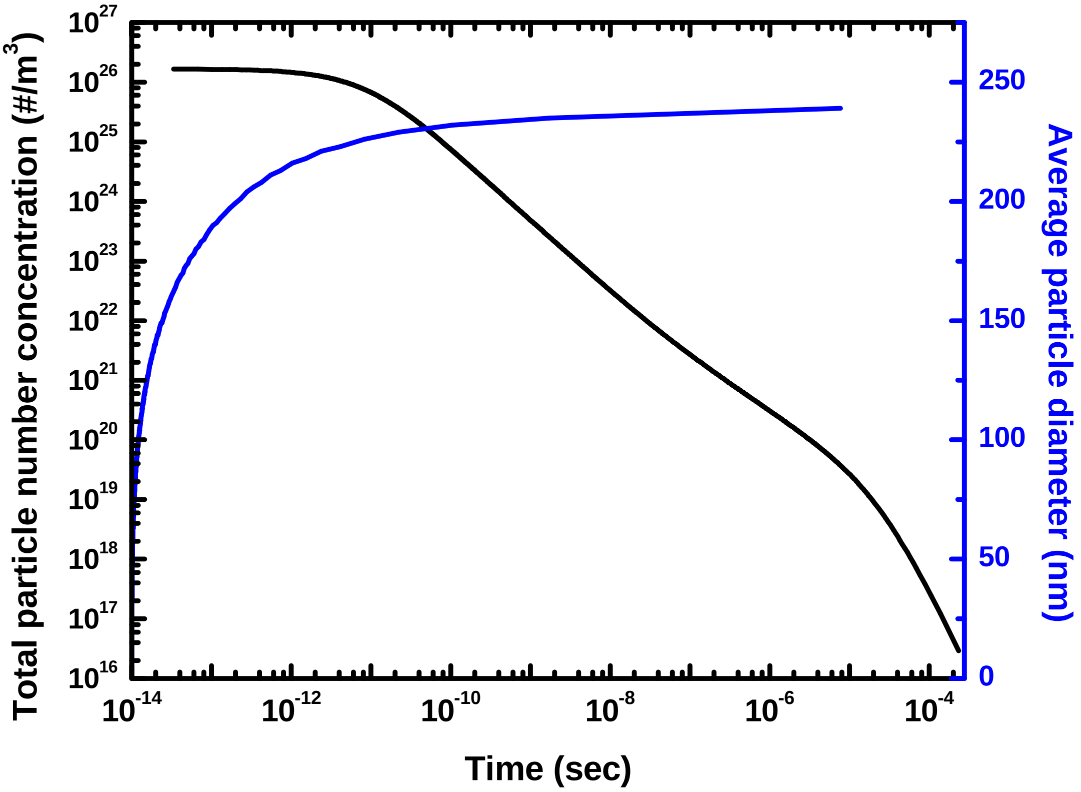

Fig. 3.2: Temporal evolution of total number concentration and average particle diameter in a burst release

The results from the volume expansion model show that when the aerosol particles in a cloud is subject to dilution by mixing with ambient air, the particle concentration decreases more rapidly and coagulation is quenched. Hence, dispersion or dilution acts to increase the total number of particles that survive coagulation after a finite interval of time, and the interplay between coagulation and dispersion determines the fraction of the particles initially present that is likely to survive after a fixed time.

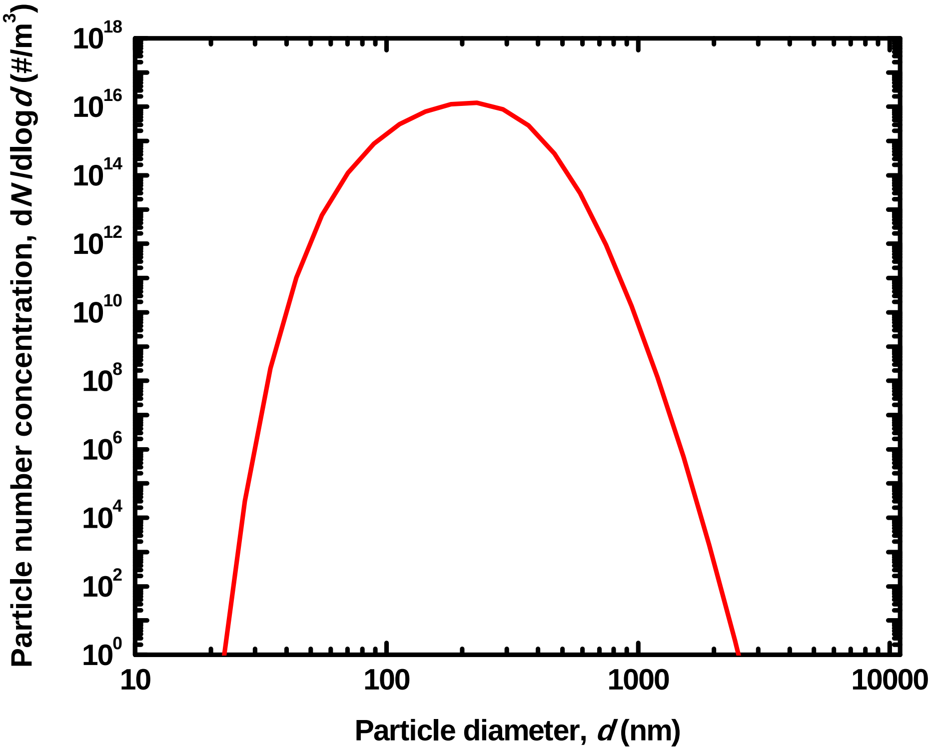

Fig. 3.3: Final aerosol particle size distribution in the cloud at t = 243 μsec

3.3. Survival fraction for puff releases

While uniformly mixed-volume expansion models or what may loosely be termed as dilution models (Radke et al, 1995; Turco & Yu, 1997; Fiebig et al, 2003) capture the combined effect of coagulation and dilution on lowering the number concentration to some extent, they cannot be related to basic atmospheric diffusion processes. In contrast to this, the prescribed diffusion approximation model used diffusion equation instead of volume expansion and approximate analytical solutions are obtained involving atmospheric and aerosol parameters, for the case of single puff release. This model explicitly postulates diffusion as the mechanistic basis of dispersion and allows for spatial gradients. Since it is difficult to solve this equation exactly even for constant coagulation kernels, approximations are developed at the level of solutions. This not only helps one to obtain practically useful analytical formulae, but also provides a systematic basis for assessing the equivalence or otherwise of the uniformly mixed-expansion model and diffusion-coagulation model.

3.3.1. Diffusion approximation model

Jaffe (1913, 1940) originally introduced the diffusion approximation to the solution in the theory of ion-recombination for obtaining simple formulae for the survival fraction of ions in alpha particle columns. It has been effectively used in the context of particle charging using alpha radiation sources (Mayya & Hollander, 1995). Its application to coagulation-diffusion appears natural considering the fundamental similarity (binary nature) between recombination and coagulation processes. In fact, Peliti showed that a mass conserving process such as the coagulation-diffusion process described by the reaction $A + A \rightarrow A$ belongs to the same universality class as the annihilation process (i.e. recombination-diffusion) described by $A + A \rightarrow \text{Ø}$ (Peliti, 1986). The underlying symmetry between the two processes has been further discussed by Lin (Lin, 1991). It must be noted that unlike two-species recombination processes, the coagulation process involves size spectrum which leads to an infinite number of coupled equations for the infinite number of interacting species. The extension of Jaffe technique to this situation involves applying the prescribed spatial diffusion approximation to each of these species.

3.3.1.1. Formulation of problem

Let us consider the case of an instantaneous release of spherical puff from a point source in a relatively calm atmosphere. The initial distribution of particles will be spatially inhomogeneous both in respect of total number concentration and size spectrum. It is assumed that there is no advection in the atmosphere. This is not a serious constraint in the present treatment since it is possible to transform the equation into pure diffusive equations through a Lagrangian framework, i.e. in a coordinate system moving along the mean advection velocity. It is assumed that the release event is quite rapid and particles are formed during the early phase of the dispersion of the puff. From this instant, the puff begins to diffuse in space and simultaneously, the particles begin to coagulate. The interplay between coagulation and diffusion determines the fraction of the initial number of particles surviving after a long time.

Let $n(u,r,t)\,du$ be the number of particles with volumes lying between u and $u+du$ per unit volume of the fluid at position r and time t. Then the general equation governing the evolution of n in the presence of coagulation, diffusion and removal is given by,

$$\begin{aligned}\frac{\partial n(u,r,t)}{\partial t} &= \nabla.\{D(r,t)\,\nabla n(u,r,t)\} + \frac{1}{2}\int_0^u K(u',u-u')\,n(u',r,t)\,n(u-u',r,t)\,du' \\ &\quad - n(u,r,t)\int_0^\infty K(u,u')\,n(u',r,t)\,du' - \lambda(u)n(u,r,t)\end{aligned} \tag{3.3}$$

where, $D(r,t)$ is the space dependent diffusion coefficient, $K(u,u')$ is the coagulation kernel between the particles of volume u and u' and $\lambda(u)$ is the removal rate of particles. In a turbulent atmosphere, the diffusion coefficients for the particles released from the point sources are generally expressed as either space dependent functions or as time dependent variables. Early work of Richardson (Richardson, 1926) suggested the now well known $r^{4/3}$ formula. On the other hand, studies of Batchelor (Batchelor, 1952) have suggested t^2 dependence. Recent numerical studies (Ott & Mann, 2000) seem to point at the superiority of space dependent formula over the time dependent approach. However, the present problem is treated under the framework of constant diffusion coefficient.

There are several expressions for the coagulation kernel depending upon the particle size range and the processes leading to the coagulation of particles. Some of the well discussed problems in the literature generally considered the case of homogeneous kernels satisfying scaling relationships of the form, $K(\sigma u, \sigma u') = \sigma^{\alpha} K(u,u')$, where σ is a scaling parameter, α is an exponent which is a measure of the degree of homogeneity of the kernel. For Brownian coagulation, $\alpha = 0$ and for free molecular kernel, $\alpha = 1/6$. However in the context of atmospheric coagulation, it has been noted that the constant kernel defined by averaging over the size distribution adequately represents the coagulation process. As noted by Turco and Yu (1997) for all practical purposes constant kernel reproduces the evolution of the size spectra quite accurately. A detailed analysis is performed for constant coagulation kernel in the first part of this section and then extended for free molecular kernel in the latter part. Additionally it is to be noted that the initial phase of the puff evolution occurs within timescales of a few tens of minutes and hence the removal process from the atmosphere is neglected, which occurs in time scales of several hours. Hence aerosol removal rate, $\lambda(u)$, is set to zero.

3.3.1.2. Method of solution

Analytical solution for constant kernel

From the above assumptions, the simplified diffusion-coagulation equation is,

$$\frac{\partial n(u,r,t)}{\partial t} = D\nabla^2 n(u,r,t) + \frac{K}{2}\int_0^u n(u',r,t)\, n(u-u',r,t)\, du' - K\, n(u,r,t)\int_0^\infty n(u',r,t)\, du' \qquad (3.4)$$

where D, K are size and space independent. Let us define the Laplace transform with respect to the particle volume variable u as,

$$\tilde{n}(p,r,t) = \int_0^\infty \exp[-pu]n(u,r,t)du\,, \qquad (3.5)$$

where, p is the conjugate parameter with respect to u.

Upon taking the Laplace transform of Eq.(3.4) on both the sides and using convolution theorem, it reduces to a differential equation,

$$\frac{\partial\tilde{n}(p,r,t)}{\partial t} = D\,\nabla^2\tilde{n}(p,r,t) + \frac{K}{2}\left[\tilde{n}(p,r,t)\right]^2 - K\tilde{n}(p,r,t)N(r,t) \qquad (3.6)$$

where, $N(r, t)$ is the total number concentration at a spatial point r, defined as

$$N(r,t) = \int_0^\infty n(u,r,t)du = \tilde{n}(0,r,t) \qquad (3.7)$$

Upon setting $p=0$ in Eq.(3.6), and noting Eq.(3.7), the following equation for $N(r, t)$ is obtained:

$$\frac{\partial N(r,t)}{\partial t} = D\,\nabla^2 N(r,t) - \frac{K}{2}\left[N(r,t)\right]^2 \qquad (3.8)$$

Eqs.(3.6), (3.8) together with initial and boundary conditions (see below) are completely equivalent to the original integro-differential coagulation equation for constant K. It may be noted that the integral term of the coagulation equation is now removed and Eq.(3.6) is essentially a non-linear partial differential equation with respect to time t with the "volume-conjugate variable (p)" appearing as essentially a parameter. Further, the equation for the total number concentration $N(r,t)$ has the same mathematical form as the diffusion-recombination equation (Mayya & Kotrappa, 1982, Mayya & Hollander, 1995) for ions. This analogy is not just limited to $N(r,t)$ but is also valid for the detailed spectral function $\tilde{n}(p,r,t)$. To see this, Eq.(3.6) is transformed by defining a new auxiliary function

$$Z(p,r,t) = N(r,t) - \tilde{n}(p,r,t) \tag{3.9}$$

Upon replacing $\tilde{n}(p,r,t)$ with $Z(p,r,t)$ in Eq.(3.6) and simplifying using Eq.(3.8), one obtains,

$$\frac{\partial Z(p,r,t)}{\partial t} = D\,\nabla^2 Z(p,r,t) - \frac{K}{2}\left[Z(p,r,t)\right]^2 \tag{3.10}$$

A physical interpretation of the auxiliary function $Z(p,r,t)$ is as follows. Since the Laplace transformed concentration $\tilde{n}(p,r,t)$ is a measure of the cumulative number concentration present below a volume of the order *1/p*, and *N*(*r,t*) is the cumulative number concentration over all sizes, $Z(p,r,t)$ is the cumulative number concentration above a size ~(1/*p*).

Eq.(3.10) combines both Eq.(3.6) and (3.8) and satisfies the condition,

$$Z(0,r,t) = 0\,. \tag{3.11}$$

Also, upon using Eq.(3.5) and Eq.(3.9), the volume concentration may be defined as

$$\phi(r,t) = \int_0^\infty u n(u,r,t) du = -\partial \tilde{n}(p,r,t)/\partial p\big|_{p=0} = \partial Z(p,r,t)/\partial p\big|_{p=0}\,. \tag{3.12}$$

Upon differentiating Eq.(3.10) with respect to *p* and plugging Eq.(3.11), the required volume conservation result is obtained. In sum, Eq.(3.10) is an elegant and compact representation of diffusion-coagulation equation for constant kernel.

The prescribed diffusion approximation of Jaffe (Jaffe, 1913, 1940) is now applied to Eq.(3.10) for obtaining analytical solutions. As the name suggests, the approximation implicitly assumes that spatial distribution function is essentially given by pure diffusion laws, and the coagulation (or recombination in the case of ions) alters essentially the spectral function and the total number concentration. Further, for mathematical tractability, let us assume a spherically symmetric Gaussian puff having a spatially homogeneous size spectrum. i.e.,

$$n(u,r,0) = \frac{N_a}{\pi^{3/2} b_0^3} \exp\left[-r^2/b_0^2\right] \frac{1}{u_0} \exp[-u/u_0], \tag{3.13}$$

where, N_a is the total number of particles contained in the puff, b_0 is the width of the puff and u_0 is the mean size of the particles at t=0. The choice of the exponential volume spectrum stems from the fact that it forms the universal scaling solution (self-preserving spectra) for the case of constant kernel (Friedlander & Wang, 1966). The size integrated number concentration function at t=0 is given by

$$N(r,0) = \frac{N_a}{\pi^{3/2} b_0^3} \exp\left[-r^2/b_0^2\right] \tag{3.14}$$

Upon taking the Laplace transform of Eq.(3.13) above with respect to u,

$$\tilde{n}(p,r,0) = \frac{N_a}{\pi^{3/2} b_0^3} \exp\left[-r^2/b_0^2\right] \left(\frac{1}{1+pu_0} \right) \tag{3.15}$$

Upon combining Eqs.(3.9), (3.14), (3.15), the following initial condition for $Z(p,r,t)$ at t=0 is obtained:

$$Z(p,r,0) = \frac{N_a}{\pi^{3/2} b_0^3} \exp\left[-r^2/b_0^2\right] \left(\frac{pu_0}{1+pu_0} \right) \tag{3.16}$$

If coagulation is absent, Eq.(3.10) is purely diffusive and its solution ($Z^{diffusive}(p,r,t)$) for the initial condition in Eq.(3.16) would have remained a spherically symmetric Gaussian at all times, with variance increasing linearly with time. Upon denoting the purely diffusive solution by $\tilde{g}(p,r,t)$ (i.e. Laplace transform of the space-size distribution, $g(u, r, t)$), we have

$$Z^{diffusive}(p,r,t) \equiv \tilde{g}(p,r,t) = \frac{N_a}{\pi^{3/2} b^3(t)} \exp\left[-r^2/b^2(t)\right] \left(\frac{pu_0}{1+pu_0} \right) \tag{3.17}$$

where, $b^2(t) = b_0^2 + 4Dt$.

In the presence of coagulation, the mathematical statement of the Jaffe (prescribed diffusion) approximation is,

$$Z(p,r,t) \approx \tilde{g}(p,r,t) f(p,t)\,, \tag{3.18}$$

where, $f(p,t)$ is the spectrum modifier function due to coagulation. The key assumption is that this function depends only on time and not on space variable. Upon setting t=0 in Eq.(3.18) and comparing Eqs.(3.16), (3.17) the initial condition is obtained as,

$$f(p,0) = 1 \tag{3.19}$$

Upon substituting Eq.(3.18) in Eq.(3.10), the Eq.(3.10) becomes,

$$\tilde{g}(p,r,t)\frac{\partial f(p,t)}{\partial t} + f(p,t)\frac{\partial \tilde{g}(p,r,t)}{\partial t} = f(p,t) D\,\nabla^2 \tilde{g}(p,r,t) - \frac{K}{2}\tilde{g}^2(p,r,t) f^2(p,t) \tag{3.20}$$

One can note that the second term on the LHS of Eq.(3.20) exactly cancels with the first term on the RHS since $\tilde{g}(p,r,t)$ satisfies the diffusion equation. The remaining part constitutes strictly speaking, an inexact equation. However, for the purpose of evaluating the spectrum modifier function, $f(p,t)$, it can be interpreted as an equation in a space averaged sense as was originally demonstrated by Jaffe. Hence, both sides of Eq.(3.20) are multiplied by $4\,\pi r^2\,dr$ and integrate it over all r. Let us note the following identities:

$$\begin{aligned} \int_0^\infty 4\pi\, r^2\, \tilde{g}(p,r,t)\, dr &= \left(\frac{N_a p u_0}{1+pu_0}\right), \\ \int_0^\infty 4\pi\, r^2\, \tilde{g}^2(p,r,t)\, dr &= \frac{1}{(2\pi)^{3/2} b^3(t)}\left(\frac{N_a p u_0}{1+pu_0}\right)^2 \end{aligned} \tag{3.21}$$

This yields the following nonlinear, ordinary, differential equation for $f(p,t)$:

$$\frac{\partial f(p,t)}{\partial t} = -\frac{1}{2}\left(\frac{K N_a}{(2\pi)^{3/2} b^3(t)}\right)\left(\frac{p u_0}{1+pu_0}\right) f^2(p,t) \tag{3.22}$$

Upon substituting the expression for *b*(*t*) from Eq.(3.17), Eq.(3.22) may be easily integrated to yield,

$$f(p,t) = \frac{1}{\left[1 + A\left(\frac{pu_0}{1+pu_0}\right)\mu(t)\right]} \tag{3.23}$$

where,

$$A = \left(\frac{KN_a}{4(2\pi)^{3/2} b_0 D}\right) \tag{3.24}$$

and

$$\mu(t) = \frac{1}{2}\int_0^{4Dt/b_0^2} \frac{dx}{(1+x)^{3/2}} = \left[1 - \frac{1}{\sqrt{1+4Dt/b_0^2}}\right] \tag{3.25}$$

It may be noted that the quantity *A* captures all the basic parameters of the problem in a single expression.

Upon combining $f(p,t)$ with Eq.(3.18) one can obtain the approximate solution for *Z*(*p,r,t*):

$$Z(p,r,t) \approx \tilde{g}(p,r,t)f(p,t) = \frac{N_a}{\pi^{3/2} b^3(t)}\exp\left[-r^2/b^2(t)\right]\left[\frac{pu_0}{1+pu_0(1+A\mu(t))}\right] \tag{3.26}$$

From the definition of Laplace transform, note that

$$\lim p \to \infty \quad \tilde{n}(p,r,t) = 0 \tag{3.27}$$

Upon applying this limit to Eq.(3.26) and noting Eq.(3.9), one obtains the expression for the size integrated number concentration *N*(*r*, *t*) as

$$N(r,t) = \lim p \to \infty \quad Z(p,r,t) = \frac{N_a}{\pi^{3/2} b^3(t)}\exp\left[-r^2/b^2(t)\right]\left(\frac{1}{1+A\mu(t)}\right) \tag{3.28}$$

It may be noted that one would obtain the same solution as Eq.(3.28) independently by solving Eq.(3.8) directly for $N(r,t)$ with Jaffe approximation. This reassures us the internal consistency between the two approaches.

Upon combining Eqs. (3.26), (3.28), and (3.9), the required solution is obtained as

$$\tilde{n}(p,r,t) = \frac{N_a}{\pi^{3/2} b^3(t)} \exp\left[-r^2/b^2(t)\right]\left(\frac{1}{1+A\mu(t)}\right)\left(\frac{1}{1+pu_0\left(1+A\mu(t)\right)}\right) \tag{3.29}$$

Upon carrying out the Laplace inversion of Eq.(3.29), the space-size spectrum of the particles is obtained as follows:

$$n(u,r,t) = \frac{N_a}{\pi^{3/2} b^3(t) u_0} \exp\left[-r^2/b^2(t)\right] \exp\left[-\frac{u}{u_0\left(1+A\mu(t)\right)}\right] \frac{1}{\{1+A\mu(t)\}^2} \tag{3.30}$$

The quantity of practical interest is the space-integrated size spectrum, rather than the detailed spatial distribution of the particles contributing to background aerosols. Upon integrating Eq.(3.30) over all space, the time evolution of the size spectrum, denoted by $\rho(u,t)$, is given by

$$\rho(u,t) = \frac{N_a}{u_0\left[1+A\,\mu(t)\right]^2} \exp\left(-\frac{u}{u_0\left[1+A\,\mu(t)\right]}\right) \tag{3.31}$$

Upon taking the asymptotic limit, and noting that $\mu(\infty)=1$, one obtains the following formula for the ultimate size spectrum of particles injected into the background:

$$\rho(u,\infty) = \frac{N_a}{u_0\left[1+A\right]^2} \exp\left(-\frac{u}{u_0\left[1+A\right]}\right) \quad \text{as } t \to \infty \tag{3.32}$$

A comparison of Eq.(3.32) with the original size spectrum contained in Eq.(3.13) indicates that while the exponential form of the size distribution has remained, the pre-factor has decreased and the characteristic size (the denominator inside the exponential term) has increased from u_0 to $u_0(1+A)$.

Let us now define an important quantity, *F*(*t*), as the fraction of space and volume integrated number of original particles N_a surviving in the puff at time *t*, or simply the survival fraction. *F*(*t*) is obtained by integrating Eq. (3.31) with respect to *u* and dividing by N_a and it is given by,

$$F(t) = \frac{1}{1 + A\mu(t)} \tag{3.33}$$

and the asymptotic survival fraction is ($t \rightarrow \infty$)

$$F(\infty) = \frac{1}{1 + A} \tag{3.34}$$

As expected, the diffusion-coagulation process admits of a non-zero survival of particles after infinite time. Of the total N_a particles with a mean size u_0 emitted from the puff, a fraction $N_a F(\infty)$ survives and becomes a part of the background aerosols with a size $u_0(1+A)$. Hence, this may appropriately be considered as the source modifier term for the total particle concentration.

Similar analysis is carried out for the case of mono-disperse initial distribution in the puff. If u_0 is the initial volume, the initial spatial and volume distribution may be given by a Gaussian form,

$$n(u,r,0) = \frac{N_a}{\pi^{3/2} b_0^{\,3}} \exp\left[-r^2/b_0^{\,2}\right]\delta(u - u_0) \tag{3.35}$$

Applying the Laplace transform and prescribed diffusion approximation, the Laplace transform of the size spectral function may be solved as

$$\tilde{\rho}(p,t) = \frac{N_a}{\left[1 + A\mu(t)\right]\left\{1 + A\,\mu(t)\left(1 - \exp\left[-pu_0\right]\right)\right\}}. \tag{3.36}$$

Upon inversion, one can obtain a discrete size spectra represented by

$$\rho(u,t) = \frac{N_a}{\left[1 + A\mu(t)\right]^2} \sum_{k=0}^{\infty} \left[\frac{A\mu(t)}{1 + A\mu(t)}\right]^{\mathrm{k}} \delta\left[u - (k+1)u_0\right] \tag{3.37}$$

The delta function series implies the occurrence of particles having integer multiple of monomers. The terms multiplying the delta functions, viz., $N_a[A\mu(t)]^k/[1+A\mu(t)]^{k+2}$, yield the amplitude of occurrence of these. The series sums up correctly to the total (all sizes considered) number of particles $N_a F(t)$, where $F(t)$ is the survival fraction given by,

$$F(t) = \frac{1}{1+A\mu(t)}. \tag{3.38}$$

$F(t)$ has the same form as that for exponential initial distribution, which confirms that it is independent of initial distribution.

It is interesting to compare Eq.(3.38) with the following formula obtained by Turco and Yu (1997) using the model of a uniformly mixed-expanding cloud. In their notation,

$$N_i(t) = N_{po}\frac{\left(N_{po}/N_T\right)^{i-1}}{\left(1+N_{po}/N_T\right)^{i+1}}; i = 1,\infty \tag{3.39}$$

where, $\frac{1}{N_T} = \frac{K_0}{2}\int_0^t \frac{1}{V(t)}dt$.

In the above, N_{po} is the total number of particles in the initial volume, $N_i(t)$ is the number of particles with i monomers at time t, K_0 is the constant coagulation kernel and $V(t)$ is the volume of the aerosol puff at time t. The survival fraction in this case is obtained by integrating the Eq.(3.39) with respect to size over the entire range of i from 1 to infinity, and dividing by the initial total number concentration (N_{po}). This survival fraction is similar to our formula if the puff volume $V(t)$ is identified by the following relationship (See Appendix - B)

$$V(t) = \pi\left(\sqrt{2\pi}\right)\left[b_0^{\,2} + 4Dt\right]^{3/2}. \tag{3.40}$$

This equivalence demonstrates that, within the framework of Jaffe approximation, the solution to the diffusion-coagulation problem is consistent with the uniformly mixed-expansion model of Turco and Yu; however, the present approach additionally provides definite pre-factors involving the physical parameters of the processes. The exponential size spectrum obtained here (Eq.(3.32)) is also consistent with their finding (Turco & Yu, 1998), providing the quantitative basis (Eq.(3.40)) for the puff volume for the case of diffusive expansion is identified. However, uniformly mixed-expansion models cannot fully replace the diffusion-coagulation models in view of their (as well as Jaffe approximation) systematic deviation in respect of the numerical results (Section 3.3.1.3).

A realistic aerosol cloud is most likely to have its size spectrum varying in space in a complex fashion. The approximation technique proposed above, can in principle, be used for obtaining essential results even when the spectrum is spatially inhomogeneous. It can be demonstrated by taking the case of a distribution, in which bigger particles are scattered to farther distances in a centro-symmetric spherical cloud, as if they are formed by an explosive process. The rough justification for this would be that due to larger mass, they have larger stopping distances and hence would be thrown farther. For example, if particles of diameter d_p are thrown with initial velocity v_0 they would stop at radial distance, $r \approx v_0 \tau \approx v_0 d_p^2 = v_0 u^{2/3}$, where τ is the relaxation time. Hence, $u \approx r^{3/2}$. For mathematical convenience, let us round it off as $u_0 = u_0(r) = \beta r^2$ (where β is a constant) without further justification. The total number concentration is assumed to be a Gaussian distribution in space. With this, the inhomogeneous distribution is written as

$$n(u,r,0) = \frac{N_a}{\pi^{3/2} b_0^{\,3}} \exp\left[-r^2 / b_0^{\,2}\right] \delta[u - \beta r^2] \tag{3.41}$$

The overall size spectrum is obtained by integrating this over all space:

$$\rho(u,0)=\frac{2N_a}{\pi^{1/2}u_c^{3/2}}u^{1/2}\exp[-u/u_c] \tag{3.42}$$

The above expression represents a well behaved spectrum having a peak at $u_m=u_c/2$ where u_c is characteristic size defined as,

$$u_c=\beta\, b_0^2 \tag{3.43}$$

The Laplace transform of Eq.(3.41) with respect to particle volume yields:

$$\tilde{n}(p,r,0)=\frac{N_a}{\pi^{3/2}b_0^{\,3}}\exp\left[-\frac{r^2}{b_0^{\,2}\xi^2(p)}\right] \tag{3.44}$$

where, a volume conjugate function,

$$\xi(p)=1/(1+pu_c)^{1/2} \tag{3.45}$$

is introduced for notational simplicity. It may be noted that Eq.(3.44) is still a Gaussian in space, made possible by our choice of the spectral function.

Since the initial distributions for *Z*-equation would involve differences between two Gaussians of different widths, it is somewhat cumbersome to apply Jaffe approximation to this equation and hence the approximation is directly applied to Eq.(3.44). i.e., in the spirit of prescribed diffusion,

$$\tilde{n}(p,r,t)\approx\tilde{n}^{diffusive}(p,r,t)\,f(p,t)$$

It may be recalled that $\tilde{n}^{diffusive}(p,r,t)$ is the evolution of the Gaussian under purely diffusive expansion and *f*(*p,t*) is the spectral modifier function under the additional action of coagulation, to be determined. The subsequent steps are similar to those carried out for homogeneous spectrum (Eq.(3.19)-(3.22)). Although tedious, the resulting nonlinear equation for *f*(*p,t*) can be integrated to a quadrature. The details are not shown here, and the final formula for the Laplace transformed spectral function $\tilde{\rho}(p,\infty)$ is provided as,

$$\tilde{\rho}(p,\infty) = \lim t \to \infty \int_{r=0}^{\infty} 4\pi\, r^2 \tilde{n}(p,r,t)dr = \frac{\xi^3(p)\exp[-\phi(1)]}{\left[1 - A\xi^3(p)\displaystyle\int_{x=0}^{1} \frac{\exp[-\phi(x)]dx}{\left\{1-\left(1-\xi^2(p)\right)(1-x)^2\right\}^{3/2}}\right]} \tag{3.46}$$

where,

$$\phi(x) = 2A\int_0^x \frac{dx'}{[1+Ax']\left[1-(1/2)\left(1-\xi^2(p)\right)(1-x')^2\right]^{3/2}} \tag{3.47}$$

The parameter A is exactly as defined in Eq.(3.24). The actual size distribution needs to be obtained by Laplace inversion. This cannot be easily done analytically over the entire spectrum. A simple numerical Laplace inversion algorithm in Mathematica (Wolfram Research, Inc., 2005) is developed to obtain the inversion of Eq. (3.46) using a 15 point Legendre polynomial expansion technique by Bellman et al. (1966) and Narayanan and Ramadurai (1992). The convergence of $\rho(p,\infty)$ was found to be quite rapid.

Analytical Solution for Free-molecular kernel

An analytical solution to Eq.(3.3) cannot be obtained by Laplace transform technique for the free-molecular kernel having the form: $K(u,v) = 1.9\sqrt{\frac{kT}{\rho}}\left(\frac{1}{u}+\frac{1}{v}\right)^{1/2}\left(u^{1/3}+v^{1/3}\right)^2$. An alternative approach is to apply scaling theory and reduce the integro-differential equation to a set of coupled differential equations, as was done by Simons and Simpson (1988). The solutions to the resulting equations can then be approximated by using prescribed diffusion approximation. Assuming a solution of self-preserving form (Simons & Simpson, 1988),

$$n(u,r,t) = \frac{\phi(r,t)}{V^2(r,t)}G\left(\frac{u}{V(r,t)}\right) \tag{3.48}$$

where, $\phi(r,t)$ is the volume fraction of particulate matter given by

$\phi(r,t) = N(r,t)V(r,t)$,

$N(r,t)$ is the number concentration, $V(r,t)$ is the mean particle volume at position *r* and time *t*. *G*(*w*) is the scaling function satisfying the constraints,

$$\int_0^\infty G(w)\,dw = 1, \text{ and} \int_0^\infty wG(w)\,dw = 1 \tag{3.49}$$

G(*w*) satisfies an integro-differential equation whose analytical solutions are available in the literature (Ruckenstein & Chi, 1974). Substituting (3.48) in Eq. (3.3), and taking zeroth and first moments of Eq.(3.3) with respect to *u*, one obtains (Appendix - C)

$$\frac{\partial \phi}{\partial t} = D\nabla^2 \phi \tag{3.50}$$

$$\frac{\partial N}{\partial t} = D\nabla^2 N - R\phi^\alpha\, N^{2-\alpha} \tag{3.51}$$

where, $R = \frac{1}{2}\int_0^\infty\int_0^\infty K(w,w')\mathrm{G}(w)\mathrm{G}(w')\,dw\,dw'$

For spherical symmetry with an initial Gaussian distribution of the volume fraction $\phi\,(r,0)$ the solution of Eq.(3.50) yields a Gaussian solution at all times exactly.

$$\phi(r,t) = \frac{\phi_0}{\pi^{3/2} b^3(t)} \exp\left[-r^2/b^2(t)\right] \tag{3.52}$$

where, ϕ_0 is the total volume of all the particles at time t=0, *b*(*t*) is the width of the plume at time *t* (Eq.(3.17)).

Apply Jaffe approximation to Eq. (3.51) by following the same prescriptions as in the constant kernel case. i.e.,

$$N(r,t) \approx g(r,t)\,F(t) \tag{3.53}$$

where, $g(r,t)=\frac{N_0}{\pi^{3/2}b^3(t)}\exp\left[-r^2/b^2(t)\right]$ is the diffusive solution and $F(t)$ is the survival fraction to be determined. The initial condition for the problem is given by $\phi(r,0)=N(r,0)\,V(r,0)$ and $N(r,0)=\frac{N_0}{\pi^{3/2}b_0^{\,3}}\exp\left[-r^2/b_0^2\right]$.

where N_0 is the total number at time t=0, b_0 is the initial width of the plume. The prescription Eq.(3.53) transforms Eq.(3.51) to the following "inexact" equation to be interpreted in the space-integrated sense:

$$g(r,t)\frac{\partial F(t)}{\partial t}\approx -R[\phi(r,t)]^{\alpha}[g(r,t)]^{2-\alpha}[F(t)]^{2-\alpha} \tag{3.54}$$

Upon integrating Eq. (3.54) over the entire space, one obtains

$$N_0\frac{\partial F(t)}{\partial t}=\frac{-R\phi_0^{\ \alpha}\,N_0^{\ 2-\alpha}[F(t)]^{2-\alpha}}{\left\{2\pi b^2(t)\right\}^{3/2}} \tag{3.55}$$

Solution of Eq. (3.55) is given by,

$$F(t)=\frac{1}{[1+A\mu(t)]^{\left(1/1-\alpha\right)}} \tag{3.56}$$

where, $\mu(t)$ has the same form as given in Eq.(3.25) and

$$A=\frac{\mathrm{R}\phi_0^{\ \alpha}\,N_0^{\ 1-\alpha}(1-\alpha)}{2(2\pi)^{3/2}Db_0}. \tag{3.57}$$

For free-molecular kernel, $\alpha=\frac{1}{6}$, and $R=6\sqrt{\frac{kT}{\rho}}$ (Simons and Simpson, 1988).

The asymptotic survival fraction is given by,

$$F(\infty)=\frac{1}{[1+A]^{\left(\frac{1}{1-\alpha}\right)}} \tag{3.58}$$

As in the case of a constant kernel, Eq.(3.58) again suggests the dependence of survival fraction on a single parameter A. Also, Eq.(3.58) is similar to the solution given by Turco and Yu (1999), with an additional feature that the quantity A is now expressed (Eq.(3.57)) in terms of known basic parameters.

It is noted that in arriving at this formula two approximations are used namely, self-preserving (scaling) solution and Jaffe's prescribed diffusion approximation theory. To test which of these approximations is more error prone, one can forgo the prescribed diffusion approximation to test the validity of scaling theory under dispersing conditions by numerically solving the differential equations (Eqs.(3.50), (3.51)). Along with the numerical solution of the full integro-differential equation, now there are two more comparisons, viz., test of only prescribed diffusion (no scaling), and scaling with prescribed diffusion, for the free-molecular kernel. Hence, in this case, the diffusion-coagulation equation (Eq.(3.51)) in three-dimensional systems under the assumption of azimuthal symmetry, may be written explicitly as

$$\frac{\partial N}{\partial t} = D\frac{\partial^2 N}{\partial r^2} + \frac{2D}{r}\frac{\partial N}{\partial r} - R\phi^{\alpha}\ N^{2-\alpha} \tag{3.59}$$

The above equation is solved by finite difference schemes described in the next sub-section. This question does not arise for constant kernel since Laplace transform was exactly possible. In what follows, a systematic numerical study of the various equations are carried out and compared with various analytical solutions.

Numerical solutions

In the present study, the integro-differential equation (3.3) is solved for spherical symmetry in 3-D by combining two numerical techniques, finite difference method for diffusion and nodal method for coagulation (Prakash et al, 2003). The particles are distributed in two-dimensional grids, one in space using Gaussian distribution function, and other in the particle volume domain. Eq.(3.3) is solved for both constant and free-molecular kernel.

The diffusion part of the Eq.(3.3) in spherical co-ordinates (assuming azimuthal symmetry) is solved by using finite difference technique. Although several schemes are available in the literature, such as the explicit, implicit and the Crank-Nicolson for solving parabolic partial differential equations, a general scheme is implemented by combining all of these. The boundary of the problem domain has been extended sufficiently far to encompass the expanding cloud. The code can handle both mono- and poly-disperse initial particle size distribution. The output of the code contains survival fraction and particle size spectral function at any particular time.

The discrete form of the coagulation part of the Eq.(3.3) is given by

$$\frac{\partial N_k}{\partial t} = \frac{1}{2} \sum_{\substack{i=2 \\ j=2}} \chi_{ijk} \beta_{i,j} N_i N_j - N_k \sum_{i=2} \beta_{i,k} N_i \tag{3.60}$$

where $\beta_{i,j}$ is the coagulation kernel and χ_{ijk} is the size-splitting operator. Eq.(3.60) is solved by Nodal method (described in Section 2.3.1.1). At every coagulation step, the size-splitting operator redistributes the particles back to nodes. The size-splitting operator (χ_{ijk}) is defined as,

$$\begin{aligned} \chi_{ijk} &= \frac{u_{k+1} - (u_i + u_j)}{u_{k+1} - u_k}; \quad u_k \le u_i + u_j \le u_{k+1}, \\ &= \frac{(u_i + u_j) - u_{k-1}}{u_k - u_{k-1}}; \quad u_{k-1} \le u_i + u_j \le u_k, \\ &= 0; \qquad\qquad \text{otherwise.} \end{aligned}$$

Sensitivity studies are carried out by varying the geometry spacing factor (q) after coupling the coagulation module with the diffusion. It is observed that the total number concentration is unaffected but the size spectrum shifts towards the larger particle sizes. To understand the extent of this error for homogeneous size spectrum and constant kernel, the Laplace transformed equations (3.6) and (3.8) are solved numerically using the differential equation solver of Mathematica (Wolfram Research, Inc., 2005). A simple numerical Laplace inversion algorithm is developed to obtain the inversion of the results of Eqs.((3.6), (3.8)) using a 15 point Legendre polynomial expansion technique by Bellman et al. (Bellman et al., 1966) and Narayanan and Ramadurai (1992). The convergence of $\rho(u,\infty)$ was found to be quite rapid. There was a reasonable, if not complete, agreement of the size spectra obtained with the nodal-finite difference technique for the geometry spacing factor q~2.0, although the accuracy increased for smaller q values. In the present study q is taken as ~2.0.

3.3.1.3. Results and Discussion

It is well-known that when only coagulation is present, the survival fraction in a puff, given by, $F(t)=\left[1+\frac{KN_0t}{2}\right]^{-1}$ (N_0 is mean initial concentration) continuously decreases with time, eventually reaching zero. In contrast, when diffusion is present, particles in a 3D puff survive coagulation, asymptotically. These results are illustrated in Fig.3.4.

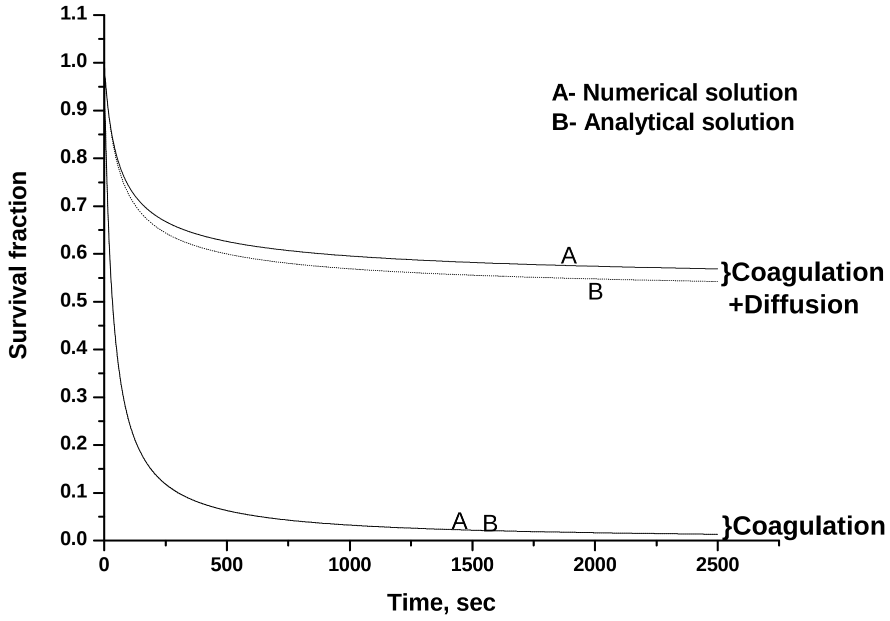

Fig.3.4: Illustration of number survival fraction of aerosol particles in a puff due to coagulation with and without diffusion.

Fig. 3.5 shows detailed comparison of the time evolution of the analytical and numerical survival fraction $F(t^*)$ for the given set of assumptions (constant kernel, constant diffusion coefficient, homogeneous size spectrum and initial size distribution - monodisperse). It is seen that $F(t^*)$ becomes almost constant beyond t^* $(= Dt / b_0^2)$ =10 units. Within analytical approximation, the asymptotic survival fraction ($F(\infty)$) can be predicted through a single parameter A (Eq.(3.24) for constant kernel), which combines all the variables, such as the coagulation kernel, plume dimension and the initial number of particles and diffusion coefficient. Larger the value of A, stronger will be the effect of coagulation in reducing the number concentration as compared to diffusive dispersion, and hence smaller will be the survival fraction.

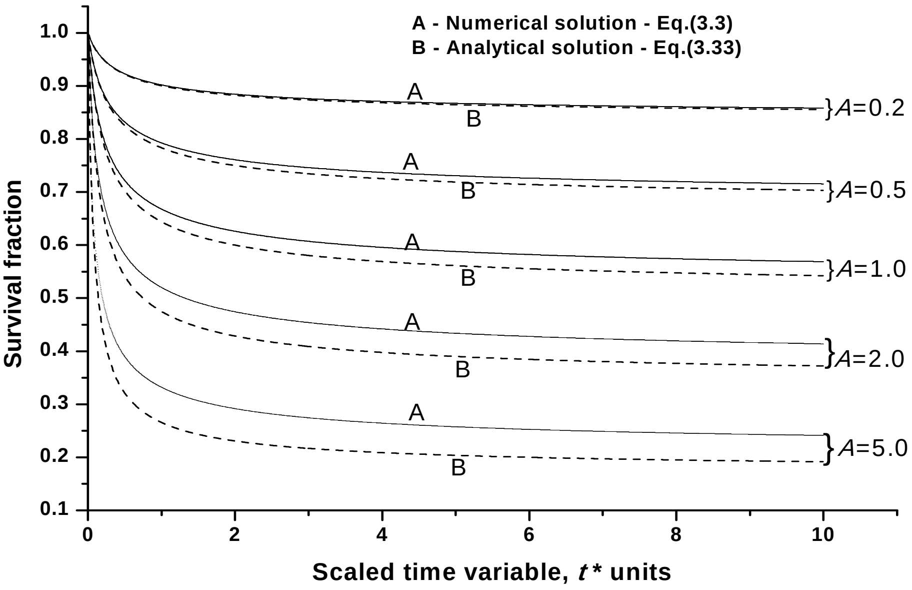

Fig.3.5: Analytical and numerical solutions for the variation of survival fraction with time for various values of A (constant kernel, homogeneous size spectrum, initial size distribution - monodisperse)

As seen in Fig.3.5, the analytical and numerical survival fractions show broad agreement with each other in respect of their overall temporal and parametric dependencies. However, quantitative differences exist which increase as the coagulation mechanism increasingly dominates over diffusion. Thus, the difference is about 2% for $F(\infty)=0.8$ (strong diffusion, $A=0.2$) and the difference is 25% for $F(\infty)$ =0.2 (strong coagulation, $A=5.0$). These results show that (i) the Jaffe solutions are less and less accurate for higher values of A, and (ii) given the similarity between the Jaffe solutions and those of the uniformly mixed-expansion model, the latter cannot exactly replace the diffusion-coagulation model.

The variation of survival fraction with time for the case of free-molecular coagulation kernel, homogeneous size spectrum (initial size distribution – monodisperse) is shown in Fig.

3.6. The maximum error between numerical solution of integro-differential equation (Plot A) and analytical solution (Plot C) obtained by Jaffe- approximation is 22% at $t^*=3$ units (for $A=3$). This deviation is due to the limitation of the prescribed diffusion approximation and not due to scaling assumption because the numerical solution to the equation obtained after scaling (Plot B) matches more closely with the numerical solution of the original integro-differential equation.

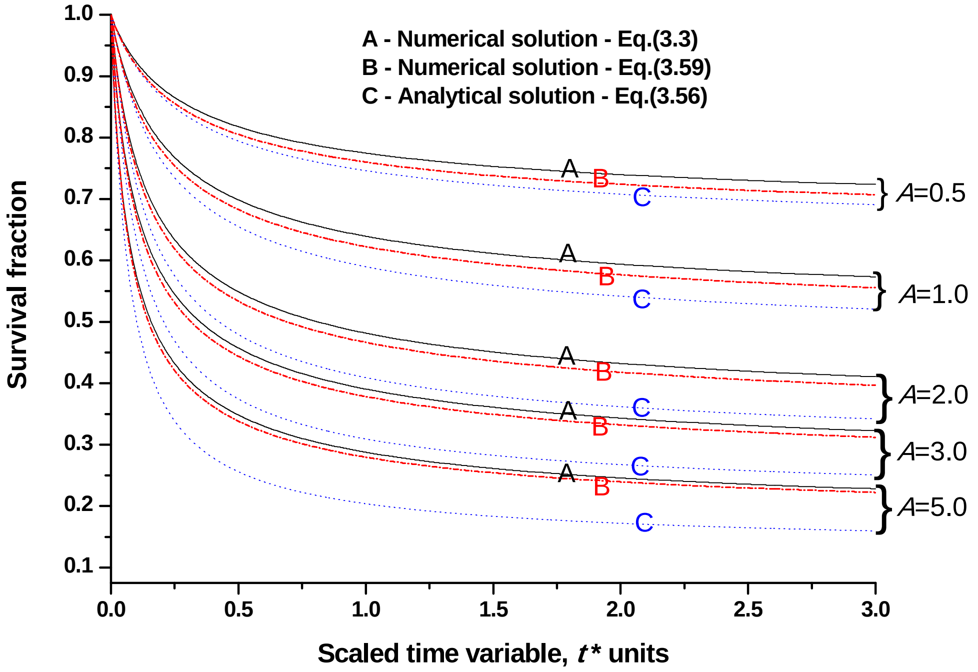

Fig.3.6: Analytical and Numerical solutions for the variation of survival fraction with time for various values of A (free-molecular kernel, homogeneous size spectrum, initial size distribution - monodisperse)

Fig. 3.7 shows the comparison of the particle size spectrum at $t^* = 10$ obtained by analytical and numerical methods along with the Turco's formula (given in the Eq. (3.39)). In this case, the particles are monodisperse of size 50 nm initially. While, as expected, the results of

Turco and Yu agree with our analytical result, both show a small but distinct deviation from the numerical result.

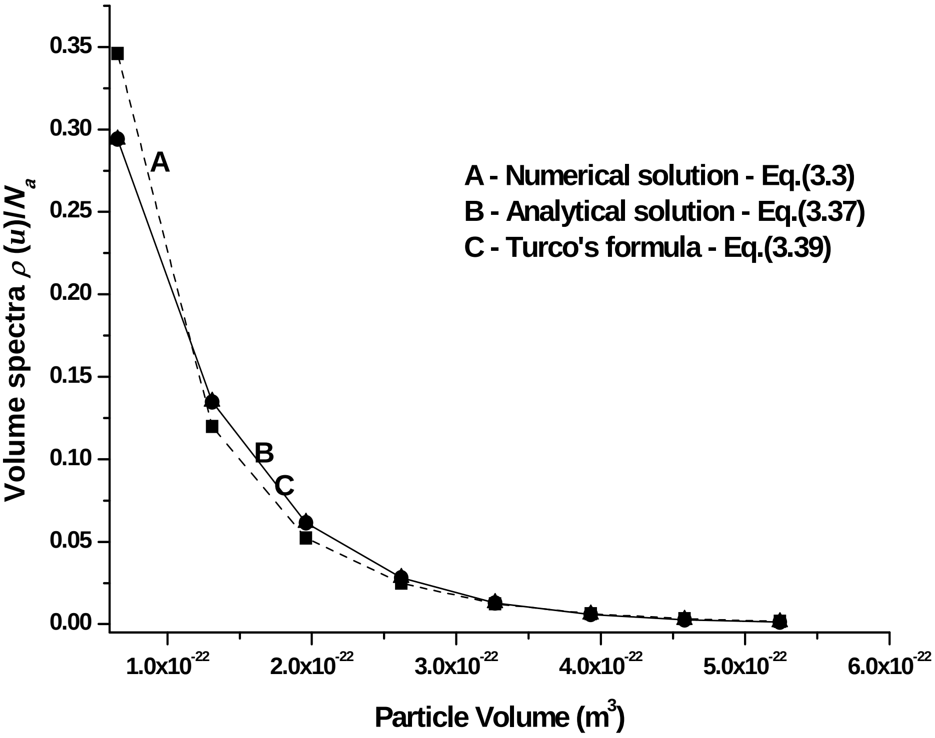

Fig.3.7: Aerosol particle size distribution for monodisperse, spatially homogeneous size spectrum at scaled time, $t^* = D\,t/b_0^2$ =10. (A =1.0, constant kernel)

Similar comparison between the numerical solutions and the analytical results for an initial exponential size spectrum and for a value A=1 are shown in Fig. 3.8. Plot-A in the figure refers to the original spectra. The numerical solutions include (i) direct solution to the integro-differential formulation (Plot C) and (ii) solution to the Laplace transformed equation and inversion, using Mathematica (Plot D). As mentioned, the two numerical approaches agree closely at smaller sizes and differ slightly at larger sizes. The analytical result (Plot B) shows deviation from the numerical solutions at smaller sizes and tends to closely follow the Mathematica based solutions at large sizes.

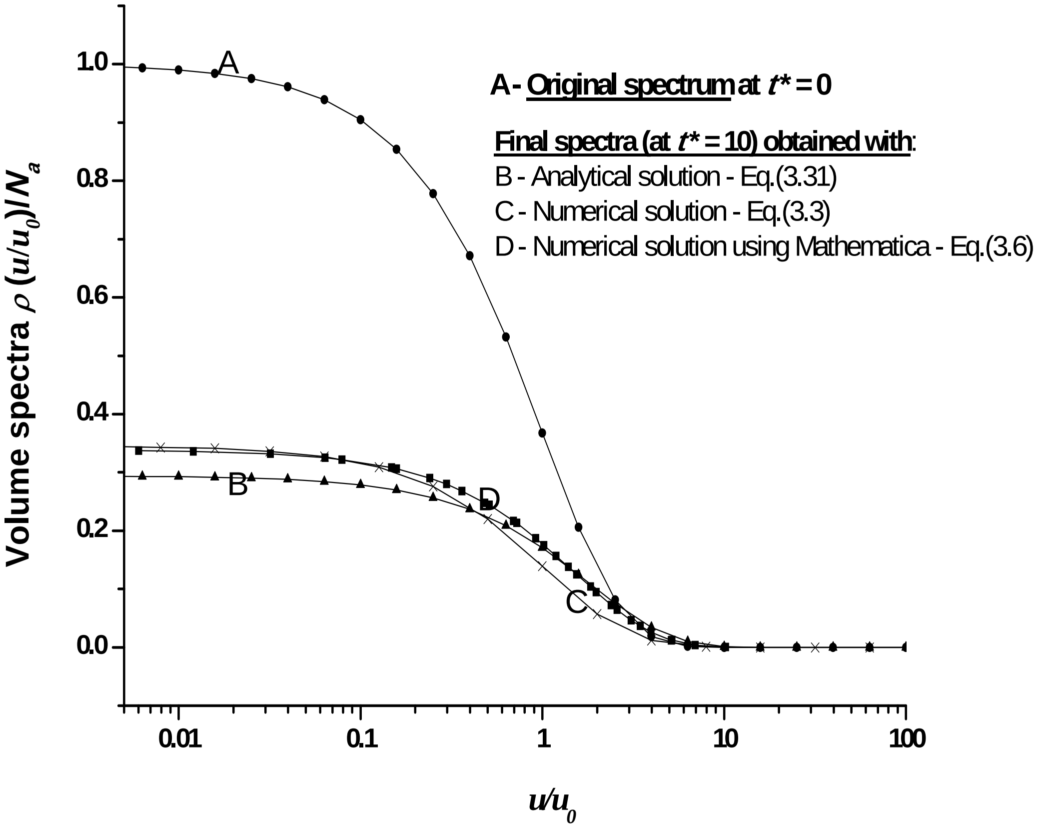

Fig.3.8: Aerosol particle size distribution for polydisperse, spatially homogeneous size spectrum at scaled time, $t^* = D\,t/b_0^2$ =10. (A =1.0, constant kernel)

The evolution of average relative particle diameter with time for the constant and free-molecular cases are shown in Figs. 3.9 and 3.10 respectively. Since the removal processes are not included in this model the volume fraction remains constant, and the average asymptotic particle size is given by, $a(\infty)=a_0/[F(\infty)]^{1/3}$. For example, considering a value of A=1, one obtains F(∞)= 0.5, and hence an aerosol puff having an initial average diameter of 50 nm would eventually attain an average particle diameter of 63 nm as it disperses to form a part of the background aerosol.

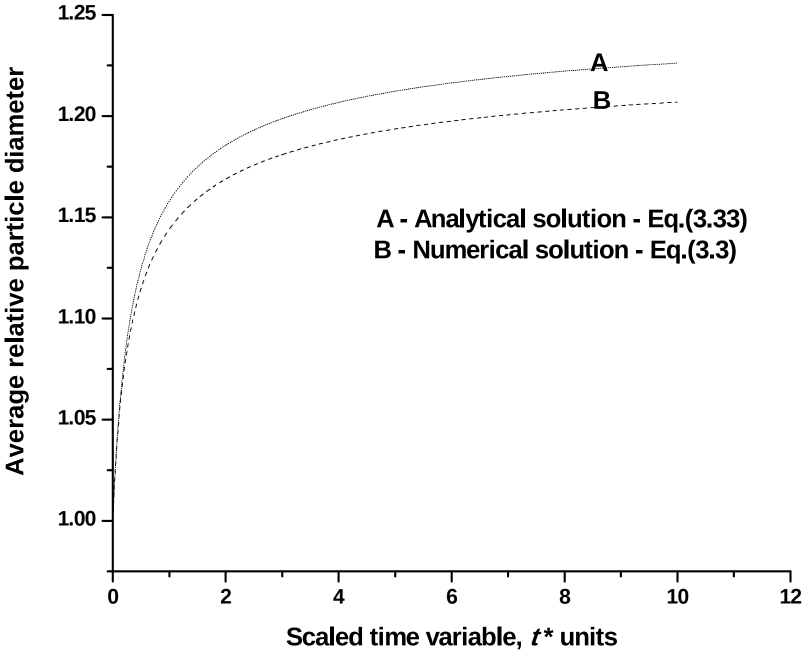

Fig.3.9: Evolution of average particle size with time for A=1.0 (constant kernel)

While the analytical results show reasonable agreement with numerical solutions when A is small, systematic deviations are seen at larger values of A. This calls for improvement in the analytical approach beyond Jaffe approximation. Nevertheless, the analytical solutions yield simple formulae for quickly estimating the survival fractions for the number concentrations of particles injected into the open environment from puff releases.

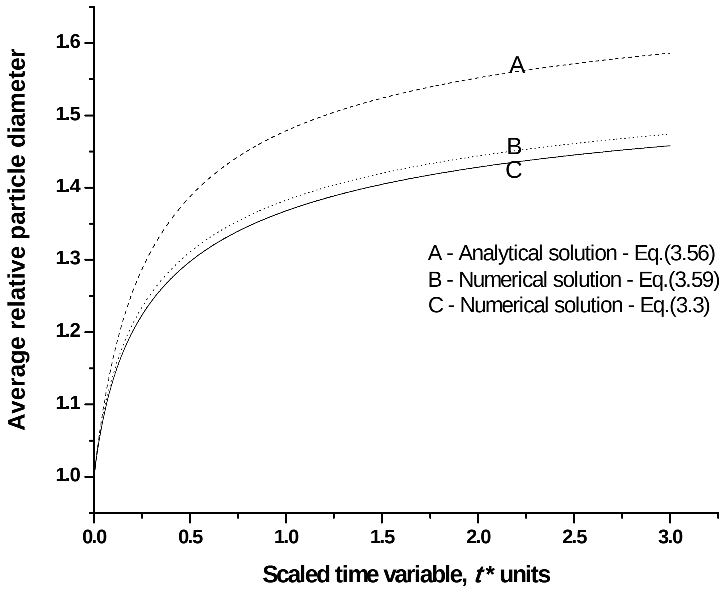

Fig.3.10: Evolution of average particle size with time for *A*=3.0 (free-molecular kernel)

3.3.2. Diffusion approximation model with coagulation-induced flattening effect

While the approximate solutions obtained by the prescribed diffusion approximation model in the previous section agreed with numerical solutions for small values of the coupling parameter between coagulation and diffusion, it deviated from the numerical solutions considerably under strong coagulation. The simple formula for larger *A* values always yielded lower survival fractions than the numerical values. This is mainly because of the restrictive assumption on the evolution of the variance of the spatial concentration distribution of the puff as the function of time. It is assumed to evolve linearly as dictated by diffusive spreading. In reality, there will be a rapid depression of concentration at the centre of the puff due to higher particle concentrations there. This would appear as a distribution, flattened at the top. When this shape is expressed as a renormalized Gaussian it would result in an apparently enhanced variance of the distribution. This is called as the 'coagulation-induced flattening effect'. This effect is accounted by a systematic mathematical procedure based on Fourier space analysis. This model is termed as 'Improved diffusion approximation model', and aims at improving the previously obtained analytical approximation through a closer look at the formulation and the solution procedure.

3.3.2.1. Formulation of problem

Upon taking the origin as the centre of the puff, Eq.(3.8) may be recast, in terms of dimensionless variables, $N^* = Nb_0^3 / N_0$, $\tau = Dt / b_0^2$, $\rho = r / b_0$, as

$$\frac{\partial N^*(\rho,\tau)}{\partial \tau} = \nabla^2 N^*(\rho,\tau) - 2(2\pi)^{3/2} A\left[N^*(\rho,\tau)\right]^2 \tag{3.61}$$

where, ρ is the radius vector, and the operator ∇^2 refers to spherically symmetric diffusion operator in ρ variable only. Let us define 3-dimensional Fourier transform of $N^*(\rho,\tau)$ with respect to its radial coordinate ρ as,

$$\varphi(k,\tau) = \iiint N^*(\rho,\tau)\exp\left(-2\pi i\vec{k}\cdot\vec{\rho}\right)d^3\rho \tag{3.62}$$

where, k is the transform variable.

Upon taking Fourier transform of Eq.(3.61) using Eq.(3.62), one obtains,

$$\frac{\partial \varphi(k,\tau)}{\partial \tau} = -k^2\varphi(k,\tau) - \frac{2A}{(2\pi)^{3/2}}\int_{k'} \varphi(k',\tau)\varphi(k-k',\tau)d^3k' \tag{3.63}$$

Eq.(3.63) is a non-linear integro-differential equation. The variance of the spatial distribution is precisely accounted for by the coefficient of k^2 terms in the k-space expansion. By treating the variance as free function yet unknown, it may be determined by matching the coefficients of k^2

terms in a systematic expansion procedure. Hence a new approximation scheme in terms of two unknown functions is proposed as,

$$\varphi(k,\tau) \approx \psi(\tau)\exp\left(-\frac{k^2}{4}\xi(\tau)\right) \tag{3.64}$$

which, in essence, replaces the classical Jaffe approximation, $\varphi(k,\tau) \approx \psi(\tau)\exp\left[-\frac{k^2}{4}(1+4\tau)\right]$.

In Eq.(3.64), $\psi(\tau)$, $\xi(\tau)$ represent the survival fraction ($\psi(\tau) = \frac{1}{N_0}\int_0^\infty N(r,t)d^3r$) and the variance (scaled in terms of b_0^2) of the distribution, respectively. The initial conditions are,

$$\psi(0) = 1, \text{ and } \xi(0) = 1 \tag{3.65}$$

Substituting Eq.(3.64) in Eq.(3.63) and comparing the coefficients of k^0 and k^2, one may obtain

$$\frac{\partial\psi(\tau)}{\partial\tau} = -\frac{2A}{\xi^{3/2}(\tau)}\psi^2(\tau) \tag{3.66}$$

$$\frac{\partial\xi(\tau)}{\partial\tau} = 4 + \frac{A}{\xi^{1/2}(\tau)}\psi(\tau) \tag{3.67}$$

Eq.(3.66) and (3.67) are a coupled set of equations for the survival fraction and the variance of the distribution. The original PDE (Eq.(3.61)) has been reduced to a system of nonlinear ODEs for two dependent variables, in this approximation.

By a careful inspection, one may note that the second term on the RHS of Eq.(3.67) represents the coagulation-induced flattening effect. The Jaffe approximation would have been equivalent to neglecting this term which would have yielded the free diffusion law, $\xi(\tau) = 1 + 4\tau$.

3.3.2.2. The ultimate survival fraction: asymptotic limit for ψ

The asymptotic solution for ψ from the Eqs. (3.66) and (3.67) in the limit $\tau \to \infty$, is obtained as follows: It may be noted that in view of the positivity of ψ and ξ, ψ is a monotonically decreasing and ξ is a monotonically increasing, function of time. This permits one to replace the τ coordinate $(0<\tau<\infty)$ with the ξ coordinate $(1<\xi<\infty)$ and seek relationship between ψ and ξ directly by dividing Eq.(3.66) by Eq.(3.67). This leads to the equation:

$$\frac{d\psi}{d\xi}=-\frac{2A\psi^2}{\xi^{3/2}\left[4+\frac{A\psi}{\xi^{1/2}}\right]} \tag{3.68}$$

with $\psi=\psi(\xi)$ and the initial condition is $\psi(\xi=1)=1$. Further, under the following transformations,

$$y=\psi^{-1}\text{, and } z=\xi^{-1/2} \tag{3.69}$$

the nonlinear equation (3.68) reduces to the following linear equation:

$$\frac{dz}{dy}+\frac{z}{4y}=-\frac{1}{A},\ (0<y<1) \tag{3.70}$$

The initial conditions will be as follows:

The fact that $\xi(\tau=0)=1 \Rightarrow z\,(\tau=0)=1$; similarly, the fact that $\psi(\tau=0)=1 \Rightarrow y(\tau=0)=1$. Hence, $z=1$ when $y=1$ is the initial condition for Eq.(3.70). This is a simple first order equation whose solution satisfying the above initial condition is

$$zy^{1/4}=\left[1+\frac{4}{5A}\right]-\frac{4}{5A}y^{5/4} \tag{3.71}$$

Since $\tau=\infty$ correspond to $z=0$, the asymptotic value of y is obtained by setting $z=0$, and transforming back to the original variables,

$$\psi^{puff}(\infty)=\frac{1}{\left(1+\frac{5A}{4}\right)^{4/5}} \tag{3.72}$$

This is the improved analytical formula for the ultimate survival fraction for the spherical puff, called as the 4/5th law. It may be easily seen from Taylor expansion of Eq.(3.72) that it reduces to the classical Jaffe formula for small A ($1/(1+A)$).

Fig. 3.11 shows the comparison of the 4/5th formula with numerical solution of the PDE (Eq.(3.61)) as well as the earlier formula, $1/(1+A)$. One may note that the new formula is in far better agreement with the numerical solution of the full problem as compared to the earlier formula without the flattening effect.

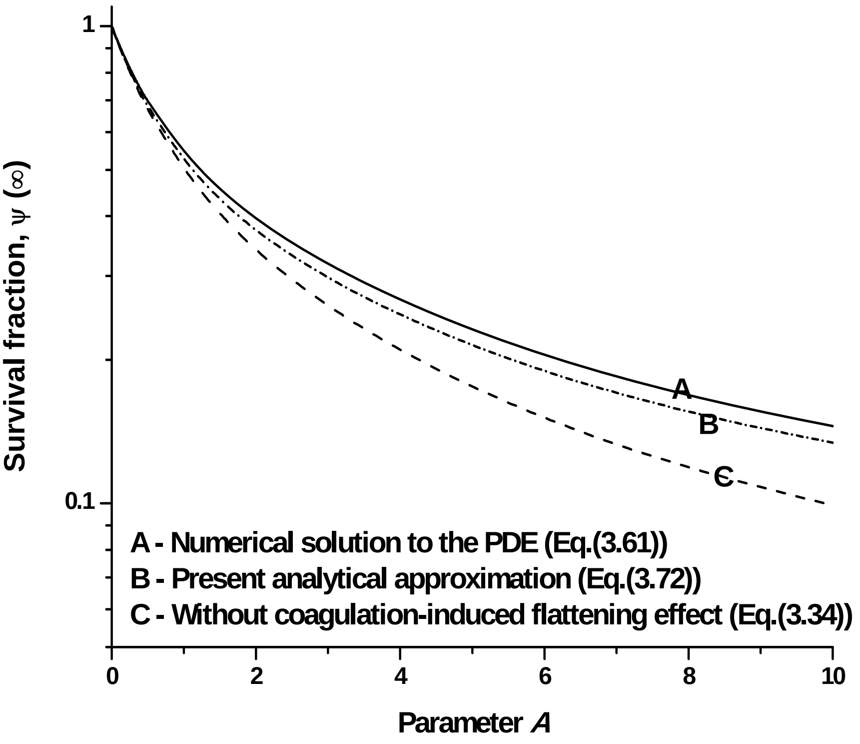

Fig. 3.11. Comparison of various solutions for the ultimate survival fraction of particles in a spherical puff as a function of the parameter A. The present solution (4/5th law) is seen to agree closely with the exact numerical solution of the coagulation-diffusion equation.

3.3.2.3. Transient analysis

To obtain temporal variation, let us start with Eq.(3.66) and note that $z=\xi^{-1/2}$. Then

$$\frac{d\psi(\tau)}{d\tau}=-2A\psi^2(\tau)z^3(\tau) \tag{3.73}$$

The above non-linear equation is converted to the following equation independent of z or ξ by transformation of variables,

$$\frac{d\psi(\tau)}{d\tau}=-\frac{2A}{\psi(\tau)}\left\{1+\frac{4}{5A}\right\}^3\left[\psi^{5/4}(\tau)-\psi_\infty^{5/4}\right]^3 \tag{3.74}$$

This may be reduced to a quadrature relating an integral over ψ, to τ.

A typical temporal variation of the survival fraction for (A=10) is shown in Fig. 3.12. It may be seen that this quantity reaches its asymptotic limit quickly (τ~1) as expected.

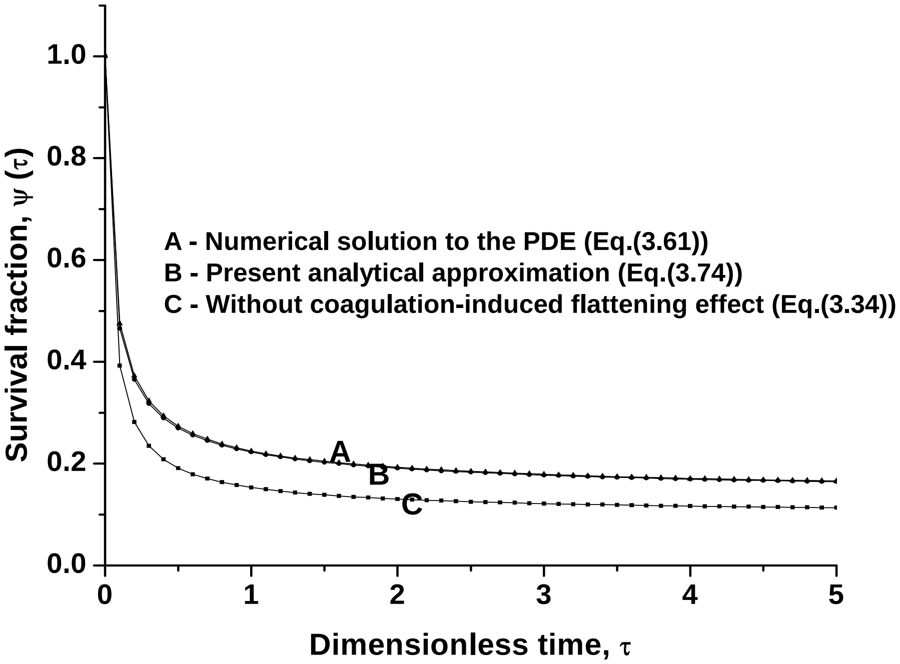

Fig. 3.12. Temporal variations of the survival fraction for a 3-D spherical puff (A = 10)

Similarly, Fig. 3.13 shows the variation of $\xi(\tau)$ as well as the purely diffusive variance as a function of time for A=10. Again, from this figure, it may be noted that the coagulation-induced flattening effect on variance occurs early in time, and at later times, $\xi(\tau)$ almost parallel to the pure diffusive variance.

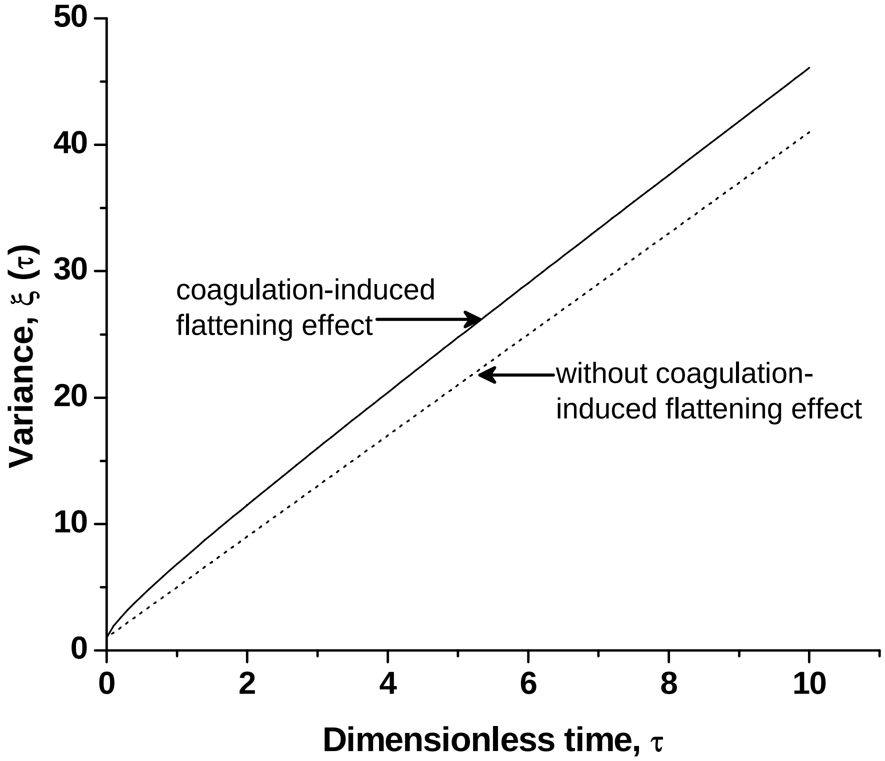

Fig. 3.13. Effect of coagulation-induced flattening on the temporal evolution of variance $\xi(\tau)$ of the spatial distribution of a spherical aerosol puff (A = 10)

3.3.2.4. Spatial variation of average particle mass inside puff

The average particle mass ($\overline{m}(\rho, \tau)$) (scaled w.r.t to the initial particle mass) is obtained from the ratio of the dimensionless mass concentration ($M^*(\rho,\tau)$) of the aerosol and the dimensionless total number concentration ($N^*(\rho,\tau)$) given by,

$$\overline{m}(\rho,\tau)=\frac{M^*(\rho,\tau)}{N^*(\rho,\tau)} \tag{3.75}$$

From Eq.(3.4), it may be easily shown that the mass concentration satisfies the free diffusion equation

$$\frac{\partial M^*(\rho,\tau)}{\partial \tau}=D\nabla^2 M^*(\rho,\tau) \tag{3.76}$$

having the solution

$$M^*(\rho,\tau)=\frac{\exp\left[-\rho^2/(1+4\tau)\right]}{\pi^{3/2}(1+4\tau)^{3/2}}. \tag{3.77}$$

From the Fourier inversion of Eq.(3.64), the total number concentration is given by,

$$N^*(\rho,\tau)=\frac{\exp\left[-\rho^2/\xi(\tau)\right]}{\pi^{3/2}\xi^{3/2}(\tau)}\psi(\tau) \tag{3.78}$$

Upon substituting Eqs.(3.77) and (3.78) in Eq.(3.75), one obtains

$$\overline{m}(\rho,\tau)=\frac{\xi^{3/2}(\tau)}{(1+4\tau)^{3/2}\psi(\tau)}\exp\left[-\rho^2\left(\frac{1}{(1+4\tau)}-\frac{1}{\xi(\tau)}\right)\right] \tag{3.79}$$

Since $\xi(\tau)>>(1+4\tau)$ due to coagulation induced flattening, the term multiplying ρ^2 inside the exponential on the RHS of Eq.(3.79) is always positive. Hence, the average mass per particle will be highest at the centre of the puff and will decrease radially. This is as expected since the coagulation rate will be highest at the centre of the puff leading to larger particles as compared to peripheral regions of the puff. As the puff expands, the average particle mass would tend to approach its asymptotic value at all radial points of the puff. These aspects are illustrated in Fig. 3.14 which shows the evolution of the average particle mass with respect to time at various radial distances of the puff, starting with an initially monodisperse mass distribution. An application of the improved diffusion approximation model is shown in the following section.

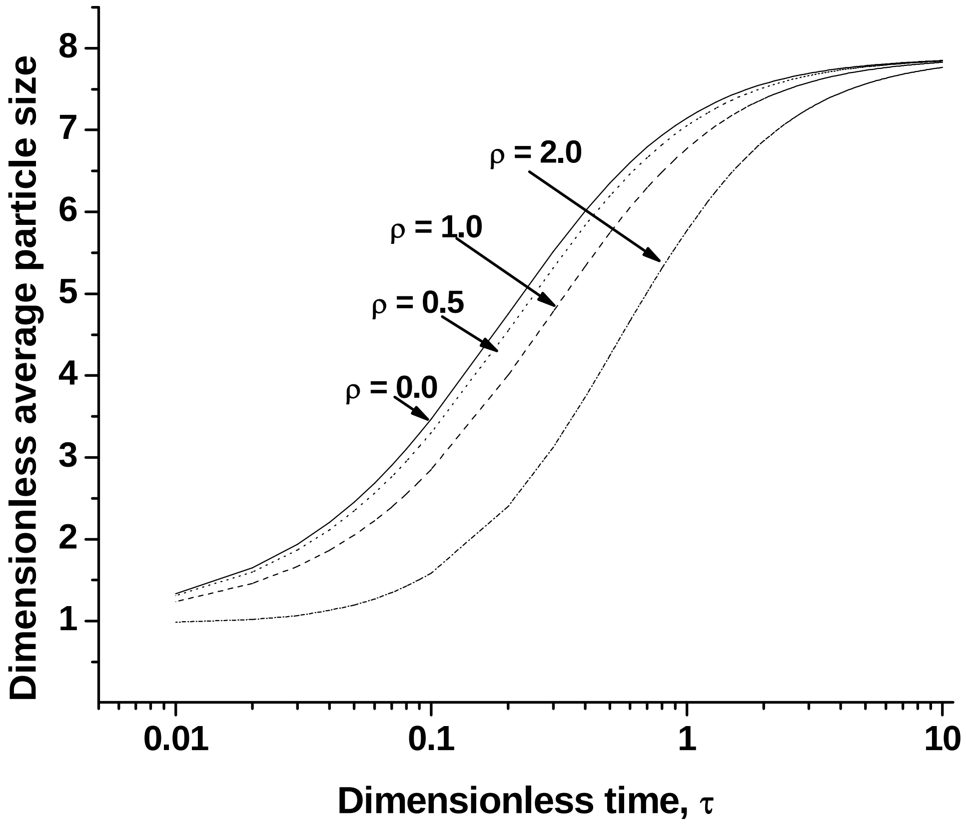

Fig. 3.14. Evolution of average particle size segregation of particles in a Gaussian puff (A = 10)

3.3.2.5. Application of the improved diffusion approximation model to vehicular emissions

The spherical puff model is an ideal case for the problems like explosive releases, fireworks, etc., but lack of data on the input parameters for these cases restricts us in applying the results. Vehicular emission is one of the major contributors of ultrafine particles (nanoparticles) in urban areas among the various sources mentioned in the introduction. It contributes significantly to the aerosol number concentration at the local scale by emitting primary soot particles (fine particles are combustion-induced) and forming secondary nucleated particles (ultrafine particles are dilution-induced). Most of the aerosol emission and transport studies for vehicular emission sources divide the study area into two distinct stages namely 'tailpipe-to-road' and 'road-to-ambient' based on different mixing forces (dilution ratio). The first stage 'tailpipe-to-road' is influenced by the traffic-generated turbulence which is a function of vehicle dimension and exit velocity of the exhaust gases from the tailpipe. The total time duration of 'tailpipe-to-road' stage is around 3 seconds (3-10 minutes for 'road-to-ambient'); the dilution ratio during this period is ~ 1000 (10 for 'road-to-ambient') (Zhang & Wexler, 2004). It is found that the nucleation process completes at very early stage, i.e., before 0.1 second (Du & Yu, 2008). Hence, coagulation is the major aerosol processes will be acting at later stage (0.1-3 seconds) of this 'tailpipe-to-road' dilution in the absence of condensation. There is thus a need to understand the effect of coagulation of aerosol particles during the puff dilution.

Vehicular releases may be approximately considered as a series of puff releases, emission point being at the end of the exhaust pipe. In the initial stage of dilution ('tailpipe-to-road'), a typical total number concentration of 10^{10} #/cm^3 contain both combustion-induced (50-60 nm) and nucleation-induced (2-5 nm) particles (Albriet et al, 2010). Coagulation kernel (*K*) of ~10^{-8}cm^3/sec is considered for the calculations. Assuming a spherical aerosol puff of width 10 cm, the initial total number in the puff is estimated to be 5.24x10^{12}. The diffusion coefficient *D* is estimated by comparing the volumes of the two different models (one from the diffusion theory and other from the dilution ratio measurements for vehicular emissions in the very early dilution stage (Du & Yu, 2008)), and it is found to be in the range of (70-300) cm^2/sec. For a weak dilution, i.e., D=70 cm^2/sec, the value of the parameter A is 1.19. With a typical value of A =1.19, the asymptotic survival fraction from Eq.(3.72) is 0.48. Thus, the effective total number in the puff/cloud at a large downwind distance is ~50% less than the initial number. This shows that the effect of coagulation is marginal in reducing the total number of particles injected into the atmosphere from vehicular emissions.

3.4. Summary

The uniformly mixed volume expansion model is simple to implement using numerical methods provided the volume expansion rate is known a-priori. The coagulation-diffusion model contrasts with the uniformly mixed expansion models developed by earlier investigators since it explicitly accounts for spatial inhomogeneity of particle concentrations, and it does not require any explicit volume expansion rate. This model holds good for diffusion dominated regime of aerosol transport. The improved diffusion approximation model (improved model developed over diffusion approximation model) brings out the special effect of the coagulation-induced flattening of the spatial concentration profiles because of which particle sizes will be larger at the centre of a Gaussian puff. Using this model one can obtain a formula for the ultimate number survival fraction as $\psi^{puff}(\infty) = (1 + 5A/4)^{-4/5}$ where, $A = KN_0 / \left\{4(2\pi)^{3/2} Db_0\right\}$ for a puff of initial width b_0 consisting of N_0 particles. This approximate analytical formula, termed as 4/5th law, obtained for the survival fraction is in close agreement with accurate numerical solutions. It is a simple formula that combines the variables of the problem into a single parameter, and proposed as modifiers of emission factors. Thus, the study provides approximate analytical solutions to predict survival fractions for the number concentrations of particles injected into the open environment from puff releases.

Chapter 4. Survival fraction for the plume releases

4.1. Introduction

Unlike the situation in respect of pure dispersion problems, the extension from puff to plume for continuous releases is far from simple when coagulation is considered. In purely dispersing linear systems, a plume can be considered as a limiting train of equally spaced puffs and therefore the distribution of the plume may be obtained as a linear superposition over all the puffs; however when coagulation is involved, one has to account for inter-puff interactions in addition to the intra-puff effects. One would therefore expect somewhat different results for the resulting distributions. There has been considerable discussion regarding Lagrangian descriptions of puffs as analogues of plume behavior (Seinfeld & Pandis, 2006) for reacting systems. The plume releases, corresponding to continuous releases, is discussed within a 2-D framework under the assumptions of constant advection velocity (U) and space dependent diffusion coefficient expressed in terms of turbulent energy dissipation rate (ε). Essentially, only the early phase inhomogeneous coagulation process during dispersal is considered; the homogeneous processes such as interaction with pre-existing background particles or the formation of new particles from the gases emitted from the sources due to photo-oxidation in the atmosphere after the dispersal is complete, are excluded. Besides this, the condensation/evaporation of volatile vapours onto and from the source particles during the early dispersal phase is not included since these are essentially number conserving processes, which mainly affect the size spectrum, but do not create or destroy particles.

The present approach (based on improved diffusion approximation model) involves construction of moment equations for the evolution of number concentration and variance of the spatial extension of plume in terms of either time or downstream distance. These equations are solved simultaneously and a simple formula is obtained to evaluate survival fraction in the context of plume (continuous) releases under the assumption of a constant coagulation kernel.

4.2. Problem formulation

Consider a continuous emission source such as an incense stick, candle or forest fire as the source region. Let us assume that particles are formed in a combustion zone of circular cross-section and are transported by advection due to wind having a speed U along X-axis. Let the initial radius of the combustion area be σ_0, which can be taken as the standard deviation of the radial distribution of particles within a Gaussian distribution framework. The evolution equation for a coagulation-diffusion system is given by,

$$\begin{aligned}\frac{\partial n(u,r,t)}{\partial t}+\nabla.[Un(u,r,t)]=\nabla.\{D(r,t)\nabla n(u,r,t)\}+\frac{1}{2}\int_0^u K(u',u-u')n(u',r,t)n(u-u',r,t)du' \\ -n(u,r,t)\int_0^\infty K(u,u')n(u',r,t)du'\end{aligned} \tag{4.1}$$

where, $n(u,r,t)du$ is the number of particles with particle volumes lying between u and $u+du$ per unit volume of the fluid at position r and time t, $K(u, u')$ is the coagulation kernel between the particles of volume u and u', $D(r,t)$ is the space dependent diffusion coefficient and $U(r,t)$ is the advection velocity. For puff releases, the study is restricted to the case of a constant, representative, diffusion coefficient chiefly because it renders itself amenable to exact analytical solution that is useful for benchmarking the functional form of solutions in more complex situations. In general, the diffusion coefficients of the particles follow the atmospheric eddy diffusion coefficients, which in turn are expressed either as space dependent functions ($r^{4/3}$ formula, Richardson, 1926), or time dependent functions (t^2 formula, Batchelor, 1952). As will be seen in this study, invoking space varying diffusion coefficients is essential for continuous 2-D plume releases, since these do not admit of non-zero ultimate survival fractions for any assumed constant diffusion coefficient. Hence for plume releases, the case of a diffusion coefficient that varies as a function of the downstream distance analogous to the t^2 law above is considered.

Ideally, one may use the Fuchs generalized kernel for $K(u,u')$ in the entire size range. However, as argued by Turco and Yu (1999), for practical purposes, an effective constant kernel is employed that essentially captures the coagulation of the particles in the dominant size range of the original particles. This would render K as a function of time only, which greatly helps in recasting the equation. It may be noted that during the entire process of coagulation, this time dependent kernel hardly changes beyond a factor of 3 and hence for all practical purposes, one can assume a representative constant kernel predominantly corresponding to the coagulation rate at the early part of the evolution of the released particles.

Let the area integrated steady mass emission rate in the plume be M_0 (kg per s) and the corresponding particle number emission rate carrying the mass be S_0 (particles per second). In combustion sources, large number of chemical species will be formed at the hot zone of the source some of which, mainly of low vapour pressure materials, will form critical nuclei as the plume cools downstream. These nuclei will grow very quickly due to the condensation of remaining vapours as the plume cools down further as well as due to rapid coagulation of the critical nuclei. Within a short downstream distance from the hot zone, most of the condensable vapour would have been exhausted and stable clusters would have been formed. The characteristic initial radius (r_c) of these clusters would be about 5-10 nm (Lighty et al, 2000). For the present, let us assume that r_c is the effective initial size parameter of particulates which carry the mass loading due to the emission source (It turns out later that the results are relatively insensitive to the choice of r_c). Then the number emission rate to mass emission rate is related through the formula

$$M_0 = S_0 \rho_m (4\pi / 3) r_c^{\,3} \tag{4.2}$$

It is postulated that the onset of the dispersal process along with further coagulation from a point located at some downstream distance from the source beyond which no new particles are formed. This location is referred as the origin of the X-axis. Unlike the 3-D puff case, the plume case is generally treated within a 2-D diffusion framework. This is based on ignoring diffusion along the wind direction under the implicit assumption that the axial Peclet number is quite large; one then treats dispersion process by considering advection along the flow direction and diffusion in the cross-wind direction. However, the cross-wind diffusion coefficients are generally assumed to increase with the downstream distance in a power law fashion. Most commonly, one expresses the diffusion coefficients through the relationship

$$D(x) = \frac{U}{4} \frac{d\sigma^2(x)}{dx} \tag{4.3}$$

where, $\sigma^2(x)$ is the variance of the plume width in the cross-wind direction. As mentioned in the introduction, the variance is taken as power-laws either of distance or of time. Most commonly used power-law is the cubic law (Ott & Mann, 2000):

$$\sigma^2(x) = \sigma_0^2 + 4D_0(x/U) + C\varepsilon(x/U)^3 \tag{4.4}$$

where, σ_0 is the initial width, D_0 is the particle diffusion coefficient in the source region and C is a constant, and ε is the turbulent energy dissipation rate. With the above, $D(x)$ assumes the form:

$$D(x) = D_0 + \frac{3C\varepsilon}{4U^2} x^2 \tag{4.5}$$

Assume cylindrical symmetry of the plume and set-up a steady-state dispersion coagulation equation for the evolution of the particle volume integrated total number concentration, under the assumption of a constant kernel. Then Eq.(4.1) becomes,

$$U\frac{\partial N(x,r)}{\partial x}=\frac{U}{4}\frac{d\sigma^2(x)}{dx}\left[\frac{1}{r}\frac{\partial}{\partial r}\left(r\frac{\partial N(x,r)}{\partial r}\right)\right]-\frac{K}{2}\left[N(x,r)\right]^2 \tag{4.6}$$

where, *x* and *r* are the spatial coordinates in the downwind and crosswind direction respectively. The initial particle distribution is given as

$$N(0,r)=\frac{S_0}{\pi U\sigma_0^2}\exp\left(-\frac{r^2}{\sigma_0^2}\right) \tag{4.7}$$

In terms of dimensionless variables $N^*(x,r')=\frac{U\sigma_0^2}{S_0}N(x,r)$, $r'=r/\sigma_0$, Eq.(4.6) reduces to

$$\frac{\partial N^*(x,r')}{\partial x}=\frac{1}{4}\frac{dW(x)}{dx}\left[\frac{1}{r'}\frac{\partial}{\partial r'}\left(r'\frac{\partial N^*(x,r')}{\partial r'}\right)\right]-\frac{\beta}{\sigma_0}\left[N^*(x,r')\right]^2 \tag{4.8}$$

where, *W*(*x*) is the dimensionless variance of the plume width:

$$W(x)=\frac{\sigma^2(x)}{\sigma_0^2}=1+\frac{4D_0}{\sigma_0^2 U}x+\frac{C\varepsilon}{\sigma_0^2 U^3}x^3\text{, and} \tag{4.9}$$

$$\beta=\frac{K}{2}\frac{S_0}{U^2\sigma_0} \tag{4.10}$$

with the initial condition

$$N^*(0,r')=\frac{1}{\pi}\exp\left(-r'^2\right). \tag{4.11}$$

As in the puff case, a Fourier space solution is developed by defining a 2-D Fourier Transform (FT) on the radial variable:

$$\varphi(x,k)=\iint N^*(x,r')\exp\left(-2\pi i\vec{k}\cdot\vec{r}'\right)d^2r' \tag{4.12}$$

Upon taking the FT of Eq.(4.8)

$$\frac{\partial\varphi(x,k)}{\partial x} = -\frac{1}{4}\frac{dW(x)}{dx}k^2\varphi(x,k) - \frac{\beta}{\sigma_0(2\pi)^2}\int_{k'}\varphi(x,k')\varphi(x,k-k')d^2k' \qquad (4.13)$$

Gaussian approach in the puff case is adopted to solve the Eq.(4.13), since the function ($W(x')$) does not have radial dependence. As earlier, the following ansatz is used that accounts for the coagulation induced flattening effect on the evolution of the variance of the plume:

$$\phi(x,k) \approx \psi(x)\exp\left(-\xi(x)\,k^2/4\right) \qquad (4.14)$$

where, $\psi(x)$ is the survival fraction and $\xi(x)$ is the variance (non-dimensional) of the spatial dispersion of particles in the cross-wind plane. By substituting Eq.(4.14) in Eq.(4.13), and collecting terms within the k^2 order, one obtains the following set of equations:

$$\frac{d\psi}{dx} = -\frac{\beta}{2\pi\sigma_0}\frac{\psi^2}{\xi} \qquad (4.15)$$

$$\frac{d\xi}{dx} = \frac{dW}{dx} + \frac{\beta}{4\pi\sigma_0}\psi \qquad (4.16)$$

4.3. Survival fraction for constant diffusion coefficient

For illustrating the analytic solvability of the plume model, one may ignore cubic dispersion and assume only constant diffusion coefficient: One then has, $W(x) = 1 + \frac{4D_0}{\sigma_0^2 U}x$ and $\frac{dW}{dx} = \frac{4D_0}{\sigma_0^2 U}$. Upon substituting this in Eq.(4.16), the coupled nonlinear ODEs (Eq.(4.15) & Eq.(4.16)) can be integrated analogous to the 3-D case. One obtains an exact, albeit implicit, relation between the survival fraction and the downstream distance as follows:

$$\int_0^{\frac{1-\psi}{B\psi}} (1 + B\,p)^{1/2}\exp(p)\,dp = \frac{4D_0}{\sigma_0^{\,2}}\frac{x}{U} \qquad (4.17)$$

where, B is the crucial dimensionless parameter, defined as

$$B = \frac{\beta\sigma_0 U}{8\pi D_0} = \frac{KS_0}{16\pi D_0 U} \tag{4.18}$$

Although this cannot be reduced any further, graph between x and ψ can be generated by evaluating the integral for various values of ψ from which x may be estimated.

An important feature of the solution given in Eq.(4.17) is that the survival fraction tends to zero as x tends to infinity. It can be shown from asymptotic expansion that for large values of the RHS of Eq.(4.17), the survival fraction approximates to the formula

$$\psi(x) \approx \frac{1}{1 + B\ln\left[1 + \frac{4D_0}{\sigma_0^{\,2}}\frac{x}{U}\right]} \tag{4.19}$$

which is also known as classical Jaffe result in columnar ion recombination theory. As may be seen, ψ tends to zero as x tends to infinity irrespective of the value of diffusion coefficient. However this monotonic reduction occurs very slowly and in practice turbulent diffusion effects, which are necessarily present in the atmosphere, will take over beyond some distances.

Eq.(4.17) is a closed form solution wherein downwind distance (x) is expressed as an integral function of ψ, which may be easily evaluated with Mathematica (2005). Figure 4.1 shows a comparison of the Eq.(4.17) and Jaffe solution with the numerical solution of the PDE (Eq.(4.6)). Again the prediction from the present analytical formula is almost indistinguishable from the accurate numerical results. In 2D, the survival fraction eventually should tend to zero since, unlike in 3D, there do not exist enough diffusive pathways to escape recombination. The difficulty arises in extending this model from puff to plume geometry due to intermixing of puffs.

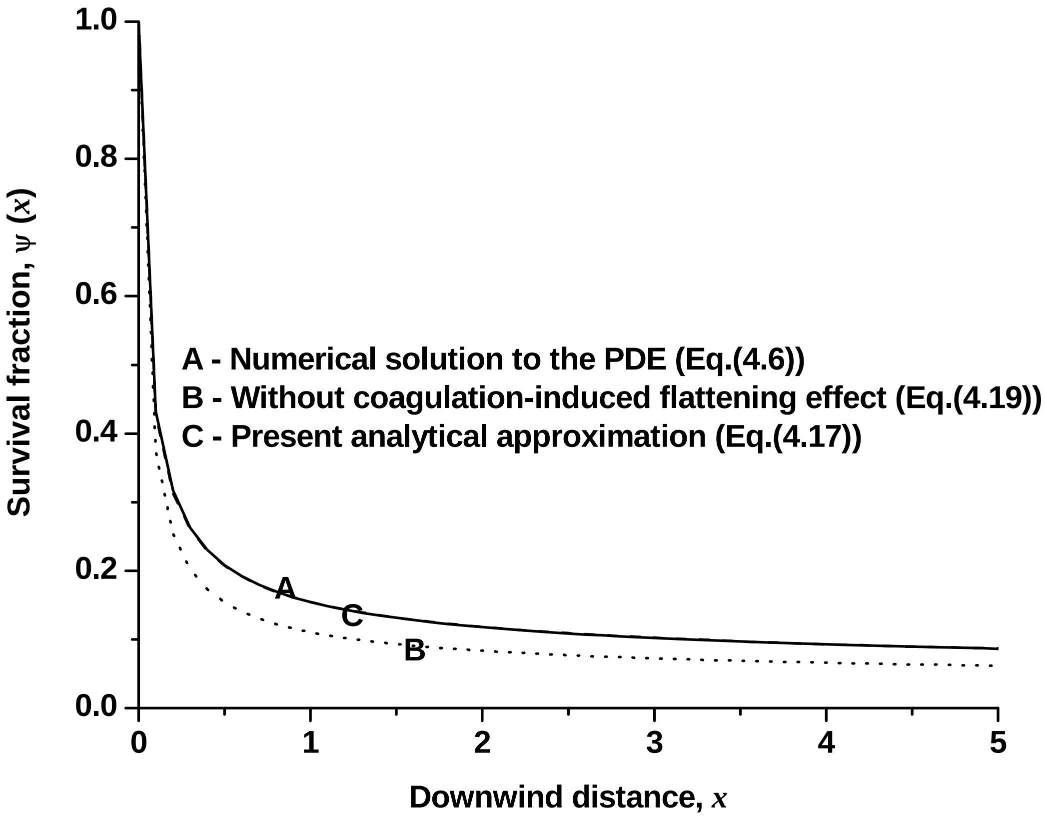

Fig. 4.1: Comparisons of different approaches for the temporal variations of the survival fraction for a cylindrical column ($d = 2$) for the case with $B = 10$.

4.4. Survival fraction for the case of turbulent diffusion

In view of the above, incorporation of turbulent diffusion is inescapable to provide estimates of the survival fraction of particles in plumes which disperse into background. One then has to necessarily solve the cubic variance equation given in Eq.(4.9).

Supposing the initial constant diffusion coefficient is very small (this has been justified by actual numerical computation as well) compared to the rapidly increasing quadratic diffusion coefficient, the second term in Eq.(4.9) can be neglected and the Eq.(4.9) can be written as

$W(x)=1+\frac{C\varepsilon}{\sigma_0^2 U^3}x^3$. Let us introduce a new dimensionless downstream distance variable $\eta=\frac{\beta}{3\sqrt{3}\mu\sigma_0}x$ to render the coupled equations ((4.15) & (4.16)) simpler. Then Eqs. (4.15) and (4.16) are modified to

$$\frac{d\psi(\eta)}{d\eta}=-\frac{3\sqrt{3}\mu}{2\pi}\frac{\psi^2(\eta)}{\xi(\eta)} \tag{4.20}$$

$$\frac{d\xi(\eta)}{d\eta}=3\eta^2+\frac{3\sqrt{3}\mu}{4\pi}\psi(\eta) \tag{4.21}$$

where, $\mu=\frac{\beta U}{3\sqrt{3}\left(C\varepsilon\sigma_0\right)^{1/3}}=\frac{KS_0}{6\sqrt{3}\,U\sigma_0^{4/3}\left(C\varepsilon\right)^{1/3}}$. (4.22)

As in the earlier case, the second term in Eq.(4.21) represents the contribution of coagulation-induced flattening to the evolution of the plume variance. It is worth noting that the case of non-constant diffusion problem also possesses a single coupling parameter μ, analogous to A in the constant D case (for puff releases) discussed in Section 3.3 of Chapter 3.

Eqs. (4.20) and (4.21) cannot be solved exactly. However, when the coupling parameter μ is small (<<1, weak coagulation), one can ignore coagulation-induced flattening of the plume and hence neglect the second term in Eq.(4.21). Under this assumption $\xi(\eta)=W(\eta)$, the survival fraction is given by,

$$\psi(\eta)\approx\frac{1}{1+\frac{3\sqrt{3}}{2\pi}\mu\int_0^{\eta}\frac{d\eta'}{\xi(\eta')}}=\frac{1}{1+\frac{\mu}{4\sqrt{3}\pi}\left[\sqrt{3}\pi-3\ln\frac{\left(1-\eta+\eta^2\right)}{\left(1+\eta\right)^2}-6\sqrt{3}\tan^{-1}\left(\frac{1-2\eta}{\sqrt{3}}\right)\right]}$$

(small μ limit) (4.23)

Upon taking the limit of η→∞, the asymptotic survival fraction is given by,

$$\psi(\infty) \approx \frac{1}{1+\mu} \qquad \text{(small } \mu \text{ limit)} \qquad (4.24)$$

In general for arbitrary μ, the coupled ODEs have to be solved numerically which can be easily executed using packages such as Mathematica (Wolfram Research, Inc., 2005). Since the quantity of crucial importance is the asymptotic survival fraction which will be a function of only one parameter, this quantity is numerically computed over a wide range of μ. For practical applicability, a function is fitted to these values, having a mathematical form analogous to that rigorously obtained in the puff case to maintain consistency between the formulae. The fitted formula for the plume model is

$$\psi^{plume}(\infty) = \frac{1}{(1+1.32\,\mu)^{0.76}}. \qquad \text{(fitted)} \qquad (4.25)$$

Fig.4.2 shows the fitted expression along with the plot of Eq.(4.24) over a wide range of μ varying from 0 to 10^5. Upon multiplying $\psi^{plume}(\infty)$ with the particle number emission rate (S_0) at the source region, the ultimate number loading rate, $S(\infty)$, of particles to the atmospheric background, which eventually survive intra-plume coagulation can be obtained.

The model has an important implication in respect of the dependency of the ultimate number loading rate on the initial data. For the purpose of illustration, the fitted exponent (0.76) in Eq. (4.25) is replaced by 0.75 (=3/4). Then for large μ, the ultimate number loading rate to the aerosol background may be expressed as

$$S(\infty) = S_0 \psi^{plume}(\infty) \sim S_0^{1/4} K^{-3/4} \sigma_0 U^{3/4} \varepsilon^{1/4} \quad (\mu >> 1) \qquad (4.26)$$

This is a remarkable result which implies that the ultimate number loading rate is relatively insensitive ($\sim S_0^{1/4}$) to the assumed value of original number emission rate. An uncertainty by a factor of 100 in the choice of S_0 would only alter the loading rate by a factor of a little over 3. Similar is the situation in respect of ε. These weak dependencies provide certain robustness to the formulation and make it possible to estimate the loading factors within far lower ranges of uncertainties than the uncertainties associated with the original parameters.

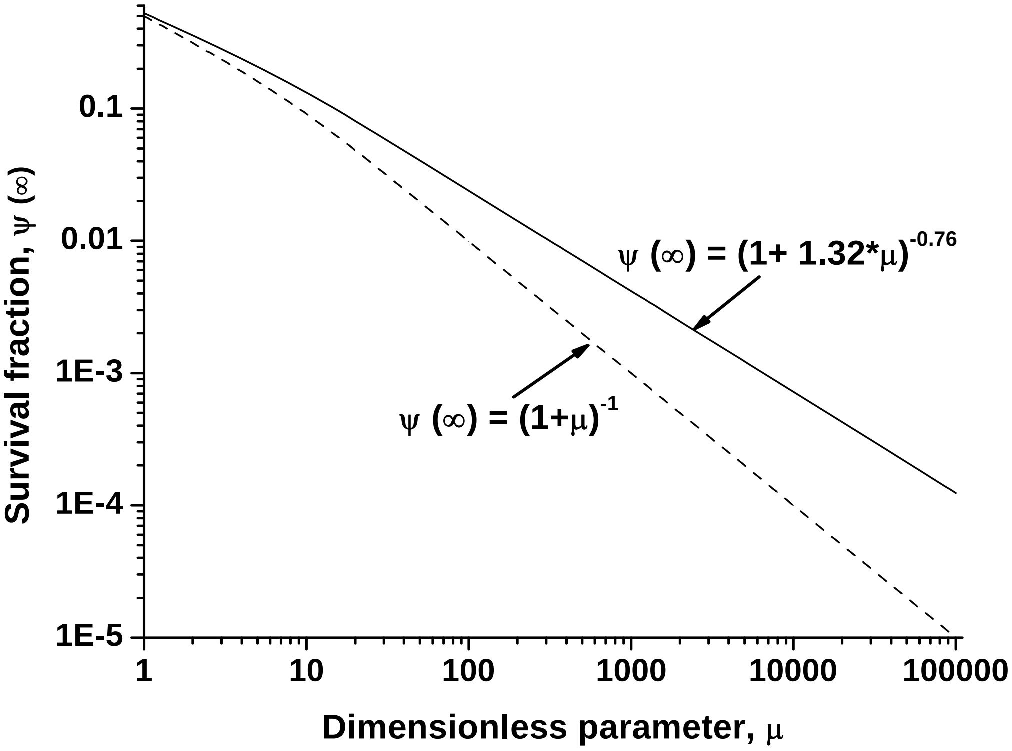

Fig.4.2: Survival fraction in the plume as a function of μ (turbulent diffusion case)

4.5. Coagulation in a spatially inhomogeneous plume: Origin of bimodal size distribution

In the previous chapters, the focus is essentially on the evolution of the total number concentration, without having to obtain detailed size distributions. When particles are nucleated from finite size sources, their concentration will be highest at the centre of the source and would decrease rapidly at the periphery. As noted in the context of studying the coagulation induced flattening, due to spatial inhomogeneity, coagulation will be most pronounced at the centre of the source giving rise to larger particles after a short time, as compared to those at the periphery. This differential coagulation rate will result in a bimodal distribution of particle sizes. We illustrate the possibility of this phenomenon below by a simple model that captures the essence of spatial inhomogeneity and coagulation.

Let us consider a circular combustion source of radius a, (say, a circular tip of burning wood) kept in a flow field having small advection velocity normal to the source plane. In the earlier treatments, we assumed Gaussian profiles for the spatial distributions under an implicit understanding that the diffusion process will eventually render all distributions into a Gaussian shape, after sufficient time. When diffusion is weak, the spatial number concentration profile will have the shape of a nearly flat top near the source. This shape represents high and uniform concentration in the central regions and a rapid fall near the periphery. Although one may construct a large number of mathematical functions having this shape, for simplicity the following form is choosen

$$N(r,0) = N_0(r) = N_0(0)\,\mathrm{erfc}\left(\frac{r-a}{s}\right) \tag{4.27}$$

where, $N_0(0)$ is the number concentration at the centre of the circle, and s is a constant.

Let us assume that these particles are monodisperse having volumes,u_0. Due to the flow field, these particles will be advected along say, X- direction normal to the plane of the source, and then let us denote time as $t = x/v$, where v is the advection velocity. Let us assume that there is no lateral diffusion. In other words, we are going to consider only an early time process of a high concentration aerosol whose coagulation time scale is far smaller than the diffusion time scale, near the source region. If the lateral diffusion is ignored, then particles at different radial points will coagulate at different rates dictated by their concentration, $N_0(r)$. Let us denote their size distribution at a radial distance r from the centre-line as $n(r,u,t)$. If the initial concentrations are very large, then the size distribution will attain self-preserving form (similarity form) having r -dependent characteristic parametters. From the standard similarity theory, this may be expressed as,

$$n(u,r,t) = \frac{N^2(r,t)}{u_0 N_0(r)}\ g\left\{\frac{u\ N(r,t)}{u_0 N_0(r)}\right\} \tag{4.28}$$

where, $N(r,t)$ is the size integrated number concentration at r, t:

$$N(r,t) = \int_0^\infty n(u,r,t)du \tag{4.29}$$

and $g(\eta)$ is the scaling function having the property:

$$\int_0^\infty g(\eta)d\eta = 1\ \ \&\ \ \int_0^\infty \eta g(\eta)d\eta = 1 \tag{4.30a, b}$$

Since we are considering nano-particles, their coagulation process may be adequately described by free-molecular kernel. Depending upon the fractal dimension of the particles, it will possess a homogeneity index α, ($1/6 < \alpha < 1/2$). 1/6 corresponds to compact clusters and 1/2 will be that for fractal dimension less than 2. Also, for a scaling kernel, similarity theory yields the result:

$$N(r,t) = \frac{N_0(r)}{\left[1 + (1-\alpha)K_0 N_0(r)t\right]^{1/(1-\alpha)}} \tag{4.31}$$

where, K_0 is an effective coagulation coefficient.

As time progresses (i.e. as the particles move away from the source), coagulation will become weaker and weaker and dispersion will eventually overtake the coagulation effect. More significantly, due to dispersion, the particles will be mixed in space resulting in an effective size distribution across the entire plume. Let us say that this happens after a time, say t_c. The size distribution over the entire plume after time t ($< t_c$) is obtained by integrating Eq.(4.28) over all r.

$$f(u,t) = \int_0^\infty 2\pi\ r\ n(u,r,t)\,dr = \int_0^\infty 2\pi\ r\ \frac{N^2(r,t)}{u_0 N_0(r)}\ g\left\{\frac{u\ N(r,t)}{u_0 N_0(r)}\right\} dr \tag{4.32}$$

In order to evaluate the integral, we need to assume a form for the scaling function $g(\eta)$. This function generally satisfies an ordinary, nonlinear integro-differential equation and excepting for constant kernel no analytical forms are available. However, these functions have been numerically evaluated for Brownian and free-molecular kernels (Friedlander, 2000). The characteristic feature of this function is that it has a well-defined peak and is skewed to the right. Hence, for practical purpose it may be approximated by a normalized lognormal distribution, with two free parameters.

$$g(\eta) = \frac{1}{\eta \ln\sigma_g \sqrt{2\pi}} \exp\left\{-\frac{\ln(\eta/\eta_0)^2}{2(\ln\sigma_g)^2}\right\} \tag{4.33}$$

The application of the additional constraint (Eq.(4.30b)) leads to the relation

$$\eta = \exp\left\{-\frac{(\ln\sigma_g)^2}{2}\right\} \tag{4.34}$$

Hence, $g(\eta)$ will have one free parameter which will vary depending on the type of the coagulation kernel. In the foregoing, we use it as a free parameter to illustrate the effect. Let us now evaluate Eq.(4.32) by using Eqs.(4.27), (4.31), (4.33), (4.34). For typical calculation, the following parameters are assumed: $\alpha = 1/6$, $\sigma_g = 1.5$, $s = 0.1a$ ($a = 1$). The time parameter is rendered dimensionless by defining

$$\tau = (1-\alpha) K_0 N_0(0)\, t \tag{4.35}$$

The integration (Eq.(4.32)) is carried out numerically using Mathematica software, for different values of τ. The results are shown in Fig.4.3.

It is seen from the figure 4.3 that the system gradually develops a second mode as τ increases. This mode broadens with time eventually becoming a long tail of the first mode.

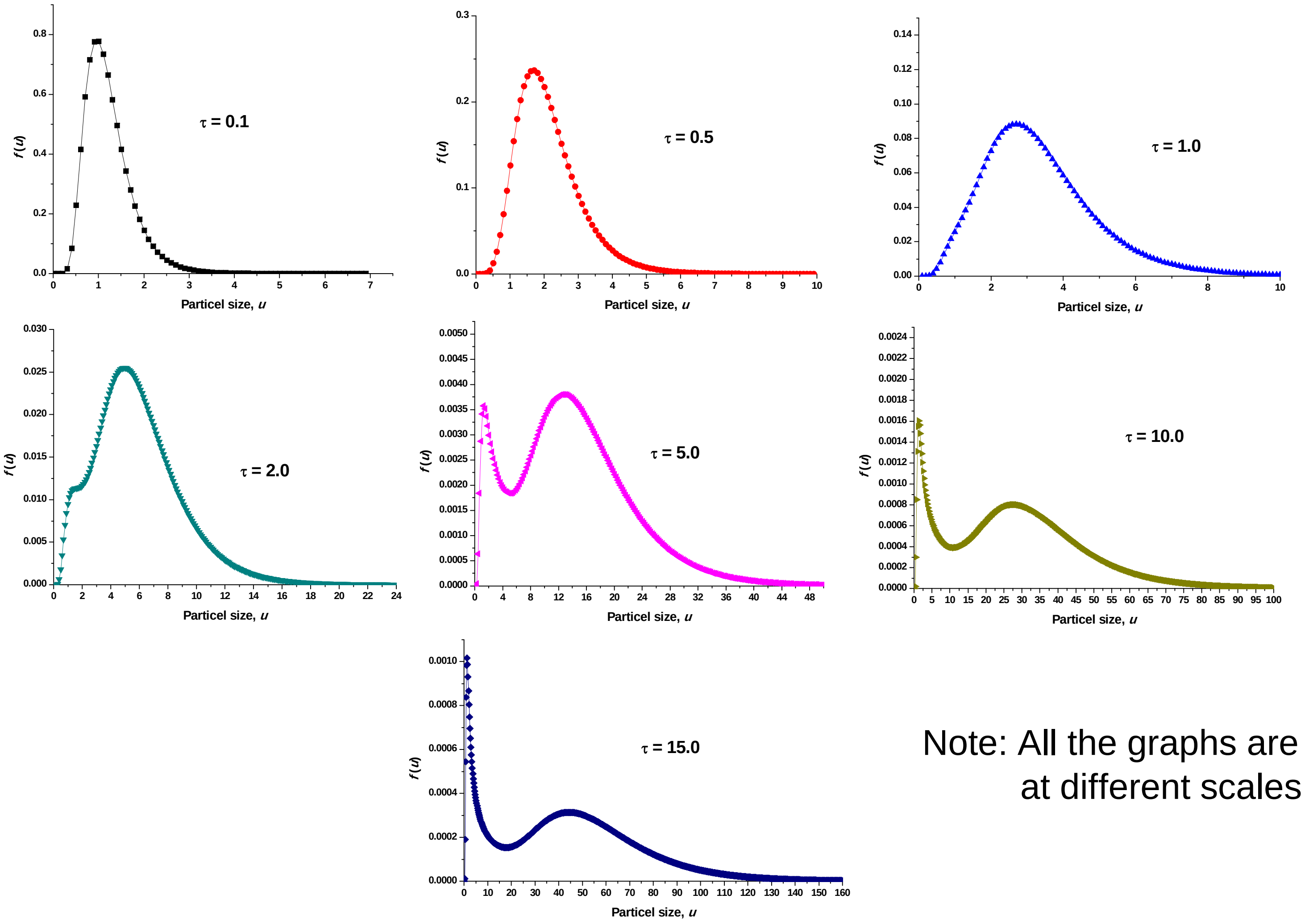

Note: All the graphs are
at different scales

Fig.4.3: Evolution of bimodal size distribution in a spatially inhomogeneous plume

Although not shown in the figure, several simulations are carried out using various values of the parameters. The features of the bimodal phenomenon are somewhat insensitive to the form of the functions chosen. Generally, the sharpness of the second mode increases as the scaling function becomes narrower, (when σ_g is decreased) and as the initial concentration distribution gets tighter (as the s parameter is reduced). An increasing α index causes the second peak to appear earlier apart from broadening it.

Although highly qualitative and phenomenological, the foregoing analysis illustrates that the bimodality induced by spatial heterogeneity is a simple consequence of differential coagulation growth rates of the particle sizes in different regions of a finite sized particle source. This would be especially more pronounced at early times when the concentrations are high. One can expect that this process will be ubiquitously present in combustion sources or sources operating by vapour condendsation processes, which will rapidly cease as the plume disperses with distance. The distributions emerging out of the combined effect can only be modeled on a case-to-case basis by taking the source distributions and disperion characteristics. In this section, it is merely demonstrated the possibility of spatial inhomogeneity as a factor to be considered in understanding bimodality (see next chapter) and we relegate further work on this topic to future studies.

4.6. Applications of the model to Forest fires

In the case of combustion aerosols, the freshly emitted particle number concentration lies in the range of (10^{11}-10^{14}) #/cm^3 near the combustion sources or the plumes of less age (Lighty et al, 2000). The forest fires are the large combustion sources that affect the climate drastically over large areas. It is found that the length of the headfire is in the range of few hundreds of meters to few kilometers (Hobbs et al, 2003), and it may be discontinuous in nature. Hence a plume width of 1000 m (1 km) is considered for this study. The mass emission rate is taken as 1000 kg/sec (Ichoku & Kaufman, 2005). The corresponding number emission rate to this mass emission is calculated to be ~2.0 x 10^{24} #/sec (Eq.4.2) by considering the average particle diameter of 10 nm and a density of 1 g/cm^3. The atmospheric turbulent kinetic energy dissipation rate (ε) is taken as 5.0 x 10^{-4} m^2/sec^3, and the constant (C) used in the turbulent diffusion model is around 0.8 (Chen, 1974; Pandey & Pandey, 2007; Ott & Mann, 2000). A typical wind velocity of 2 m/sec is considered for this case study. With these input values, the value of the parameter μ is 1.31x10^5, and the asymptotic survival fraction (Eq.(4.25)) is ~1.1 x 10^{-4}. It may be noted that the Jaffe type solution (Eq.(4.24)) yields a much lower survival fraction of 7.7 x 10^{-6} which clearly demonstrates that coagulation induced flattening has a significant effect in intense, large and extended time sources such as forest fires. The total particle injection rate becomes 2.2 x 10^{20} #/sec. One may estimate the corresponding number averaged particle diameter injected into background as ~200 nm.

The robustness of the result in respect of the initial data on number emission rate may also be illustrated as follows. Considering the case discussed above, if S_0 = 2.0 x 10^{20} (lower by a factor of 10^4) and other parameters remained the same, then μ=13.1, the survival fraction $\psi^{plume}(\infty)$=0.11. However the ultimate number loading rate $S(\infty)$ would still be about 2.1 x 10^{19} #/sec, which is only one order lower than the previous value. Similarly one can show that if ε increased by factor of 1000, $S(\infty)$ would reduce only by about a factor of 10. These illustrations indicate that it is not quite crucial to have very accurate values for some of the "difficult to estimate" initial parameters for predicting the number of particles contributed by strong continuous sources to the atmosphere that persist as background aerosols. While it is recognized that there is no alternative to full numerical computations for detailed information on aerosol distributions, the summary formulae presented here could still serve as useful guidelines for establishing the relative importance of processes in implementing these models.

4.7. Summary

The present study addresses the question of plume emissions from localized sources in the presence of atmospheric turbulence. It provides simple scaling relations for the survival fractions and the number loading factors. In the case of plume model, the results demonstrate a certain level of robustness of the ultimate particle loading rates with respect to the initial data on the initial number emission rates and atmospheric turbulence energy dissipation rates, which is reassuring in view of the practical difficulties in obtaining these data accurately. For plume of initial width σ_0 emitting S_0 particles per unit time, the formula for the survival fraction obtained by fitting the numerical solutions is obtained as $\psi^{plume}(\infty) = (1 + 1.32\,\mu)^{-0.76}$ where, $\mu = KS_0 \Big/ \left\{6\sqrt{3}\,U\sigma_0^{4/3}(C\varepsilon)^{1/3}\right\}$ and C is a constant (~0.8). Further, it is shown that the atmospheric ultimate number loading factor ($S(\infty)$) is relatively insensitive to the original number emission rate (~$S_0^{1/4}$), and the turbulent energy dissipation rate (~$\varepsilon^{1/4}$), when the source is intense. It is hoped that it might be possible to test some of the results by both direct numerical simulations and experimental measurements in future studies.

Chapter 5. Coagulation of nanoparticle aerosols released continuously into a well stirred chamber

5.1. Introduction

The presence of sources of anthropogenic nanoparticles, particularly in the indoor atmosphere of workplaces and schools, is of considerable concern with regard to their impact on human health. One characteristic feature of nanoaerosols is their dynamic evolution with respect to concentration and size distribution during the time of transport from the source to the receptor due to various mechanisms. In a recent study, Schneider et al. (2011) discuss the importance of such modifying factors for the metrics used to estimate the potential hazard of ENPs and, indeed, efforts are increasing to understand how such aerosols evolve in the indoor environment (Seipenbusch et al, 2008, Schneider & Jensen, 2009, Schneider et al, 2011).

The factors responsible for changes in the number concentration and size distribution of an aerosol include homogeneous and heterogeneous coagulation, as well as particle removal due for example to ventilation or wall losses. These mechanisms are linked to the characteristics of a nanoparticle source, interaction with preexisting particles, as well as the transport, mixing and dilution conditions specific to a given environment. Although well understood in principle, it is not at all a trivial task to develop meaningful models and to estimate changes, even the order of magnitude of changes, in aerosol size distribution for a given situation; and it is even more difficult to distill general conclusions which will be relevant for a broader type of situation. For this reason, one often resorts to scenarios.

One such scenario of particular relevance to engineered nanoparticles involves their continuous emission into a confined space or a chamber, from a volume source. Several analytical and numerical studies have been carried out for a variety of aerosol systems with continuous source injection (Barrett & Mills, 2002; Schneider & Jensen, 2009; Landgrebe & Pratsinis, 1989; Kim et al. 2003). The details of these studies are discussed in the Literature survey section of Chapter 1. While these studies provide general insight into the phenomena to expect, and of course demonstrate that simulation techniques are well established, they do not offer insights into long time system behaviour and interplay of various mechanisms. Also, they fall short of providing general conclusions relevant for workspaces, i.e. large enclosed volumes of air with constant aerosol sources. It is still of considerable interest to explore the relative influence of various factors driving such systems, and to obtain a better understanding, e.g. of when multimodal aerosol distributions evolve, the relative importance of the modes, etc.

In this context, there exist interesting experimental observations of aerosol evolution for a scenario in which nanoaerosol is continuously injected at different rates into a large, well mixed volume of air, with and without the presence of a background aerosol (Seipenbusch et al, 2008). One such observation is the occurrence of a transient peak in the total number concentration during filling of the chamber, as well as indications of an asymptotic stabilization of the total chamber concentration due to the interplay between freshly injected aerosol and the removal of particles by coagulation or ventilation. It is of considerable practical interest to know under what conditions the concentration would eventually stabilize in the chamber, and how this would depend on source strength and removal rate parameters. Similarly, the conditions for the aerosol to develop a distinct secondary large-particle mode need to be explored because this has a direct impact on the coagulation processes taking place.

Some of the features observed in these experiments are not easily explained or reproduced by straightforward models using constant coagulation kernels, because the dynamics of such systems must exhibit pronounced size dependent features. It is therefore necessary to extend the simulation to realistic coagulation kernels and also examine other effects such as changes in collision radius of particles due to the formation of large fractal aggregates. Given these motivations, the application of a discrete numerical simulation covering the entire particle size regime to investigate solutions to the general dynamic equation with a constant source term and a constant removal term by ventilation is described. Coagulation is treated on the basis of the practically relevant Fuchs kernel and allowing for the growth of fractal particles. A two-group analytical model is developed to assess the asymptotic behaviour of the nanoparticles injected into a closed chamber. Laboratory experiments are carried out to validate these models.

5.2. Formulation of the problem

Let us consider a scenario adapted to the experiments described by Seipenbusch et al. (2008) in which nanoparticles are released continuously into a large volume. The aerosol system evolves by continuous injection of particles at a constant rate, by coagulation, and by removal / dilution with clean air at a constant rate. It must be pointed out that spatial inhomogeneity (Kasper, 1984) is more of a rule than an exception when particles are released from localized sources, and the complexity of addressing these problems has been discussed in previous chapters. Particularly, the effect of spatial inhomogeneity on the size distribution is discussed in the section 4.5 of the chapter 4. However, if the aerosol is mixed rapidly through mixing elements such as fans or induced ventilation, one may, to a first approximation, treat the aerosol concentration as spatially homogeneous at all times. Then the rate of change of aerosol concentration in the chamber is given by

$$\begin{aligned}\frac{\partial n(u,t)}{\partial t} &= S(u,t) + \frac{1}{2}\int_0^u K(u',u-u')\, n(u',t)\, n(u-u',t)\, du' - n(u,t)\int_0^\infty K(u',u)\, n(u',t)\, du' \\ &\quad - \{\lambda_v + \lambda_d(u)\}\, n(u,t)\end{aligned} \tag{5.1}$$

where $K(u, u')$ is the coagulation kernel (m^3s^{-1}) between particles of volumes u and u', $n(u, t)$ is the number concentration (m^{-3}), λ_v is the ventilation rate (s^{-1}), $\lambda_d(u)$ is the removal rate due to wall/surface deposition processes, $S(u,t) = (\dot{V}_s/V)Q$ is the particle number injection rate of the source ($m^{-3}s^{-1}$), $\dot{V}_s$ is the source volume flow rate to the chamber (m^3s^{-1}), V is the volume of the chamber (m^3), and Q is the number concentration at the source (m^{-3}). The initial number concentration in the chamber is assumed to be zero ($n(u, 0) = 0$). The first term in the RHS of Eq.(5.1) represent continuous source injection, the second and third terms represent coagulation, and the fourth for ventilation and size dependent removal processes.

Supposing, for the sake of simplicity, one makes an assumption that the coagulation coefficient may essentially be approximated by an effective constant, i.e. $K(u, v) = K$. Further we assume that the removal rate due to deposition is negligible as compared to ventilation. Then, one obtains the following nonlinear equation from Eq.(5.1) for a constant source term:

$$\frac{dN(t)}{dt} = S - \frac{K}{2}N^2(t) - \lambda N \tag{5.2}$$

where, the total number concentration is defined as, $N(t) = \int_0^\infty n(u,t)\,du$. For the initial condition $N(0) = 0$, the solution to this equation may be easily obtained by quadrature as follows:

$$N(t) = -\frac{\lambda}{K} + \left(\frac{2A}{K}\right)^{1/2}\left[\frac{\exp\left(\sqrt{2AK}\,t\right)\left\{\sqrt{4AK}+\sqrt{2\lambda^2}\right\} - \left\{\sqrt{4AK}-\sqrt{2\lambda^2}\right\}}{\exp\left(\sqrt{2AK}\,t\right)\left\{\sqrt{4AK}+\sqrt{2\lambda^2}\right\} + \left\{\sqrt{4AK}-\sqrt{2\lambda^2}\right\}}\right] \tag{5.3}$$

where, $A = S + \frac{\lambda^2}{2K}$.

At large times, the above expression tends to a steady-state given by,

$$N(\infty) = -\frac{\lambda}{K} \pm \left(\frac{\lambda^2}{K^2} + \frac{2S}{K}\right)^{1/2} \tag{5.4}$$

In the absence of removal processes, the solution of the Eq.(5.2) is given by,

$$N(t) = \left(\frac{2S}{K}\right)^{1/2} \left[\frac{\exp\left(\sqrt{2SK}\ t\right) - 1}{\exp\left(\sqrt{2SK}\ t\right) + 1}\right] \tag{5.5}$$

This leads to a steady-state concentration, $N(\infty) = \left(\frac{2S}{K}\right)^{1/2}$. This is an interesting result that deserves attention. In the absence of ventilation removal, one expects the mass concentration to diverge to infinity after sufficiently long time because of the continuous injection of particles. However, the presence of the coagulation manages to limit the number concentration to a finite value for constant kernel. This raises a question as to whether a finite number concentration will be sustained for size dependent kernels?. The assumption of a constant kernel is reasonable for homogeneous problems involving one time injection of monodisperse particles. In contrast, under continuous injection, the number concentration will be dictated by the fact that the injected nanoparticles will be scavenged by the coagulated large particles and the rate of this scavenging increases with particle size. Constant kernel is a too simplistic an assumption to handle this effect and to address the question raised above, it is necessary to go for the next level of approximation, achieved by formulating the two-group model.

5.3. Two-group model

In order to provide quantitative insights into the temporal behaviour of the total number concentration, the approach of Jeong and Choi (2003) is followed and a simplified two-group model of the coagulation problem under continuous injection is proposed. Let us assume that essentially the behaviour can be described by the interactions between the particles of two different size groups; the first one corresponds to the mean particle volume of the injected nanoparticles (v_1), and the second group to the mean particle volume of the part of the size spectrum of the already coagulated particles ($v_2(t)$) (i.e. excluding the first group). The entire spectrum of the second group is represented by a single effective size determined by mass conservation. This approach is somewhat similar to the two-group model proposed by Jeong and Choi (2003) for the case of coagulation of coalescing particles. Unlike their formulation, we do not consider coalescence. The two-group model results in a purely differential formulation of the coagulation equation which can be easily subjected to mathematical analysis, also at long times. Let $N_1(t)$ be the number concentration of the particles of the first group having constant size v_1, and $N_2(t)$ be the number concentration of the particles of second size group of volume $v_2(t)$ at any given time t. Then, the total number concentration $(N(t))$ is given by,

$$N(t) = N_1(t) + N_2(t) \tag{5.6}$$

The evolution of $N_1(t)$ and $N_2(t)$ proceeds via the coagulation processes described by three kernel types, i) the coagulation coefficient $K_{11}(v_1,v_1)$ among particles of first size group, ii) the coefficient $K_{12}\{v_2(t),v_1\}$ for the coagulation between first group size particles of volume v_1 and second size group particles of volume $v_2(t)$, and iii) the coagulation coefficient $K_{22}\{v_2(t),v_2(t)\}$ between the second size group particles themselves. The effect of externally maintained ventilation is included by introducing a size independent removal term. With this, one can write down the following equations for the process of evolution of $N_1(t)$ and $N_2(t)$:

$$\frac{dN_1(t)}{dt} = S_1 - K_{11}N_1^2(t) - K_{12}\{v_2(t), v_1\}N_1(t)N_2(t) - \lambda N_1(t) \tag{5.7}$$

$$\frac{dN_2(t)}{dt} = \frac{1}{2}K_{11}N_1^2(t) - \frac{1}{2}K_{22}\{v_2(t), v_2(t)\}N_2^2(t) - \lambda N_2(t) \tag{5.8}$$

The evolution equation for the total number concentration (Eq.(5.2)) is now split into two separate evolution equations (Eq.(5.7) & Eq.(5.8)). In Eq.(5.7), the first term on the RHS is the number of particles injected into the study volume per unit time per unit volume, the second term represents the loss of particles from the first group due to homogeneous coagulation. The loss term will not involve the usual factor 1/2 because of the following reason. There will be $1/2\,K_{11}N_1^2(t)$ coagulation events between the primary particles themselves per unit time and since two particles are lost in each event and the coagulated particle is lost from this group to the higher group, the loss rate in the first group will be $2*\left(1/2\,K_{11}N_1^2(t)\right) = K_{11}N_1^2(t)$. The third term on the RHS represents loss of first-size-group particles due to the interaction with the second-size-group particles. Similarly, in the second equation (Eq.(5.8)), the first term (gain term) in the RHS represents the contribution due to homogeneous coagulation of first size group particles, and the second term in the RHS represents the loss of the second size group particles due to their homogeneous coagulation. Heterogeneous coagulation between the first and second size group particles does not contribute to the change in the concentration of second-size-group particles. These two equations need to be supplemented with the mass conservation law which will provide equation for $v_2(t)$ as follows:

Let $\phi(t)$ be the total volume concentration (of both size groups) in the air space (i.e., mass concentration divided by particle density). Since coagulation is a volume (mass) conserving process, $\phi(t)$ increases linearly with time because of steady and continuous injection satisfying the following equation.

$$\frac{d\phi(t)}{dt} = v_1 S_1 - \lambda\phi(t) \tag{5.9}$$

However, $\phi(t)$ is related to $v_2(t)$ and v_1 through the following closure equation,

$$\phi(t) = N_1(t)v_1 + N_2(t)v_2(t) \tag{5.10}$$

From Eqs. (5.9) and (5.10), one can obtain the following relation for the volume of the second size group,

$$v_2(t)=\frac{\phi(t)-N_1(t)v_1}{N_2(t)} \tag{5.11}$$

The initial conditions for this model are,

$$N_1(0)=0; N_2(0)=0; v_2(0)=0; \phi(0)=0 \tag{5.12}$$

Although the above set of equations is nonlinear and complex, it is attractive because it can be easily solved for any type of kernel using differential equation solver packages such as Mathematica. More importantly these equations are amenable to asymptotic analysis in order to elicit the long time behaviour of the solutions analytically.

5.3.1. Additive coagulation kernel

In order to illustrate the usefulness of the two-group model, we first apply it for a size dependent, yet relatively simple, coagulation kernel such as the (*u*+*v*) kernel, which is analytically solvable. The additive coagulation kernel ((*u* + *v*) kernel) arises in the study of cloud droplet coalescence (Bertoin, 2002; Scott, 1968; Berry, 1967; Hidy & Brock,), gravitational clustering in the universe (Sheth & Pitman, 1997), and phase transition for parking (Chassaing & Lochard, 2001). This kernel has the following form,

$$K(u,v)=\alpha(u+v) \tag{5.13}$$

where, α is a constant.

By substituting the Eq.(5.13) in Eqs.(5.7) & (5.8), one can obtain,

$$\frac{dN_1(t)}{dt}=S_1-2\alpha\, v_1N_1^2(t)-\alpha[v_1+v_2(t)]N_1(t)N_2(t)-\lambda N_1(t) \tag{5.14}$$

$$\frac{dN_2(t)}{dt}=\alpha\, v_1N_1^2(t)-\alpha\, v_2(t)N_2^2(t)-\lambda N_2(t) \tag{5.15}$$

The evolution equation for total number concentration can be obtained from Eqs.(5.14) & (5.15) by using the relations, $N(t)=N_1(t)+N_2(t)$,and $N_2(t)v_2(t)=\phi(t)-N_1(t)v_1$, and is given by,

$$\frac{dN(t)}{dt} = S_1 - \alpha\phi(t)N(t) - \lambda N(t) \qquad (5.16)$$

Let us non-dimensionalise the above equation by introducing the following dimensionless variables,

$$\left.\begin{aligned} &t^* = t/t_c, && \text{where, } t_c = \left(S_1 K_{11}\right)^{-1/2} \\ &N^*(t^*) = N(t)/N_c, && \text{where, } N_c = \left(S_1 / K_{11}\right)^{1/2} \\ &\lambda^* = \lambda\, t_c, && \\ &\phi^*\left(t^*\right) = \alpha\, \phi(t)\, t_c && \end{aligned}\right\} \qquad (5.17)$$

where, $K_{11} = K\left(v_1, v_1\right) = 2\alpha\, v_1$, from Eq.(5.13). By substituting the parameters defined in Eq.(5.17) in Eqs.(5.16) & (5.9), the following set of equations can be obtained:

$$\frac{dN^*(t^*)}{dt^*} = 1 - \phi^*\left(t^*\right)N^*(t^*) - \lambda^* N^*\left(t^*\right) \qquad (5.18)$$

$$\frac{d\phi^*(t^*)}{dt^*} = \frac{1}{2} - \lambda^* \phi^*\left(t^*\right) \qquad (5.19)$$

Eq.(5.18) and (5.19) together form the complete set of equations for the total number concentration. It may be easily verified that one arrives at the same set of equations starting from the unapproximated coagulation equation (Appendix - D), for the kernel under consideration. In view of this and the fact that the equations are simple to solve, the predictions from this case provide valuable guiding results on the general behaviour for more complex, size dependent kernels. Let us examine the behaviour of this system when $\lambda^* = 0$. In this case, the Eq.(5.18) becomes,

$$\frac{dN^*(t^*)}{dt^*} = 1 - \frac{1}{2} N(t^*)\, t^* \qquad (5.20)$$

where, ϕ^* is replaced by $t^*/2$. The solution of the Eq.(5.20) is obtained by quadrature and given as,

$$N^*(t^*) = \int_0^{t^*} \exp\left\{-\frac{1}{4}\left(t^{*2} - t'^2\right)\right\} dt' \tag{5.21}$$

Let $(t^*\text{-}t') = x$, then the Eq.(5.21) can be written as,

$$N^*(t^*) = \int_0^{t^*} \exp\left\{-\frac{1}{4} x\left(2t^* - x\right)\right\} dx \tag{5.22}$$

Since major part of the contribution to the integral will arise from points near $x \sim 0$, we may assume $x << t^*$ in the integrand above in which case Eq.(5.22) is reduced to,

$$N^*(t^*) \approx \int_0^{t^*} \exp\left\{-\frac{t^* x}{2}\right\} dx = \frac{2}{t^*}\left[1 - \exp\left\{-\frac{t^{*2}}{2}\right\}\right] \tag{5.23}$$

From Eq.(5.23), the asymptotic number concentration (as $t^* \to \infty$) is,

$$N^*(t^*) \approx \frac{2}{t^*} \qquad \text{(for } \lambda^*\text{=0)} \tag{5.24}$$

Eq.(5.24) shows an important result that the total number concentration decays as t^{*-1} in the absence of removal processes.

For nonzero λ^*, the analytical solution is not very convenient as it involves higher mathematical functions. In view of this, Eqs.(5.18) & (5.19) are solved together using the numerical solver of Mathematica. For various removal rates, the temporal variation of total number concentration is plotted in Fig. 5.1. One notes that for $\lambda^* = 0$, the concentration falls monotonically with time. A fit to the graph for large times shows that $N^* \sim 1/t^*$, which is in agreement with analytical theory (Eq.(5.24)). When a slight ventilation removal is present, the concentration tends to approach a nonzero steady state. The value of this steady state increases with ventilation for $\lambda^* = 0.01, 0.1, 0.6$ and decreases for higher ventilations (e.g. $\lambda^* = 2.0, 10.0$). This is an interesting result that predicts a critical ventilation parameter for which the steady-state particle concentration will be maximum.

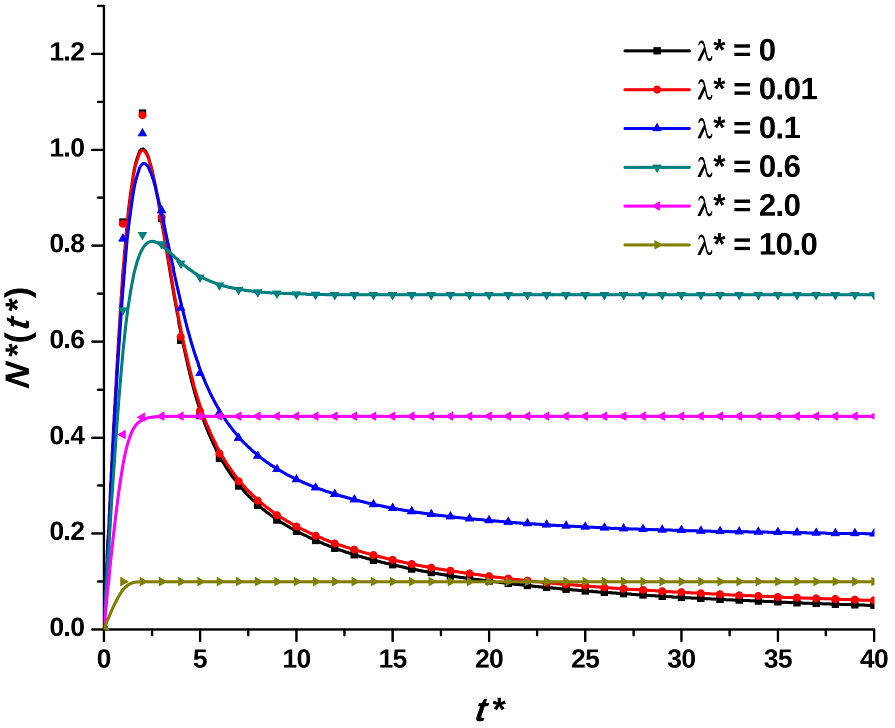

Fig. 5.1: Temporal evolution of the scaled concentration ($N^*(t^*)$) for various removal rates (λ^*)

In order to understand this somewhat intriguing result, we solve the equation analytically for the special case of steady-state (i.e., $d/dt^* = 0$). The following steady-state solutions may easily be obtained from Eq.(5.18, 5.19):

$$N^* = \frac{2\lambda^*}{1+2\lambda^{*2}} \qquad \text{(Steady-state number concentration)} \qquad (5.25)$$

$$\phi^* = \left(1/2\lambda^*\right) \qquad \text{(Steady-state volume/mass concentration)} \qquad (5.26)$$

This example clearly demonstrates in a simple way that the steady-state concentration is achievable only in the presence of removal processes as shown in the Eq.(5.25). From Eq.(5.25), it can be shown that steady-state concentration attains a peak value for a removal rate $\lambda^* = \left(1/\sqrt{2}\right) = 0.707$. This removal rate is called as critical ventilation rate. Beyond the critical ventilation rate, the concentration decreases as expected (Fig.5.2). Considering the practical importance of this result in ventilation design for removal of high particle concentration in workplace environments, it is pertinent to explore the consequence for other kernels. More detailed discussion on this topic is presented in Section 5.5.1.4 (for the case of Fuchs coagulation kernel).

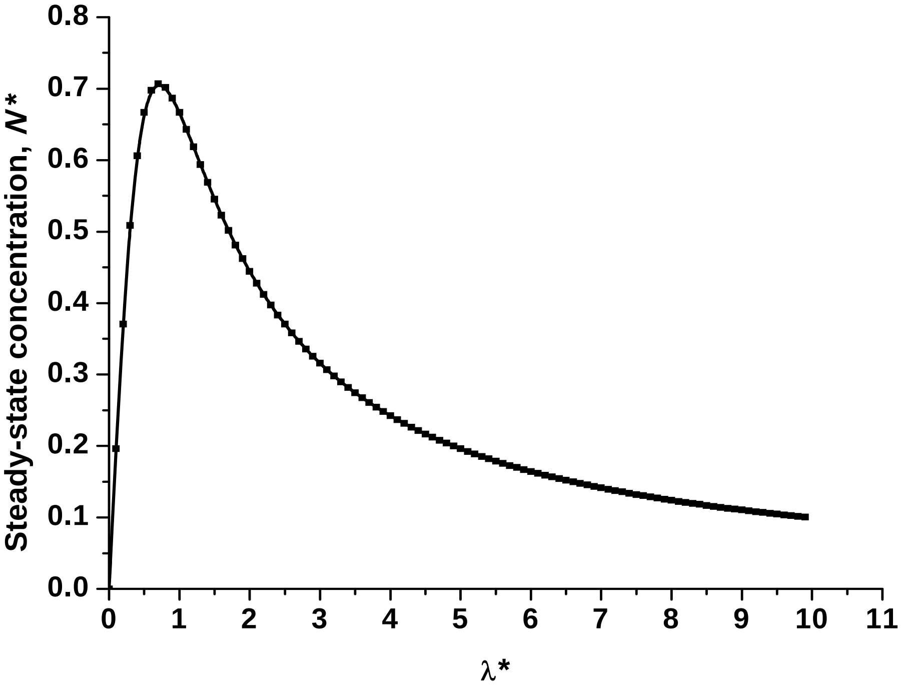

Fig. 5.2: Steady-state number concentration vs. removal rate in the case of ($u + v$) type kernel

5.3.2. Fuchs coagulation kernel

Fuchs coagulation kernel is very often used in the study of Brownian coagulation process, and it is applicable for the entire particle regime (from free-molecular regime to continuum regime). Since the Fuchs kernel has a form of complex function unlike the additive kernel mentioned above, the analysis is carried out by numerical methods to obtain complete solution of

Eqs.(5.7) & (5.8). However, the asymptotic behaviour of this system is obtained analytically as follows:

Since the particle sizes of the first group (primary) do not change with time, the homogeneous coagulation coefficient will be a constant quantity, say $K_{11} = \sqrt{\frac{16\pi kTr_0^4}{\rho v_0^2}}2^{d_f} v_1^{1/2}$, given by the free-molecular limit of the Fuchs kernel. Here, d_f is the fractal dimension, k is the Boltzmann constant, T is the temperature, μ is the air viscosity, r_0 is the radius of the individual spherule of volume v_0, and ρ is its density. In the asymptotic limit of long times, the characteristic volume $v_2(t)$ of the second group particles will be large and hence the Fuchs kernel corresponding to their mutual coagulation will approach the continuum Smoluchowski kernel ($K_{22}\{v_2(t), v_2(t)\} = \frac{8kT}{3\mu}$) which will be again a constant regardless of time. On the other hand, the heterogeneous coagulation coefficient (K_{12}) between first group and second group particles will be time dependent according to the formula,

$$K_{12}\{v_2(t), v_1\} = \frac{2kT}{3\mu}\left[v_2^{1/d_f}(t) + v_1^{1/d_f}\right]\left[\frac{1}{v_2^{1/d_f}(t)} + \frac{1}{v_1^{1/d_f}}\right] \approx const\left(\frac{v_2(t)}{v_1}\right)^{1/d_f} \tag{5.27}$$

To render the equation more transparent for mathematical analysis, it is advantageous to introduce non-dimensional variables (some of them as in the text) as follows:

$$\left.\begin{aligned}
&t^* = t/t_c, \qquad\qquad \text{where, } t_\mathrm{c} = \left(S_1 K_{11}\right)^{-1/2}\\
&\left\{N_1^*(t^*), N_2^*(t^*)\right\} = \left\{N_1(t), N_2(t)\right\}/N_c, \text{where, } N_\mathrm{c} = \left(S_1/K_{11}\right)^{1/2}\\
&u(t^*) = \frac{v_2(t^*)}{v_1}\\
&k_1 = \frac{1}{u^n}\frac{K_{12}}{K_{11}}\\
&k_2 = \frac{K_{22}}{K_{11}}\\
&n = d_f^{-1}
\end{aligned}\right\} \tag{5.28}$$

With these notations and by using the appropriate asymptotic limits of the Fuchs kernel, Eqs. (5.7-5.11) may be written in the following simpler form:

$$\frac{dN_1^*(t^*)}{dt^*} = 1 - \left[N_1^*(t^*)\right]^2 - k_1\left[u(t^*)\right]^n N_1^*(t^*)N_2^*(t^*) \tag{5.29}$$

$$\frac{dN_2^*(t^*)}{dt^*} = \frac{1}{2}\left[N_1^*(t^*)\right]^2 - \frac{1}{2}k_2\left[N_2^*(t^*)\right]^2 \tag{5.30}$$

$$u(t^*) = \frac{t^* - N_1^*(t^*)}{N_2^*(t^*)} \tag{5.31}$$

Let us now hypothesize that, after sufficiently long time, the concentrations $N_1^*(t^*)$ and $N_2^*(t^*)$ vary according to the following power laws:

$$N_1^*(t^*) = a\,t^{*^{\alpha}}, (\alpha < 1) \tag{5.32}$$

$$N_2^*(t^*) = b\,t^{*^{\beta}} \qquad \text{as } t^* \to \infty \tag{5.33}$$

where, *a*, *b* are positive quantities. We do not impose any restriction on α, β (they are positive or negative depending on whether $N_1^*(t^*)$, $N_2^*(t^*)$ are increasing or decreasing) except that $N_1^*(t^*)$ cannot increase faster than linearly (i.e. $\alpha < 1$) so that $u(t^*)$ in Eq. (5.31) (the size of the secondary group) always remains a positive quantity. This implies, from Eq. (5.31), that asymptotically,

$$u(t^*) \sim b^{-1}\, t^{*1-\beta} \qquad \text{as} \quad t^* \to \infty \tag{5.34}$$

Upon using Eqs.(5.31)-(5.33), Eqs. (5.29) and (5.30) transform to the following equations:

$$a\alpha\, t^{*\alpha-1} \sim 1 - a^2\, t^{*2\alpha} - a\, b^{1-n} k_1\, t^{*\alpha+n+\beta-n\beta}, \; (\alpha < 1) \tag{5.35}$$

$$b\beta\, t^{*\beta-1} \sim \frac{1}{2} a^2\, t^{*2\alpha} - \frac{1}{2} k_2 b^2\, t^{*2\beta} \tag{5.36}$$

Let us first argue that **α cannot be greater than β.** Supposing the opposite were true, (i.e. $\alpha > \beta$), then the first term on the RHS of Eq. (5.36) will dominate over the second term at large times. In that case,

$$b\beta\, t^{*\beta-1} \sim \frac{1}{2} a^2\, t^{*2\alpha} \tag{5.37}$$

and upon matching the exponents one obtains,

$$2\alpha = \beta - 1. \tag{5.38}$$

Similarly, matching the pre-factors of both sides of Eq. (5.37), one obtains

$$\frac{a^2}{2b} = \beta \tag{5.39}$$

But the condition $\alpha > \beta$ implies that $2\alpha > 2\beta$ which together with the condition obtained in Eq. (5.38) yields the constraint

$$\beta < -1. \tag{5.40}$$

But β cannot be negative since it violates the constraint (Eq.(5.39)) on the pre-factor requirement which should be positive. Hence, **α cannot be greater than β.** One can also arrive at the same conclusion by plugging Eqs. (5.38) and (5.39) in Eq. (5.35) and examining the condition under which exponent of the leading term (third term on RHS of Eq.(5.35)) matches with the exponent (0) of the source term.

Now, let us similarly argue that ***α* cannot be less than *β*.** If the converse is true (i.e. $\alpha < \beta$), the second term on the RHS in Eq.(5.36) will dominate over the first term, and hence,

$$b\beta\, t^{*\beta-1} \sim -\frac{1}{2} k_2 b^2\, t^{*2\beta} \tag{5.41}$$

The exponent and pre-factor matching implies that

$$\begin{aligned} &\beta = -1 \\ &b = -\frac{2\beta}{k_2} = \frac{2}{k_2} \end{aligned} \tag{5.42}$$

and the sign of the pre-factor (b) is positive which is acceptable. However, the above result $\beta = -1$ is not consistent with Eq.(5.35). The first term (i.e. unity = $(t^*)^0$) on the RHS of Eq. (5.35) can only be matched by the third term providing

$$\alpha + \beta + n - n\beta = 0 \tag{5.43}$$

With the result $\beta = -1$, one can obtain (from Eq.(5.43)) the relation $\alpha = 1 - 2n$ which implies that $\alpha > -1$ (since $n = \left(1/d_f\right) < 1$). This violates the starting premise that $\alpha < \beta$, i.e. $\alpha < -1$. Hence by contradiction, ***α* cannot be less than *β*.**

In view of the above, **the only possibility is that $\alpha = \beta$.** In order to determine this value, match the source term in Eq.(5.35) with the remaining terms which lead to Eq.(5.43). With $\alpha = \beta$**,** this immediately yields the result

$$\alpha = \beta = -\frac{n}{2-n} = -\frac{1}{2d_f - 1} \tag{5.44}$$

The corresponding pre-factor from Eq.(5.35), yields

$$ab^{1-n}k_1 = 1 \tag{5.45}$$

and from Eq.(5.36),

$$a^2 = b^2 k_2 \tag{5.46}$$

Eq.(5.44) determines uniquely the power of the leading terms in the asymptotic behaviour of $N_1^*(t^*)$, $N_2^*(t^*)$. The total number concentration may be given by,

$$N^*(t^*) = N_1^*(t^*) + N_2^*(t^*) \sim (a+b)\, t^{*^{-\{1/(2d_f-1)\}}} \tag{5.47}$$

This completely determines the law of asymptotic behaviour of the number concentration of particles for the problem of coagulation with continuous injection in the absence of removal.

From Eq.(5.44), for the case of a fractal dimension d_f=1.75, the value of the exponent $\alpha\,(=\beta)$ works out to be -0.4 and hence the total number concentration is expected to decay as

$$N^*(t^*) \sim const.\, t^{*^{-0.4}}, \text{ for } d_f=1.75 \tag{5.48}$$

Hence for the Fuchs kernel too, the number concentration will approach zero in the absence of removal, albeit more slowly (exponent of -0.4 instead of unity) as compared with (u+v) kernel. This effect has been validated by the numerical simulation of the original integro-differential coagulation equation (Eq.(5.1)), as discussed in the next section.

5.4. Numerical model

The evolution of the size distribution is simulated by the nodal method as described in Section 2.3.1.1. The discrete form of the coagulation part of Eq.(5.1) is given by

$$\frac{\partial n_k}{\partial t} = \frac{1}{2}\sum_{\substack{i=1 \\ j=1}} \chi_{ijk} K_{i,j} n_i n_j - n_k \sum_{i=1} K_{i,k} n_i \tag{5.49}$$

$K_{i,j}$ is the coagulation kernel for the interacting particles of size i and j, and χ_{ijk} is the size-splitting operator given by

$$\chi_{ijk} = \begin{cases} \dfrac{u_{k+1} - (u_i + u_j)}{u_{k+1} - u_k}; & u_k \le u_i + u_j \le u_{k+1}, \\ \dfrac{(u_i + u_j) - u_{k-1}}{u_k - u_{k-1}}; & u_{k-1} \le u_i + u_j \le u_k, \\ 0; & \text{otherwise.} \end{cases} \tag{5.50}$$

where, u_i is the volume of the particle at the i^{th} node, and i, j and k are the corresponding particle sizes. At every coagulation step, the size-splitting operator redistributes the particles back to nodes to conserve the mass. The aerosol size distribution of the freshly injected nanoparticles (the source) is described by a log-normal distribution in terms of a series of discrete particle nodes, with the number of particles in each node representing the particle number concentration integrated between two consecutive nodes.

The most widely used Fuchs coagulation kernel $K(r_i, r_j)$ that accounts for transition regime effects is employed. It is given by,

$$K(r_i, r_j) = \frac{4\pi (r_i + r_j)(D_i + D_j)}{\dfrac{(r_i + r_j)}{(r_i + r_j) + \sqrt{\delta_i^2 + \delta_j^2}} + \dfrac{4(D_i + D_j)}{\sqrt{\bar{v}_i^2 + \bar{v}_j^2}\,(r_i + r_j)}} \tag{5.51}$$

wherein r_i is the radius of the particle of size i, D_i is the particle diffusion coefficient, δ_i is the mean distance from the centre of a sphere reached by particles leaving the sphere's surface and traveling a distance of particle mean free path λ_i, and v_i is the mean thermal speed of a particle. These parameters are given by

$$\delta_i = \frac{(2r_i + \lambda_i)^3 - (4r_i^2 + \lambda_i^2)^{3/2}}{6 r_i \lambda_i} - 2r_i; \quad \lambda_i = \frac{8 D_i}{\pi \, \bar{v}_i}; \quad D_{m,i} = \frac{kT}{6\pi \, r_i \eta_a} G_i \tag{5.52}$$

where, k is the Boltzmann constant, T is the temperature, η_a is the air viscosity, and G_i is the slip-flow correction which further depends on the Knudsen number of the particle.

Implicit in the traditional derivation of rate kernels for clusters is the assumption that they are compact objects, which may be approximated by equivalent spheres. This is no longer found to be true. Fractal-like agglomerates are formed due to coagulation of solid primary particles. Experimental studies on the structure of metal smoke indicated that particle aggregates may be better described by fractal geometry. Fractals are self-similar objects; a small part, when magnified, appears exactly like the original cluster. Also, the clusters are spongy, having voids on all length scales. For real aggregates, self-similarity breaks-down at length scales of the order of the monomer size. Hence, the fractal description is adequate for clusters which are much larger than their constituent monomers. In brief, fractal clusters differ from compact clusters in the following important aspect. For a compact cluster, one can assign a constant density (ρ) such that its mass (M) is related to its radius (R) by

$$M = \rho R^3 \tag{5.53}$$

Compact objects can have voids; but these give rise to size independent porosities and hence size independent effective densities. For fractals, on the other hand, the porosity monotonically increases (the effective density decreases) with the cluster size. The mass therefore scales as a fractional power of the size, i.e.,

$$M = constant\ R^{df} \tag{5.54}$$

where, d_f is the fractal dimension of the cluster (d_f <=3). For metal smoke, d_f = 1.74. The above equation implies that the effective density of the cluster decreases as

$$\rho = constant\ R^{-(3-df)}. \tag{5.55}$$

Two important models, viz., diffusion-limited aggregation (DLA), and cluster-cluster aggregation (CCA) models have been put forward in order to understand the origin of fractality. In the DLA model valid at low monomer concentrations, a given seed particle grows by the successive accretion of monomers. The probability of a monomer being added at a given surface site is proportional to the Fickian flux, $\nabla C.\hat{n}$, where, C is the monomer concentration field satisfying the Laplace's equation $\nabla^2 C = 0$ outside the aggregate, with the irreversible sticking condition, $C = 0$ on the surface. Since the Fickian flux is higher at points having greater curvature, tips formed due to fluctuations tend to grow more rapidly than the shallower regions of the cluster. This leads to a progressive increase in the fractional void space as the cluster builds up, giving rise to a fractal object. Computer simulations of this model yield a fractal dimension of 2.5, which agrees with that obtained in laboratory experiments with colloids. It has been shown that the electrical charge on monomers has no effect on the cluster structure.

In the cluster-cluster aggregation model, many clusters are formed simultaneously in the suspension and the clustering of these clusters occurs. This is more like what happens in a high-density aerosol as is implied in the coagulation equation. The inter-penetrability between a cluster and another cluster is much less than that between a monomer and a cluster, and hence larger voids are left in CCAs than in DLAs. Therefore, CCAs are far more ramified objects. In this case, the computer simulations give a fractal dimension of 1.78 which is close to that observed for smoke aggregates.

Implications of fractality to aerosols are manifold. In the coagulation equation, the rate kernels have to be re-derived for fractal clusters. In order to include the effect of particle morphology (i.e. fractality) in Fuchs kernel, the particle radius (r_i) in Eq.(5.51) is replaced by the collision radius of the agglomerate of volume u_i, which is taken as the fractal radius ($r_{f,i}$) given by (Matsoukas & Friedlander, 1991)

$$r_{f,i} = r_s N_i^{1/d_f} \tag{5.56}$$

where, r_i is the volume-equivalent radius defined as radius of a sphere with the same volume and density as the agglomerate, r_s is the radius of each individual spherule, N_i is the number of individual spherules or primary particles in the agglomerate, and d_f is the agglomerate fractal dimension. The particle diffusion coefficient, the Knudsen number, and the mean distance traveled by the particles (δ_i) are evaluated at the mobility radius using the prescription proposed by Jacobson (2005).

Indoor particles are generally removed by the combined action of wall deposition and ventilation mechanisms. The former has a complex dependence on size, atmospheric turbulence, surface characteristics and room geometry, which has been a topic of considerable research interest in recent years. In contrast, removal by ventilation occurs at a uniform rate for all sizes and is independent of environmental parameters other than the air-exchange rate or ventilation rate. (Recall that a well-stirred reactor is assumed at all times.) From the perspective of capturing the peculiar effects that might arise because of the removal process combined with coagulation under continuous injection, we consider the simpler case of ventilation removal only.

5.5. Results and Discussion

5.5.1. Evolution of total particle number concentration

The numerical method described in the previous section is used to study the temporal evolution of *total number concentration*, *particle size distribution*, and *average particle size* during simulation periods of ten hours each. The following parameter sets are considered to construct the evolution scenarios:

- 2 fractal dimensions (1.75 and 3.0; i.e. “branched” and “compact”),
- 3 source injection rates (2 x10^8, 2 x10^9 and 2 x10^{10} $m^{-3}sec^{-1}$), assumed to be constant in time,

- 2 initial particle size distributions (count median diameters (CMDs) 15 and 30 nm; constant σ_g of 1.3)
- Ventilation rate (0, 0.15, 4 ("normal"), and 10 h^{-1} ("high")).

Temperature and pressure are fixed at 300 K and 1 atm respectively.

The total particle number concentration is one of the major metrics used to estimate the toxicological hazard of particles in the workplace environment. Its dependency on the above parameter sets is therefore of central interest.

5.5.1.1. Effect of particle fractal dimension on the total concentration

It is by now well established that droplets evolve as compact spheres with $d_f = 3$ while solid particles evolve as more or less branched, fractal aggregates depending on the mode of their generation and the chemical nature of particles. Fractality of particles tends to increase the value of the coagulation kernel thereby enhancing the coagulation rate at a given particle concentration (Maynard & Zimmer, 2003, Jacobson, 2005). In the present study, two extreme cases are considered, one with fractal dimension 3.0 and the other with 1.75, in order to examine the effect of fractal dimension on the evolution of particle characteristics *in the absence of any removal process*. Although not unique, the choice of 1.75 corresponds to the fractal dimensions seen in cluster-cluster aggregation models (Schneider & Jensen, 2009). This value has been used by other investigators as well. It is further assumed that the fractal aggregates are made up of spherules of 5 nm diameter. The formation of these fractal aggregates takes place at an early stage near the aerosol source before the actual measurements could take place. In the present simulations, the initial particles (measured near the injection point) are assumed to be aggregates comprised of such 5 nm dia. spherules. As mentioned, two initial size spectra of the fractal aggregates, viz., 15 and 30 nm CMDs are examined, and the particle size distribution is assumed to be lognormal with a GSD of 1.3. The numerical model was suitably modified to take into account the appropriate definitions of the mobility and the area equivalent radii (Jacobson, 2005) required for the Fuchs kernel for fractal agglomerates.

The temporal evolution of the total particle number concentrations for $d_f = 3$ and 1.75, with other parameters fixed as above, are shown in Fig. 5.3. In both cases, the concentration initially increases rapidly as the chamber fills, reaches a peak and then tends to decrease with time as coagulation sets in. The simulation for compact particle morphology (d_f=3.0) shows that the peak concentration of 2.2 x 10^{12} m^{-3} occurs after about 50 min. In the case of fractal particles (d_f=1.75), the total number concentration of 1.37 x 10^{12} m^{-3} peaks at around 25 min. Apparently both the peak concentration and the time of its occurrence are reduced considerably, in fact nearly cut in half, for fractal particles (d_f=1.75) as compared to compact particle d_f=3.0.

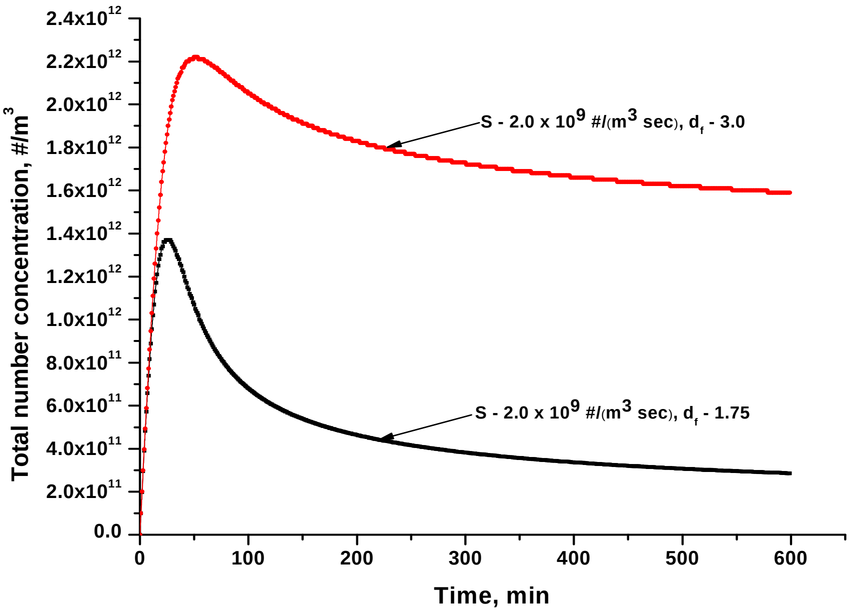

Fig.5.3. Effect of particle fractal dimension on the total number concentration. The ventilation rate is zero.

The initial steep increase, which is almost linear in time, is mainly due to steady injection coupled with the fact that significant coagulation is yet to take effect. After some time when the number concentration has increased sufficiently, coagulation sets in. The increase in the coagulation rate decreases the rate of rise of the number concentration. During this time, significant numbers of secondary particles will also be formed due to coagulation. Subsequently, the coagulation process will be dominated by primary-primary, primary-secondary and secondary-secondary particle interactions. Since the coagulation kernel for the primary-secondary interactions increases in value with the size of secondary particles, the injected primary particles will be removed at an increasingly rapid rate as time progresses. Seen in another way, one can visualize an overall increase of the effective coagulation coefficient for the entire size spectrum with time. This mechanism leads to the peak in the number concentration.

The Fuchs kernel which calculates the coagulation rate for the entire size regime is able to capture the peaking effect of the total number concentration; in contrast, a constant coagulation kernel which does not account for size-dependent effects will be unable to produce this kind of system behavior. Although not shown, a similar peaking behaviour is found for most of the commonly used, size dependent kernels including the free-molecular kernel and the continuum kernel.

After peaking, the concentration gradually decreases. In fact, when the ventilation rate is zero – a parameter discussed in more detail later on -, this trend of decreasing concentration appears to continue indefinitely, at least within the simulation time period. This strongly points to a fundamental behavior of coagulating systems, that asymptotically they would tend to zero number concentration, in spite of steady injection, perhaps even regardless of injection rate. As shown in the Section 5.5.1.2, the concentration appears to fall at least as fast as $\sim t^{*-0.33}$ for the case of $d_f = 1.75$, the exponent being independent of the strength of the source, where t^* is the scaled time. In fact there are strong indications, obtained by analysing a simplified 2-group version of the coagulation model that the long time decay might be $N^*(t^*) \sim t^{*-0.4}$.

One may anticipate the conclusion of an ever-decreasing concentration from the fact that in the absence of any removal mechanism, the average secondary particle sizes will increase indefinitely with time and the ever increasing rate of primary-secondary coagulation will dominate the depletion of number concentration. Basically, the effective coagulation coefficient for the entire aerosol system continually increases which cannot be balanced by the source term. However, in the case of constant kernel, the effective coagulation coefficient is a constant and the continuous injection rate balances coagulation rate thereby leading to a non-zero steady state. These results are noteworthy since they advise against the use of a constant kernel throughout the process in cases where the size distribution broadens continuously with time.

5.5.1.2. Effect of source strength on the total concentration

Here we consider different source strengths with otherwise fixed parameters identical to those of the preceding section; in particular the ventilation rate is zero. According to figure 5.4, an increased injection rate both increases the peak in total number concentration and reduces the peaking time sharply. For example, the total number concentration reaches its maximum around 8 minutes for an injection rate $S = 2\text{x}10^{10}$ particles per m^3 and sec, compared to 80 minutes for a 100 times lower injection rate.

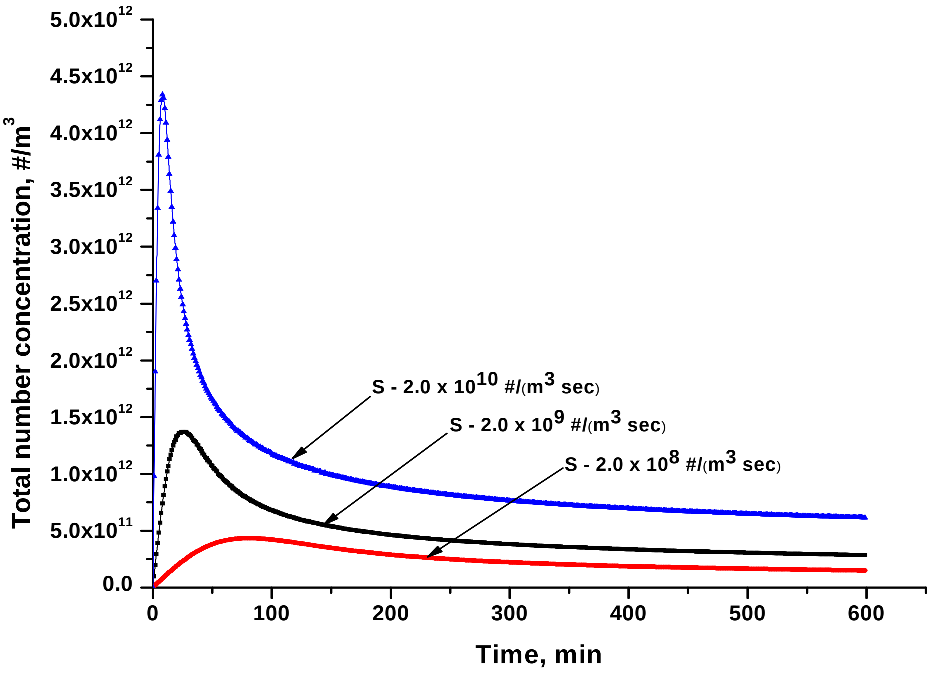

Fig.5.4: Effect source injection rate on the total number concentration of particles with d_f=1.75. The ventilation rate is zero.

In the following, possibilities of capturing the effect of varying source strengths on the total concentration in a single plot is examined through an appropriate scaling transformation of variables. It must be noted up front that similarity transformations under steady-injection conditions do not exist, even for scaling kernels: hence the question of a similarity transformation does not arise for a non-scaling kernel such as the Fuchs kernel. Nevertheless one may attempt to scale the number concentrations and the time in terms of respective characteristic variables referring to the primary particle sizes. Suppose let us define a characteristic number concentration $N_c = \sqrt{S/K(u_0,u_0)}$ and a characteristic time $t_c = 1/\sqrt{S\,K(u_0,u_0)}$, where, u_0 is the volume of the particle corresponding to the CMD of the size distribution of the source injected into the system. We may then obtain a dimensionless number concentration and dimensionless time as follows:

$$N^*(t^*) = N(t)/N_c \qquad (5.57)$$

$$t^* = t/t_c \qquad (5.58)$$

Fig. 5.5 shows plots of $N^*(t^*)$ vs. t^* for various source injection rates in the absence of any removal processes in the system. Quite interestingly, all the plots for different injection rates in this graph collapse to a single curve. This is a useful result which shows that the prediction of the total number concentration for any source injection rate can be obtained through these scaling parameters, provided all removal processes operating in the system are negligible.

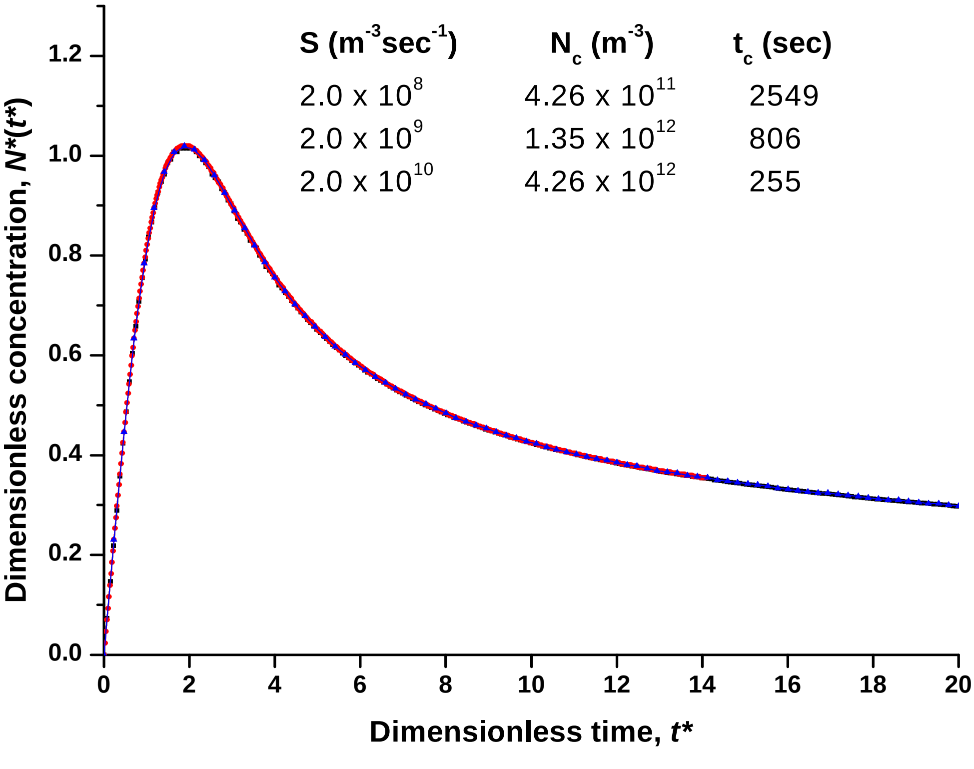

Fig.5.5: Non-dimensionalized representation of total concentration $N^*(t^*)$ vs. time for various source injection rates. The ventilation rate is zero.

A power-law fitting to the tail of Fig. 5.5 shows that for $d_f = 1.75$, the concentration appears to fall as $N^* \sim const.\, t^{*-0.33}$ at around $t^* \sim 20$. However, since numerical simulation for longer times is computationally very intensive it is difficult to establish whether asymptotic limit has been attained at time t^* about 20. The exponent is still different from the theoretical prediction of -0.4 (Eq.(5.48)). To understand the origin of this difference, numerical solutions to the set of the simplified equations (5.29-5.31) have also been obtained for the Fuchs kernel using the differential equation solver in Mathematica. These solutions closely agree with the asymptotic predictions of the long-time decay exponents for various d_f 's ranging from 1.5-3, thereby confirming the formula (Eq.(5.44)). However, it is found that the asymptotic law sets in at very large times, i.e., for scaled times t^* greater than about 1000. Around t^*~20, the decay exponent is still about -0.34, hence very close to the value observed in our simulations of the integro-differential equation. Considering that numerical simulation of the original coagulation equation for scaled times beyond 20 becomes increasingly time consuming, the predicted exponents of the simplified differential formulation may be taken as representative of the true asymptotic behaviour of the aerosol number concentration for continuous injection without external removal.

It should be pointed out that the power law $t^{*-0.4}$ dependence for the monotonic decrease in concentration with continuous injection is far slower than the decrease following a one-time (instantaneous source) injection, which is well known to merge asymptotically into a t^{-1} dependence. In terms of real variables, the asymptotic number concentration will be $N(t) \sim const. S^{0.3}\, K_{11}^{-0.7} t^{-0.4}$ for continuous injection, and $N(t) \sim K^{-1} t^{-1}$ for one-time injection. These relations show that the pre-factor for continuous injection will depend upon the source strength, unlike the latter case in which the number concentration after long time no longer depends upon the initial concentration. This latter property of a rate of decrease independent of initial conditions is sometimes utilized (e.g. Koch et al, 2008) to establish an aerosol concentration standard; i.e., a system with a predictable particle concentration which becomes an inherent property of the aerosol and does not depend on its initial size or concentration. Our finding implies that one cannot generally establish such a standard on the basis of steady injection.

5.5.1.3 Effect of initial particle size on the total concentration

Fig. 5.6 shows the effect of the size of the source particles. The comparison is made between two CMDs, 15 nm and 30 nm, while keeping all other parameters constant; in particular the ventilation rate is zero. For source particles with CMD = 30 nm, the total number concentration peaks earlier (*t* = 18 min) at a peak concentration which is lower by a factor of ~0.7 as compared to particles with CMD = 15 nm. However, at about 150 minutes, the concentration for 30 nm particles crosses over and thereafter tends to remain higher by about 25%. Thus larger source particles have a greater persistence at long times.

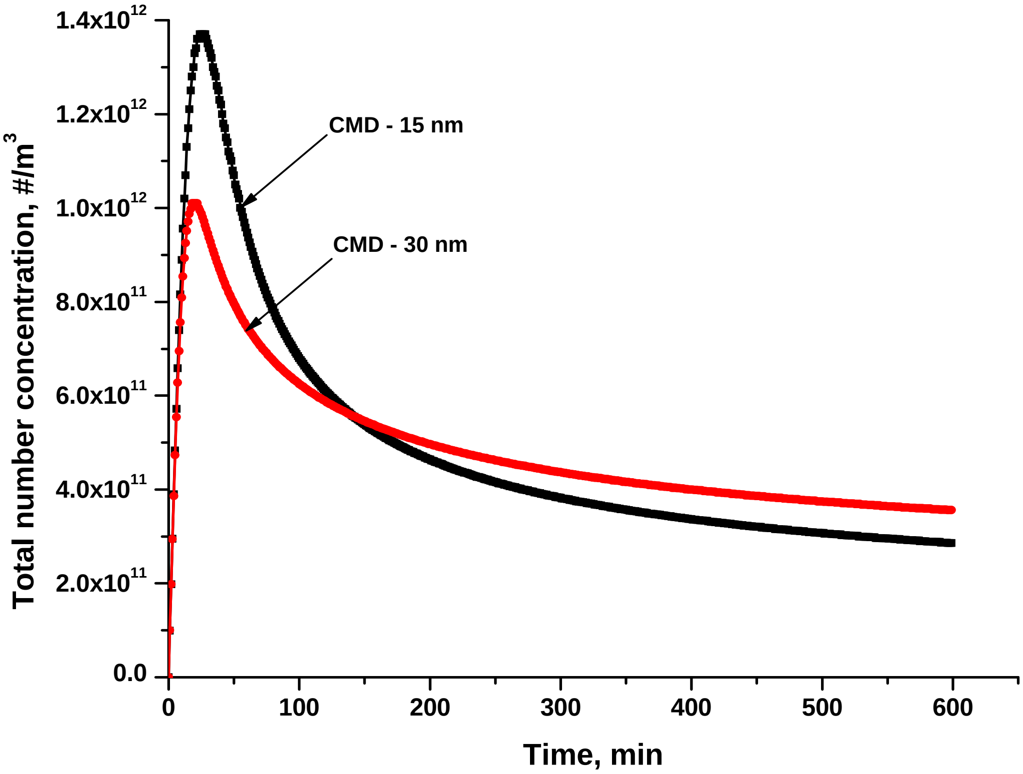

Fig.5.6: Effect of source particle size on the total number concentration. Source strength and fractal dimension are constant at $S=1.67x10^9$ m^{-3} s^{-1} and $d_f=1.75$.

5.5.1.4. Effect of the removal rate due to ventilation on the total concentration

Fig. 5.7 compares the temporal evolution of the total particle number concentration at increasing ventilation rates with the case of no removal ($\lambda_v=0$) corresponding to the scenarios of the previous sections. The other parameters are as given earlier.

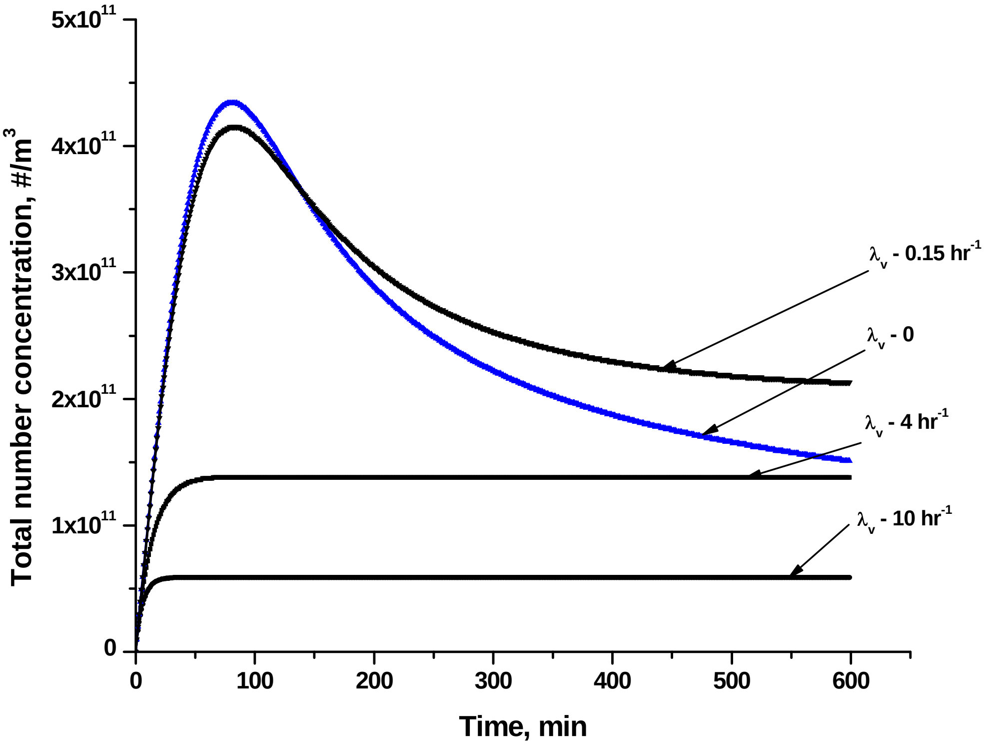

Fig. 5.7: Effect of ventilation rate on the total number concentration. $S = 2\text{x}10^8\ \text{m}^{-3}\text{s}^{-1}$; $d_f = 1.75$

Most importantly, the figure shows that (within our parameter range) ventilation always causes the total number concentration to reach an asymptotic steady state, while in the λ_v=0 case there is a continuous decline as discussed earlier. The higher the dilution (applicable for dilution rates above the critical ventilation rate defined later in this section), the lower the final plateau and the less prominent the initial concentration peak. The principal reason for this apparent stabilization of the concentration even at these ventilation rates is the dilution of very large secondary particles. Without dilution, the ageing aerosol contains an increasing number of very large agglomerates (This is discussed on more detail in Section 5.5.2). The ever increasing size and number of these secondary particles leads to a growing loss of freshly injected primary particles due to heterogeneous coagulation in such a way that the total concentration tends to fall continuously. Thus a small amount of ventilation suffices to remove enough larger particles from the airspace to slow down heterogeneous coagulation sufficiently to balance it with injection of new aerosol. On the other hand, strong dilution appears to also affect the primary particle concentration sufficiently to reduce the asymptotic plateau.

Interestingly, Fig.5.7 shows a cross-over between the cases of λ_v =0 and 0.15 h^{-1}, with the low-dilution case leading to higher concentrations after the peak than no dilution at all (Recall that in Fig.5.7 all parameters are kept constant except the ventilation rate). Thus, Fuchs kernel too seems to predict a critical ventilation rate at which the stabilized concentration is maximum, between insufficient suppression of heterogeneous coagulation on the one hand and too much primary aerosol dilution on the other.

This finding has significant implications for control strategies of a nanoparticle leak in the workplace. Introducing a ventilation rate below this critical value may be counterproductive from the point of view of nanoparticle reduction. In fact it is seen from Fig.5.7 that a dilution of 4 h^{-1} is required at the prevailing source injection rate, in order to maintain the aerosol concentration within about 10^{11} m^{-3}. A higher source injection rate of 2 x 10^9 $m^{-3}s^{-1}$ (curves not shown here), would require a ventilation rate >15 h^{-1}, amounting to 15 turn-overs of the chamber volume per hour, to bring down the total number concentration. Note that such high ventilation rates would also bring the flow conditions in the chamber close to those of a well-stirred reactor.

5.5.2. Evolution of particle size

5.5.2.1. Evolution of the particle size distribution

The experimental study of Seipenbusch et al. (2008) has clearly established the formation of a bimodal size distribution under continuous aerosol injection. It is interesting to examine model predictions with regard to the effect of various parameters on the evolution of the size spectrum and in particular on the appearance of the secondary size mode which cannot be generated with constant-kernel coagulation simulations. It is worth to mention here that the bimodal distribution may also be produced near the source due to the effect of spatial heterogeneity (See Section 4.5 of Chapter 4). However, in the present model, we assume that the aerosols released into the chamber is having unimodal (lognormal) size distribution. Further, it is assumed that these aerosols are uniformly mixed well in the chamber. The effect of source strength, choice of fractal dimension and CMD are again investigated.

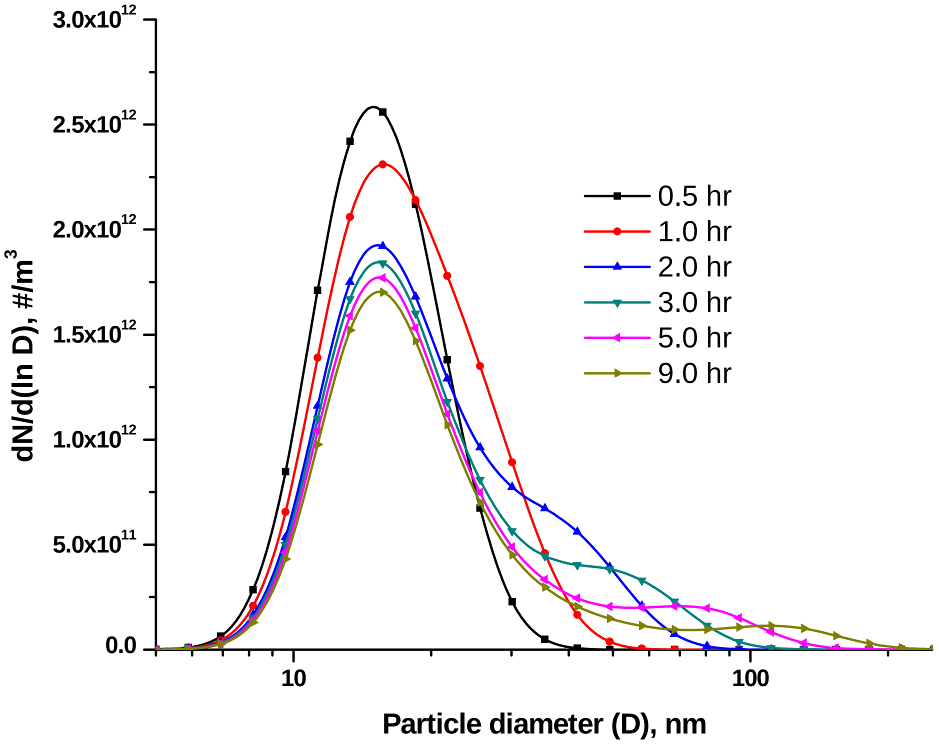

Fig. 5.8: Evolution of particle size spectrum for compact particles with $d_f = 3.0$ ($S = 2\text{x}10^9$ m^{-3}s^{-1}, CMD=15 nm; zero ventilation rate)

Fig.5.8 shows the evolution of particle size spectra for the case of a constant injection rate S=2 x 10^9 m^{-3}s^{-1} with compact spherical particles ($d_f = 3.0$) with an initial size of 15 nm. The simulations are carried out with $\lambda_v = 0$. The size distribution remains unimodal at early times (up to~ 1 hr) and the second mode appears to gradually evolve at a later stage. While the first peak remains nearly stationary at the primary size, a distinct second peak, although of much smaller height as compared to the first mode, appears after about 5 hours and then continues gradually to move to larger sizes. This secondary mode becomes less prominent at lower injection rates (not shown in the figure).

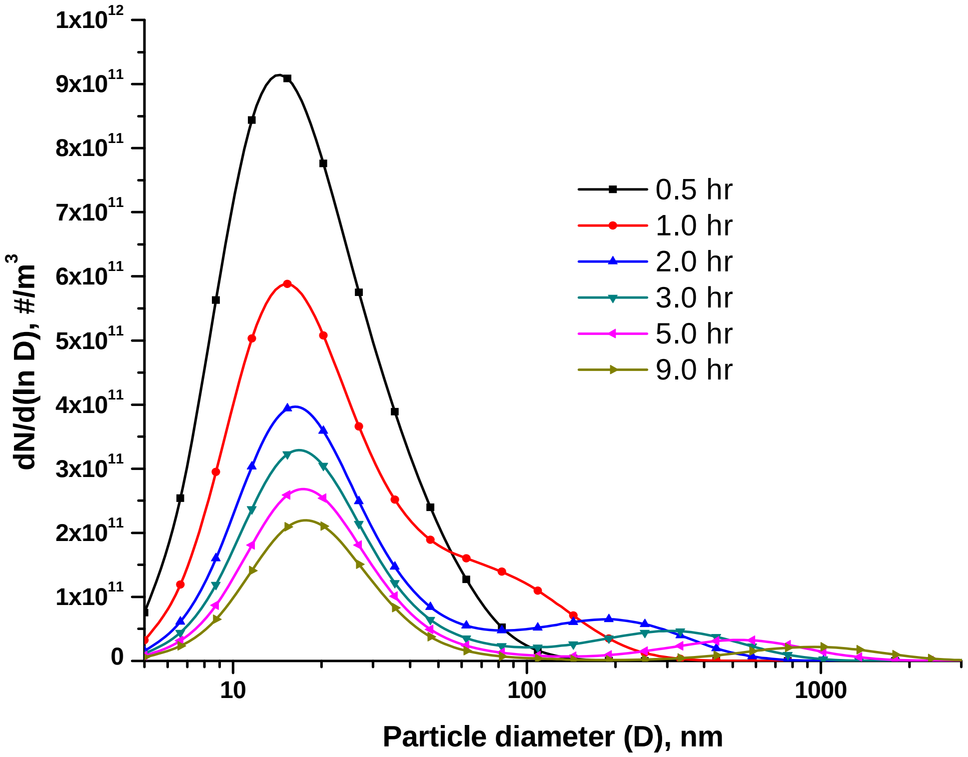

Fig. 5.9: Evolution of particle size spectrum for fractal particles with $d_f = 1.75$. ($S = 2\text{x}10^9$ m^{-3}s^{-1}, CMD=15 nm; zero ventilation rate)

The secondary mode forms earlier if we consider particles of a fractal nature (Fig. 5.9). For $d_f = 1.75$ it appears at $t = 2$ h around the particle diameter of 110 nm. With increasing time, the mode flattens and extends to larger diameters as one would expect from a self-preserving-size-distribution-like behavior. Another interesting feature of the fractal particles is the continuous decrease of the primary peak with time, while for compact particles (Fig.5.8) the first mode height remains almost unchanged. Also the secondary mode shifts more rapidly to higher sizes for fractal particles. The above features appear more markedly at higher injection rates (Fig.5.10).

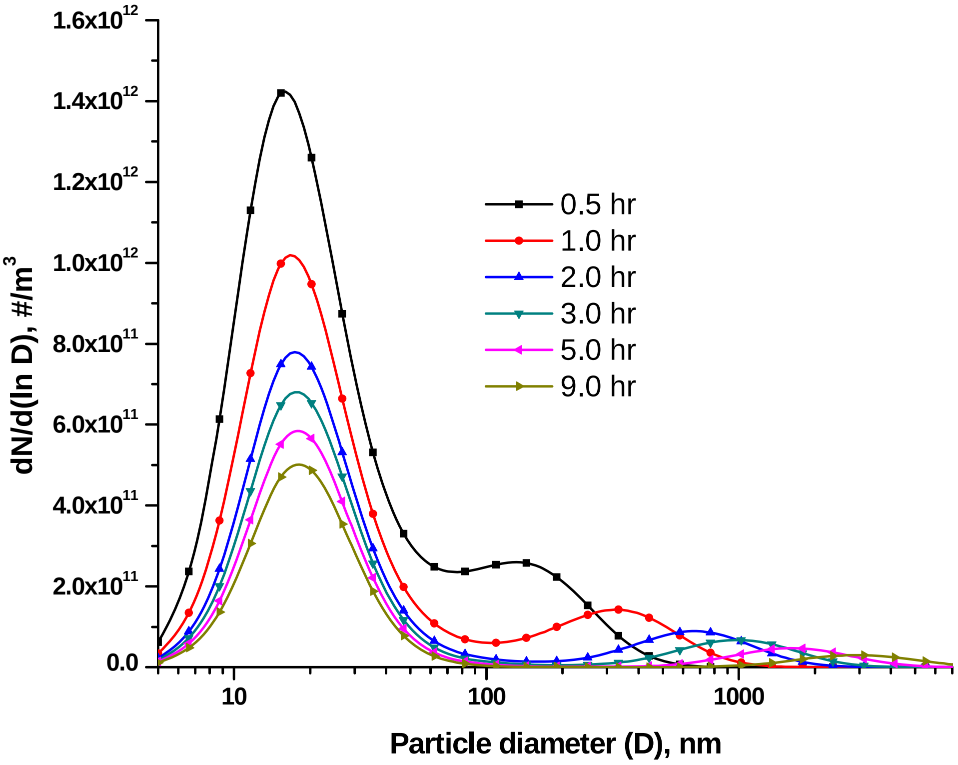

Fig. 5.10: Evolution of particle size spectrum for fractal particles at a higher injection rate of S = 2 x 10^{10} $m^{-3}s^{-1}$. (d_f – 1.75, CMD=15 nm; zero ventilation rate)

In Fig. 5.11 the effect of a larger primary particle size (30 nm) for the case of a fractal kernel is also examined. Compared to Fig. 5.11, the 30 nm case shows a more prominent secondary mode. On the whole, it appears that lower fractal dimensions lead to a more distinctive secondary peak (which it is further enhanced for larger primary particle sizes) due to the increased value of the coagulation kernel. This is perfectly consistent with the more rapid decline in concentration for d_f = 1.75 already observed in Fig. 5.3 – although there for zero ventilation rate. The impact of the secondary peak on the overall spectrum will be discussed in more detail in the following section.

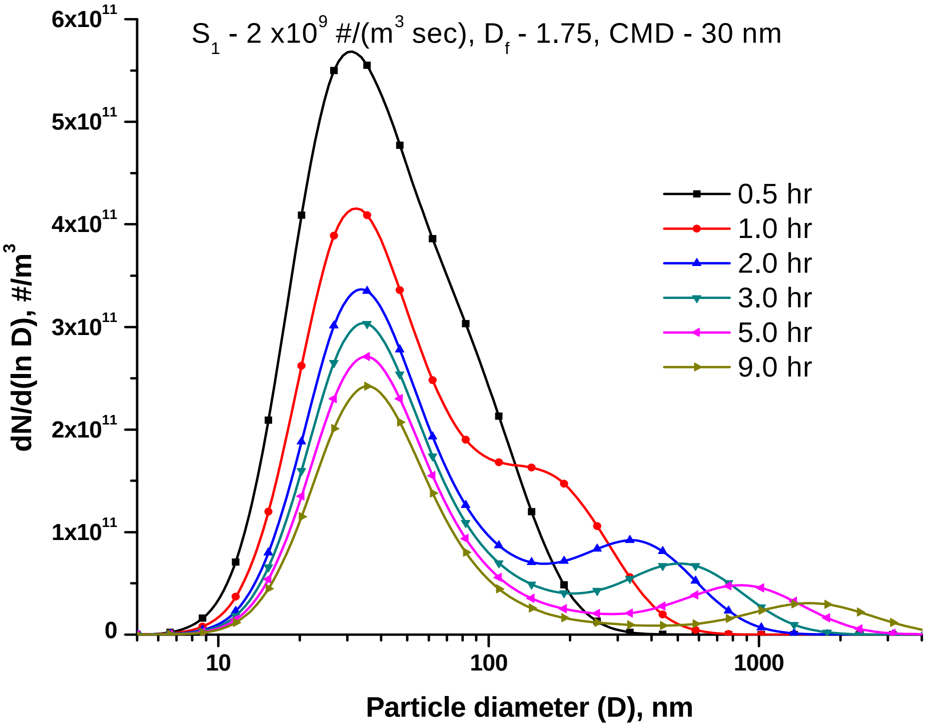

Fig. 5.11: Evolution of particle size spectrum for a larger initial particle size CMD=30 nm. (S = 2 x 10^9 $m^{-3}s^{-1}$, d_f – 1.75, zero ventilation rate)

5.5.2.2. Evolution of the mean particle size

Fig. 5.12 shows the evolution of average particle diameter for a variety of cases discussed in the preceding sections. Although the mean particle size has only limited value in characterizing bimodal particle systems as they are encountered here, it does provide information about the prominence of the secondary size peak compared to the primary aerosol injected into the chamber. The figure illustrates how widely the mean particle diameter can differ over the course of 10 h, depending on the scenario. All the simulations shown in Fig.5.12 are with zero ventilation except the fourth curve from the top.

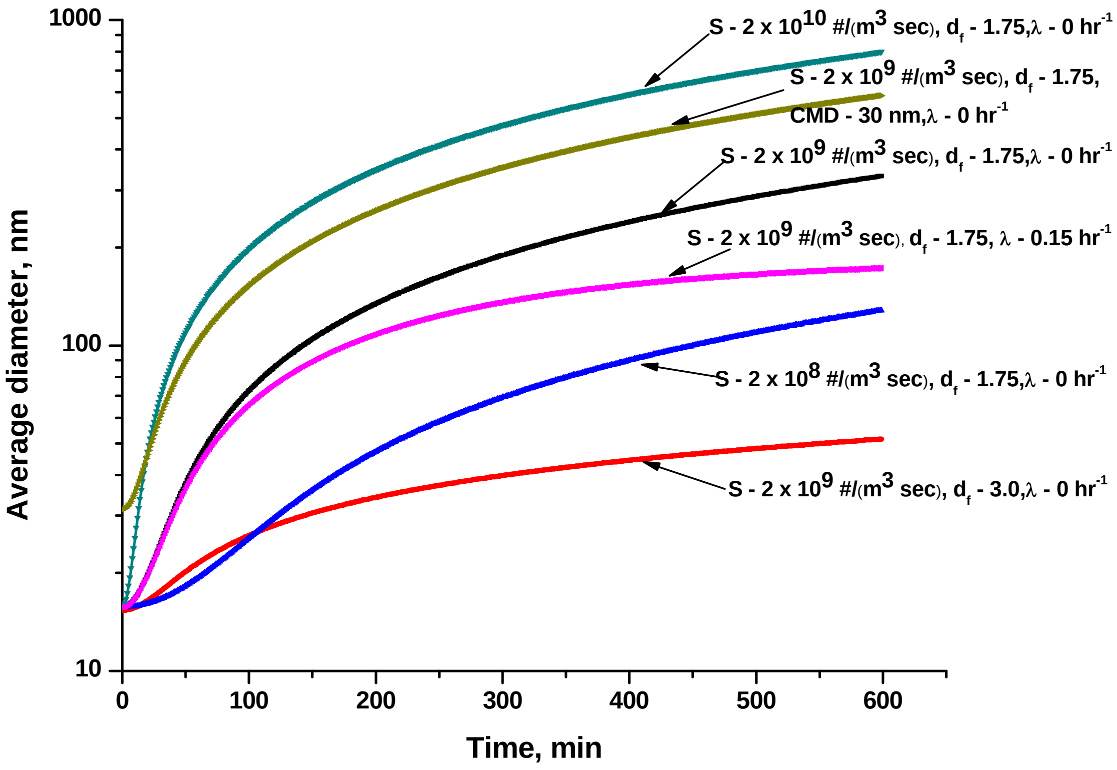

Fig.5.12: Evolution of mean particle diameter with time for various combinations of parameters.

Not surprisingly, the particle diameter increases more rapidly with source injection rate, lower ventilation (up to a point!) and for particles of lower fractal dimension. For example, an increase of the source injection rate by a factor of 10 (from $2x10^8$ to $2x10^9$) is easily outweighed by a reduction in d_f from 3 to 1.75. When comparing the two lowest curves of Fig. 5.12, the respective size increases are about 3-fold for the spherical particles vs. nearly 9-fold for the fractal particles. For the fractal particles, an increase of the source injection rate by a factor of

100 (from 2x10^8 to 2x10^{10}) increases the final size after 10 h by about 50x, from roughly 130 nm to 800 nm.

5.5.2.3. Evolution of the surface area concentration

As pointed out by Schneider et al (2011), the surface area concentration is another important metric apart from the number and mass concentrations. For solid particles evolving as fractal aggregates, the total surface area will be conserved in the same way as the mass of the aggregate during the coagulation process. As a result, the total surface area concentration ($A(t)$) may be expressed in terms of the total volume concentration $\phi(t)$ as follows:

$$A(t) = \frac{a_1 \phi(t)}{v_1} \tag{5.59}$$

Similarly for instantly coalescing droplets the surface area concentration can be estimated by the formula

$$A(t) = (36\pi)^{1/3} \int_0^\infty v^{2/3} N(v,t) dv = a_1 N_1(t) + a_1 N_2(t) \left(\frac{v_2(t)}{v_1} \right)^{2/3} \tag{5.60}$$

where, a_1 is the surface area of the primary mode particles.

In both these cases, the surface area metric is not an independent quantity, but is related to the particle number concentration and mean sizes, which in turn may be obtained from the simplified equations given in the two-group model.

Jeong and Choi (2003) considered a general case of change of surface area concentration in systems having finite coalescence time (τ) originally formulated by Koch and Friedlander (1990). Within their framework the two situations mentioned above pertain to $\tau = \infty$ (solid particles), and $\tau = 0$ (liquid droplets). For a general case, one is required to establish a separate equation for $A(t)$ in addition to those for $N_1(t)$ and $N_2(t)$. Non-zero and finite coalescence times are important for aerosols injected into in a high temperature reactor system; however, these may not be quite relevant to particles injected into ambient environment. In view of this, the formulae given above are sufficient to estimate $A(t)$ for practical purposes of releases to workplace and ambient environments.

5.5.3. Comparison with experimental results

5.5.3.1. Experiment carried out by Seipenbusch et al (2008)

When allowing for a fractal nature of particles, the present numerical simulations reproduce some of the salient features of the experimental observations of Seipenbusch et al. (2008). The most significant of these is the peaking effect in the total number concentration. We compare the observed value of the peak number concentration and the time of occurrence of the peak with that predicted by the simulations. The source emission rate measured in the experiments is 1.67×10^8 #/(m^{3}sec) of platinum nanoparticles and the estimated size of the primary particles (as seen by their first mode) is 15 nm. Since the chamber volume is 2 m^3, the emission rate of the platinum hot wire generator is estimated to be 3.34×10^8 #/sec. Upon combining this data with the simulation results (Fig.5.5) showing the variation of the scaled concentration as a function of scaled time, we may calculate the peak concentration to be 2.6×10^{11} #/m^3 and the time of occurrence of this peak to be 50 minutes. This is fairly in agreement with the experimental value of the peak concentration of 2.1×10^{11} #/m^3 occurring after 30 minutes in Seipenbusch et al. (2008, Fig.(4)). In the simulations, we have used the primary particle density as the platinum density (21450 kg m^{-3}) and the agreement improves if one uses lower densities, as is expected if the primary particles are not fully compact.

Similarly, Seipenbusch et al. (2008) obtained a value of about 1.5 for the ratio of the peak number concentration to that attained after about 250-minutes (nearly steady-state). For a ventilation rate of 0.15 per hour used in their experiments, the simulation also yields a value of 1.5 for this ratio. Although the exact agreement may be fortuitous, it may be stated with confidence that the model predictions compare reasonably well with the experimental data for the total number concentration.

The simulation results also provide qualitative support to the occurrence of a bimodal size distribution demonstrated in the experimental studies cited above. However, the experimental results have shown a secondary mode peak comparable in magnitude to the first peak at an injection rate of ~10^8 particles/(m^3sec) after about 120 minutes, which is not supported by simulations. Similarly, the experiments have shown a more rapid decrease in the primary mode concentration than the simulations, and the secondary mode is larger than the first mode during the early stages (up to 2 hrs). Although it is not possible to reconstruct the reasons for this disagreement, certain non-ideal factors such as the finite time required for the expansion and mixing of the plume during injection into the chamber could have played a role in accentuating the modal results. Possibly, the injection of unimodal particles in the form of a spatially inhomogeneous plume can also lead to a bimodal distribution. In fact, we have noted that in a spatially inhomogeneous aerosol plume, the particles at the centreline of the plume will grow to larger sizes than at the periphery due to coagulation (Chapter 4), which can result in pronounced bimodality as the plume gets mixed subsequently due to increased turbulence in the chamber. As this effect may add to the prominence of the second mode in experimental systems, it needs to be examined separately.

5.5.3.2. Experiments carried out using Nichrome hot wire generator

In this section, we present experimental results of the study of aerosol evolution in a closed chamber with continuous source. The experimental setup is shown in Fig. 5.13. An important requirement of this setup is a continuous nanoparticle generator; other requirements are such as narrow size distribution, and stability of the source during many hours (constant emission rate). This is satisfied by using a hot wire generator. It was widely used as an aerosol generator for the calibration of particle counters (Liu et al, 1975, Trueblood et al, 2000), and for nucleation studies (Vali et al, 1978) which produces narrow, approximately log-normal size distributions with a peak particle diameter of 24 nm. The particle number concentrations could be varied over two orders of magnitude by adjusting the voltage (or heating current).

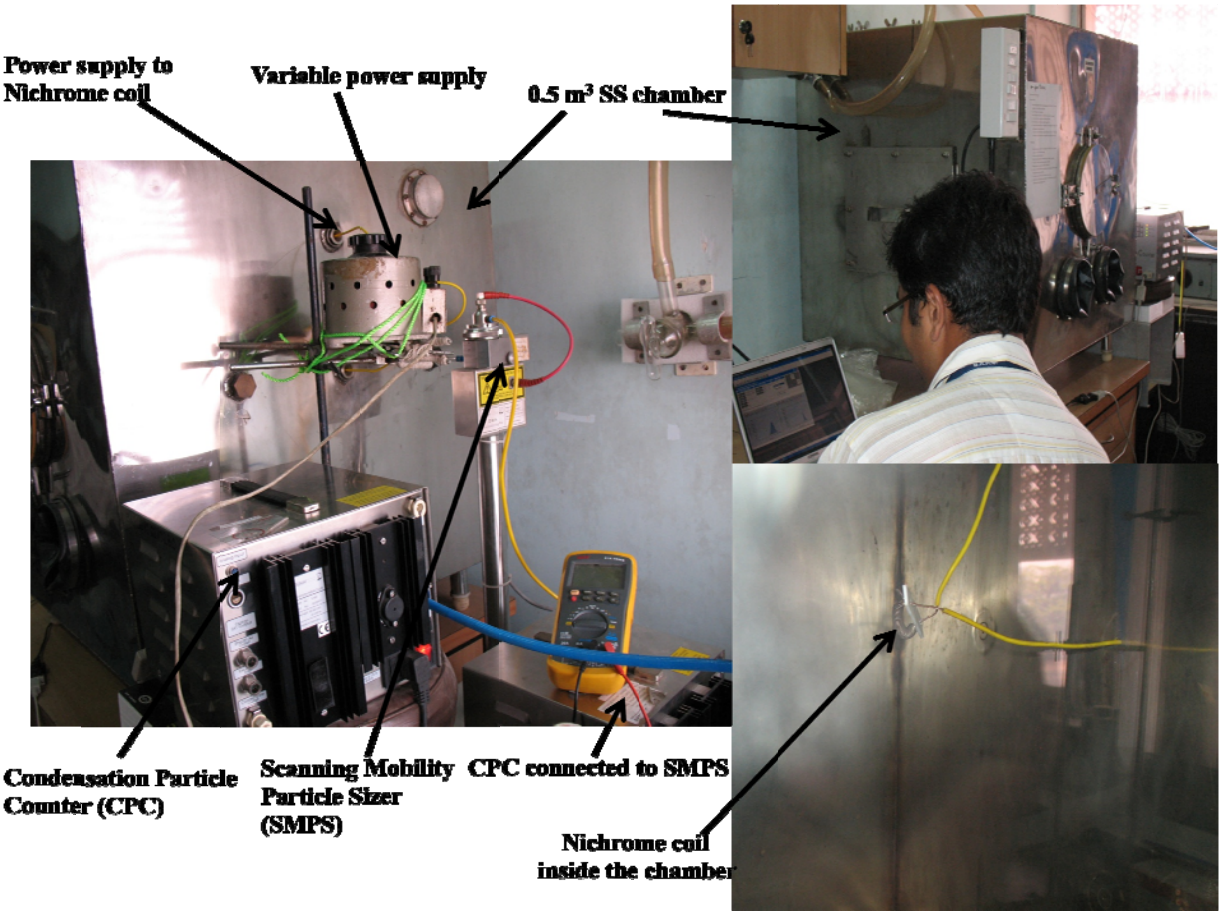

Fig. 5.13: Experimental setup to study the aerosol evolution in a well-stirred chamber

In the present study, a small coil of nichrome is used to generate nanoparticles on-line by an evaporation/condensation method. When the electric current passes through this coil, it gets heated to higher temperature. Due to this, the material evaporates from the surface thus producing vapour continuously. Then, the vapour emitted by the coil condenses and nucleates to produce nanoparticles (primary source particles). The nichrome coil is placed inside a cubical chamber of volume 0.512 m^3 with dimensions 0.8 m x 0.8 m x 0.8 m, and it is connected to a variable power supply. The chamber has inlet or outlet ports distributed over the chamber walls as shown in Fig. 5.13. The inlet ports are used for the electrical connection to the nichrome coil placed inside the chamber, and ventilation. Small sample flows (0.3 lpm) are extracted from outlet ports located in the chamber walls for the purpose of monitoring the aerosol size distribution, and concentration as functions of time. The chamber is also equipped with an external pump to flush it with filtered air in order to obtain a particle-free environment. Two small fans are operated inside the chamber to homogenise the concentration. The quality of mixing is tested by simultaneously measuring the temporal evolution of aerosol from two different sampling ports (one at the top, and other at the bottom of the chamber).

The particle number concentrations are measured using Grimm Aerosol Spectrometer (model 1.108) and Grimm Scanning Mobility Particle Sizer (SMPS 5.403) which covers the size ranges 0.3–20 μm and 9.8–874.8 nm, respectively. The size distributions measured by SMPS consists of a Condensation Particle Counter (CPC, Grimm Series 5.400) and an intermediate length DMA (Grimm Vienna/Reischl type). The aerosol spectrometer works on the principle of scattering of light by the particles. The light source is a solid state laser and the scattering is measured using a set of compact photo-diodes having an effective area of the order of 0.12–0.5 mm^2 which have high sensitivity, high speed and a response over a spectral range of 320–1060 nm. The sample flow rate of this system is 1.2 lpm. The GRIMM SMPS was used for the measurement of particles in the fine sizes. In this system, the size-classification is based on the mobility of the particles in an applied electric field and the counting of particles is by CPC where they undergo condensational growth until they are sufficiently large to be detected optically (diameter growth factor −100 to 1000). These larger sized particle droplets cross a laser beam where each droplet scatters light onto a photo-diode. These signals are continuously counted, stored and converted to particles/cm^3 which are displayed on the screen. The sampling flow rate of this model is 0.3 lpm. It should be noted, however, that the chemical nature of the particles has no importance for the present investigation because aerosol dynamic properties are governed entirely by size and concentration.

The release scenario represents the release of nanoparticles from a moderately strong aerosol source (>10^6 cm^3) into the well-stirred chamber continuously for ~ 2 hours. The voltage applied to the nichrome coil in the present experiment is 8.9 V. The voltage applied to the coil is verified at constant intervals to confirm whether the release rate is a constant or not. The size distribution is monitored over the entire duration of the experiment by SMPS (Fig. 5.14) from a sampling port located at top corner of the chamber. The SMPS takes 8 minutes to complete a single scan of the entire size spectrum. Since our SMPS measuring range starts from 9.85 nm, we are unable to measure the primary particle size emitted by the source. The first spectrum at *t* = 8 min (3:37:39 PM curve in Fig. 5.14) shows that the primary particle spectrum lies below the lower detection limit, and hence the primary particle size at the source is assumed to be less than 9.85 nm. A secondary peak at 15 nm due to the homogeneous coagulation of primary particles appears after eight minutes as shown in the next size distribution (3:45:15 PM curve). Subsequent measurements at a time interval of 8 min show the rapid emergence of a secondary peak which moves towards larger particle sizes. But their concentration (mode of the second peak) continuously decreases with time as shown in Fig.5.14. The formation of the secondary peak is due to the homogeneous coagulation mechanism between the primary particles injected into the chamber as discussed in the Section 5.5.2.

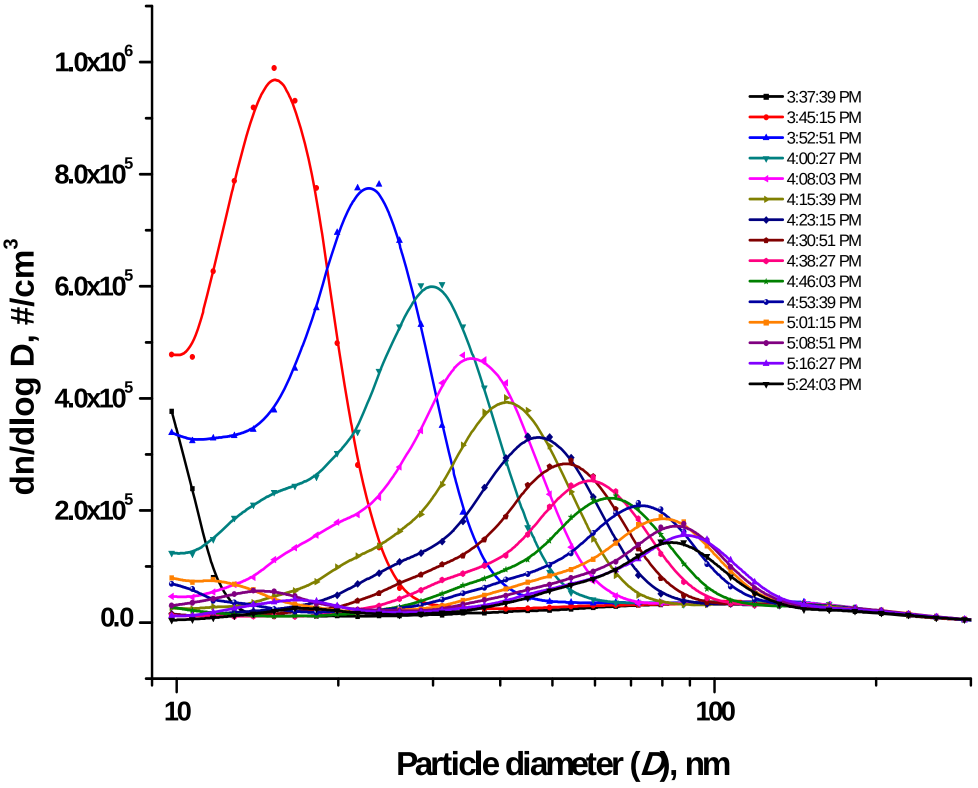

Fig. 5.14: Temporal evolution of particle size spectrum (Each curve was obtained at an interval of ~8 minutes)

The evolution of the total number concentration and mean particle diameter are shown in figures 5.15 and 5.16. From the Fig. 5.15, it is observed that the total number concentration increases rapidly to a peak value and then decreases slowly. The time taken to reach the peak concentration is 633 seconds. During this period, the number concentration increases linearly due to the source injection. The coagulation process is weak during this time period since the number concentration is low. Once the chamber attains sufficiently high aerosol number concentration, significant rate of coagulation is initiated since the coagulation rate is proportional to the square of the number concentration.

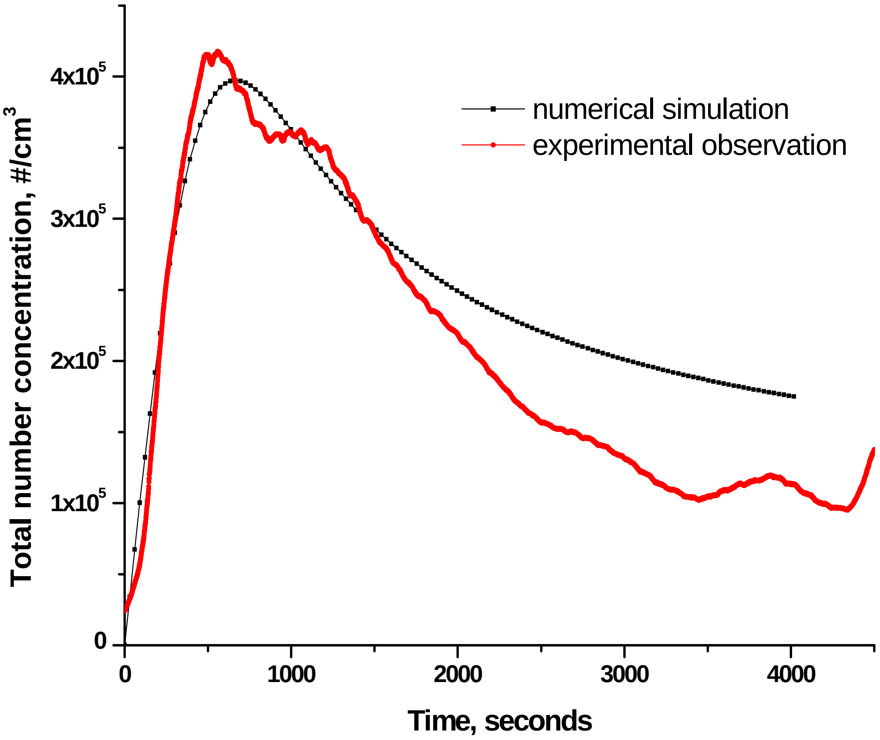

Fig. 5.15: Evolution of total number concentration in the 0.5 m^3 chamber - comparison of experimental results with numerical simulation

Fig.5.15 shows that the theoretical predictions compares well with the experimental results during the initial period (upto 1500 seconds). After this duration, the experimental results show faster decay of total number concentration as compared to simulated results. This may be due to the increase in the coagulation rate. The coagulation rate increases because of the particle growth by vapour condensation (vapour being continuously emitted by the source) in addition to the coagulation. Also, the observed multiple peaks suggest that the nulceation bursts are taking place whenever the vapour concentration reaches above the saturation value in this system.

These processes (nucleation and condensation) are not accounted in the present numerical model, and hence the deviation of the predicted values from the experiments in the later part.

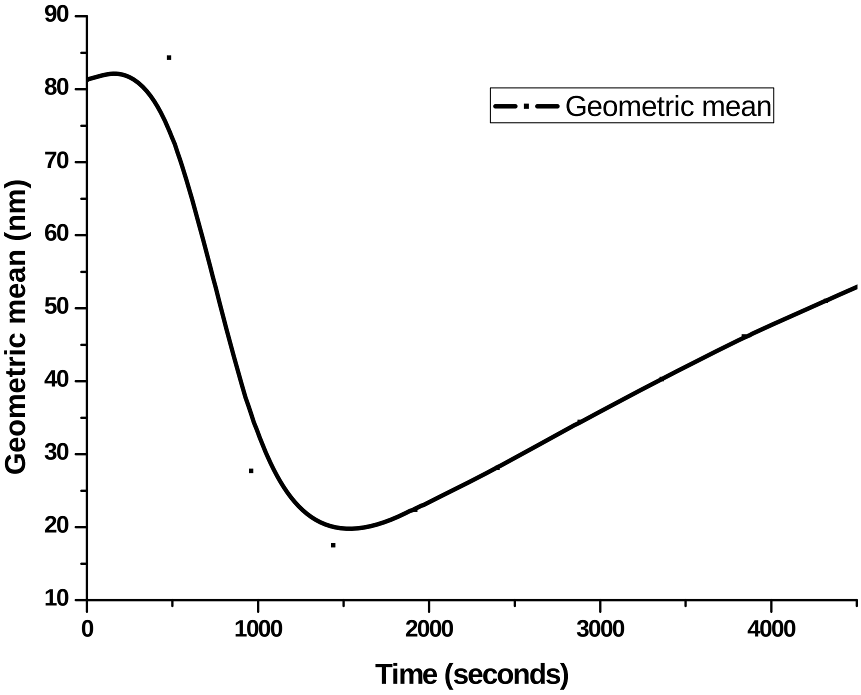

Fig. 5.16: Temporal evolution of particle diameter (geometric mean) in the 0.5 m^3 chamber

From the experimental measurements, one can predict the source emission rate using the non-dimensional variables defined in Eq.(5.28). Using the peak concentration and the time to reach peak concentration (3.98 x 10^5 #/cm^3 and 633 seconds respectively) from the experiments and the characteristic concentration (N_c = N_p/N^*) and time (t_c = t_p/t^*) from simulations, we estimated the source emission rate ($S = N_c/t_c$) as ~ 1.2 x 10^9 #/(m^3 sec). Then, the primary particle emission rate of this hot wire generator is estimated at ~ 6.0 x 10^8 #/sec. This result is in comparison with typical particle generation rates observed in hot-wire based particle generators (for example, the particle generation rate reported by Seipenbusch et al, 2008 is about 3.4 x 10^8 #/s). This study demonstrates that the theory is useful in characterising particle emission rates from sources using transient concentration buildup data in closed chambers. This opens up the possibility of an important application for assessing the particle emission rates of variety of fossil fuel based combustion sources used in domestic environments which are responsible for large scale indoor air pollution in rural areas.

5.6. Summary

A non-dimensional form has been found for the concentration decay $N^*(t^*)$ in the limit $t^*\to\infty$ of a coagulating system with constant source term. Simulations combined with analytical results using two-group model (Fuchs coagulation kernel) indicate an asymptotic decay of number concentration in the form $N^*\left(t^*\right) \sim t^{*-0.4}$ which is in marked contrast with the well known t^{-1} behavior for systems with a one-time aerosol injection.

The detailed numerical study brings forth several important features of coagulation of particles injected continuously into an air space:

Fractal dimension, initial particle size, injection rate, and ventilation are identified as key variables that influence the evolution of particle characteristics. It is shown that, indeed, the number distribution of this system gradually assumes a bimodal shape, with the larger mode attaining prominence more rapidly for fractal particles and at higher injection rates. In general, the overall concentration of a coagulating system with a constant source term attains a peak soon after nanoparticle emission starts, and then tends toward an asymptotic steady-state limit. An asymptotic law ($t\to\infty$) for the decay of number concentration is derived using an analytical model (two-group model).

The number concentration attains a peak when the air space is sufficiently filled with particles, followed by a gradual concentration, which is more pronounced for fractal aggregates as compared to compact particles. Peaking occurs more rapidly at higher concentrations when source injection rate is increased. For the total number concentration these features agree well even quantitatively, with the experimental data observed by Seipenbusch et al. (2008).

Ventilation of the air space, even a small amount of ventilation, causes the particle concentration to stabilize (i.e. converge toward a finite asymptotic value), as opposed to no ventilation which always seems to lead to an asymptotic concentration of zero regardless of source strength. Particle concentrations may thus be larger at low ventilation rates as compared to an unventilated space. Also, there appears to exist a concentration maximum for a certain ventilation rate. Little ventilation may therefore be a worse prevention measure for nanoaerosols than no ventilation at all.

A prominent effect of applying coagulation dynamics to rapidly mixed systems having continuous injection, is the shift of aerosol mass from the nanoparticle regime into micrometer sized particles. This shift is stabilized by the presence of ventilation rate. The stabilizing effect of ventilation is due to dilution of the secondary particle concentration, which would - without this continued dilution - continue to grow with time in both concentration and particle size, thereby leading to an ever increasing rate of coagulation between the primary and secondary modes. Note that this very relevant feature of aerosol dynamic behavior in a workplace cannot be reproduced by simulation with a size-independent collision kernel.

It was further found that the secondary mode occurs more prominently for fractal particles having larger initial sizes. Several of these results are qualitatively consistent with the experimental observations, but do not match quantitatively, possibly due to the presence of initial inhomogeneity of the aerosols during source injection.

Chapter 6. Summary and Conclusions

This chapter summarises the accomplishments of this work and provides a final overview on the study of coagulation of dispersing aerosol systems. It then offers suggestions for further research work.

6.1. Summary

A key question for assessing the impact of anthropogenic aerosols on the environment pertains to the estimation of the fraction of particles that persist in the atmosphere to form background aerosols. Among the various factors that contribute to this, coagulation is an important and numerically the most difficult issue to handle. The study addresses this question by combining coagulation with dispersion and different emissions scenarios to understand the long time and far field behaviour of aerosol size spectra and number concentrations. To this end, numerical and analytical models have been developed for modeling aerosol evolution in the atmosphere, emitted from localized sources under the combined action of coagulation and dispersion. This work presents the study of coagulation of the following dispersing aerosol systems:

- instantaneous puff releases,
- continuous plume releases, and
- continuous and homogeneous volumetric releases.

In this study, the following aspects are focused:

1) Temporal – spatial variations of aerosol particle number size distributions,

2) Temporal variations of total particle number concentrations,

3) Emission rates and fate of aerosol particles in the atmosphere,

4) Factors influencing the particle number concentrations and its size distributions, and

5) Modal structure of aerosol particles.

Four mathematical models are developed and evaluated in this study. They are (the first three models are solved using analytical methods),

1) Diffusion approximation model to obtain particle number survival fractions for puff releases.

2) Improved diffusion approximation model with coagulation-induced flattening effect to obtain particle number survival fractions for puff and plume releases.

3) Two-group aerosol particle model to investigate and characterize the indoor aerosol particles released continuously in to a closed environment.

4) Comprehensive numerical model to obtain solutions to the coagulation-dispersion equation for the puff, plume, and continuous volumetric releases mentioned above.

From these models,

1) simple useful formulae to estimate the effective source emission factors/survival fractions for puff and plume releases, and

2) temporal evolution of aerosol characteristics for continuous volumetric releases

are obtained.

In particular, the study introduces the concept of survival fractions as a means of predicting the atmospheric number loading factors of particles released from localized sources such as instantaneous puff and continuous plume releases.

In the case of instantaneous puff releases, the analytical solutions have been obtained for constant and free-molecular coagulation kernels by combining prescribed diffusion approximation with Laplace transforms and scaling theory, respectively. While, the formulae for the survival fractions obtained within the framework of Jaffe approximation have similar functional forms as those obtained by earlier investigators based on a uniformly mixed-expansion model, the present approach provides definite pre-factors involving the physical parameters of the processes. The results have been tested against numerical solutions developed by combining finite-difference with nodal method as well as using differential equation solver package of Mathematica. Although the analytical results for the temporal variations of the survival fractions follow similar trends as numerical predictions, they show systematic deviations up to about 25% under strong coagulation. This suggests that the expansion-coagulation models are not fully equivalent to diffusive-coagulation models except in the limit of Jaffe approximation.

An improved diffusion approximation model is introduced to improve the predictions of analytical solutions. The underlying assumptions in this model are, (i) representative constant kernel coagulation coefficient is used and (ii) dispersion is handled by a constant diffusion coefficient for spherical symmetric puffs and a down-stream distance dependent diffusion coefficient for plumes. The approach consists of constructing moment equations for the evolution of number concentration, mass concentrations and variance of the spatial extension of puff or plume in terms of either time or downstream distance. The equation for the variance includes a special effect due to coagulation induced flattening of the concentration in-homogeneity in high concentration regions in addition to the normal atmospheric dispersion effect. From these equations, the number survival fractions surviving coagulation, are defined as

(i) for puffs: ratio of the particles present in the entire space at any given time with respect to initially emitted number of particles and (ii) for plumes: ratio of fluence rate of particles transported by advection across a given downstream distance reckoned with respect to the emission rate at the source region. The fraction of particles contributed by these sources to persist as background aerosols in the atmosphere are then obtained as the asymptotic limits of the survival fractions ($\psi(\infty)$) either as time or downstream distance tends to infinity (as the case may be). For the puff case, we propose a formula,

$$\psi^{puff}(\infty) = \left(1 + \frac{5\text{A}}{4}\right)^{-4/5}$$

where, $A = \dfrac{KN_0}{4(2\pi)^{3/2} Db_0}$, and for plume

$$\psi^{plume}(\infty) = (1 + 1.32\,\mu)^{-0.76}$$

where, $\mu = \dfrac{KS_0}{6\sqrt{3}\,U\sigma_0^{4/3}(C\varepsilon)^{1/3}}$ for the asymptotic survival fractions. The implications of these results for a few practically important problems such as vehicular emissions, forest fires, etc are demonstrated.

In the case of continuous and spatially homogeneous volumetric releases, a detailed numerical study is carried out to bring forth several important features of coagulation of particles injected continuously into an air space. The number concentration attains a peak, followed by a gradual concentration, which is more pronounced for fractal aggregates as compared to compact particles. Peaking occurs more rapidly at higher concentrations when source injection rate is increased. The limit concentration is nonzero finite only in the presence of ventilation, even for very low ventilation rates. Furthermore, there exists a critical ventilation rate at which the steady-state number concentration attains maximum value. It was further found that the secondary mode occurs more prominently for fractal particles having larger initial sizes. Several of these results are consistent with the experimental observations, but the presence of initial spatial inhomogeneity of the aerosols during source injection needs to be studied separately. The total concentration is found to scale reasonably well when expressed in terms of a characteristic concentration $N_c=(S/K_{11})^{1/2}$ and a characteristic time $t_c=(SK_{11})^{-1/2}$, where S is the injection rate density (# m^{-3} s^{-1}) and K_{11} (m^3 s^{-1}) is the coagulation coefficient of injected particles. When the ventilation is zero, the simulations suggest that, following the initial peak, the scaled concentration $N^*(t^*)$ continuously decreases by a power law ~ $t^{*\alpha}$ with $\alpha \approx -0.33$ for particles with fractal dimension of 1.75 and for $t^* < 20$. Simulations combined with analytical results using simplified model (two-group coagulation model) indicate an asymptotic decay of number concentration in the form $N^*(t^*) \sim t^{*-0.4}$, ($t^* > 1000$) which is in marked contrast with the well known t^{-1} ($\alpha = -1$) behavior for systems with a one-time aerosol injection.

6.2. Conclusions

The study brings out several important features of the coagulation-dispersion process affecting the evolution of particles released into environment. These include the effects of mode of release and the various aerosol and environmental parameters on particle number concentrations and effective sizes. In the case of burst releases, the study estimates the time scales in which the concentration falls, from a large initial value, to normal levels. Although it is too ideal to be of direct practical applications to radiological dispersal devices, it provides the basic formulations for stepping up onto the inclusion of other processes such as heterogeneous coagulation with ground dust. The concept of survival fraction and number loading factors introduced in the context of puff and plume releases capture the essential quantity of environmental significance for anthropogenic sources. The formulae derived have great simplicity for practical evaluations and capture the essential parameters of the problem.

One of the major challenges in simulating the aerosol number concentration and size distribution in regional and global atmospheric scales is the description of aerosol dynamics near sources of primary particles. Unfortunately, simulation of the rapid dilution of particles as they disperse away from their source together with their coagulation and removal is prohibitively expensive for regional and global chemical transport models. There is a need to be able to simulate the dominant behaviour of sub-grid aerosol dynamics (or near-source aerosol dynamics) without having to resolve processes at the individual plume level. The present study of coagulation of dispersing aerosols near the emission sources paves a concrete platform to address these issues. The source modifier functions obtained for the puff and plume releases may serve as a useful tool in reducing the computational time by eliminating the need to embark on detailed modeling at the near source region. The near-source aerosol dynamics may be incorporated as a lumped term modifying the source itself at sub-grid level for application in 3-D models.

The results obtained from the continuous and homogeneous volumetric releases will have implications for an assessment of toxicological risk as well as in planning of safety measures in the context of industrial processing and applications of nanoparticles. They reinforce the notion that number concentration and the effective particle size standout as crucial metrics. Also, the broader results related to the effect of concentration and ventilation rate may yield modifying factors to be used in a predictive exposure model for workplace environment such as Advanced REACH Tool (ART) (Schneider et al., 2011). This however calls for more studies by combining realistic situations such as the effect of background particles, deposition rates, and the spatial dispersion of the releases. It is also important to look for alternative, less time consuming models to yield reliable and quick results to address nanoparticle toxicological issues.

6.3. Future work

A. It is of considerable value to integrate the main results obtained in this thesis for puff and plume releases with detailed regional aerosol dynamics models to calculate the long term contributions from various emission sources to air pollution. In this context, the plume release problem enables us to obtain source term modifications (accounting for local coagulation effects) by using the information on the source area, mass emission rate and local atmospheric turbulence conditions. With these modified source term, one can study their long range mixing and dispersion by pure advection diffusion equations, without having to worry on intra-coagulation effects.

B. Investigation of coagulation-diffusion dynamics of aerosol puffs/plumes interacting with the background aerosol particles is an important issue, which will be useful for the atmospheric aerosol transport models. An immediate application will be the development of first principle model for radon progeny attachment dynamics to a coagulating aerosol. This may be validated against various activity distributions of radionuclides measured in the environment.

C. Numerical simulation can be further pursued for the uniformly mixed volume expansion model by including nucleation and condensation processes to the existing model. Addition of interaction with the background aerosols will lead to realistic estimate of the aerosol loading. Experiments are also required to validate these models.

D. It is required to carry out detailed investigation on the asymptotic behaviour of the aerosols continuously injected into confined environments by including size dependent removal processes. Although an experimental study has been made to examine the model results, many more experimental studies will be required to bring out the various processes taking place in an evolving aerosol system. The experimental observation of multiple aerosol concentration peaks is a case in point that cannot be explained by coagulation alone. It may be necessary to improve the models by including nucleation and condensation processes to handle these situations. As there exists very little past work in this area it offers a rich and relevant topic for future investigations.

References

1. Albriet, B., Sartelet, K. N., Lacour, S., Carissimo, B., & Seigneur, C. (2010). Modelling aerosol number distributions from a vehicle exhaust with an aerosol CFD model. Atmospheric Environment, 44, 1126-1137.
2. Allen, M.D., & Raabe, O. G. (1982). Reevaluation of Millikan's oil drop data for the motion of small particles in air, J. Aerosol Science. 13, 537-547.
3. Aloyan, A. E. (2009). Modeling aerosol dynamics during forest fires, Izvestiya, Atmospheric and Oceanic Physics, 45, 55-68.
4. Andersson, K. G., Mikkelsen, T., Astrup, P., Thykier-Nielsen, S., Jacobsen, L. H., Schou-Jensen, L., Hoe, S. C., & Nielsen, S. P. (2008). Estimation of health hazards resulting from a radiological terrorist attack in a city, Radiation Protection Dosimetry, 131(3), 297-307.
5. Arya, S.P. (1999). Air pollution meteorology and dispersion. Oxford University Press
6. Barrett, J. C., & Mills, R. (2002). An approximate treatment of aerosol coagulation and removal, Aerosol Science, 33, 1327-1339.
7. Batchelor, G. K. (1952). Diffusion in a field of homogeneous turbulence. II. The relative motion of particles. Proceedings of the Cambridge Philosophical Society, 48, 345-363.
8. Bellman, M.D, Kalaba, R.E., & Lockett, J.A. (1966). Numerical inversion of the Laplace transform: Applications to biology, economics, engineering and physics. Elsevier, NY.
9. Berry, E.X. (1967). Cloud droplet growth by collection, Journal of the atmospheric sciences, 24, 688-701.
10. Bertoin, J. (2002). Eternal solutions to Smoluchowski's coagulation equation with additive kernel and their probabilistic interpretations. Annals of Applied Probability, 12(2), 547-564.

11. Brock, C. A., Washenfelder, R. A., Trainer, M., Ryerson, T. B., Wilson, J. C., Reeves, J. M., Huey, L. G., Holloway, J. S., Parrish, D. D., Hübler, G., & Fehsenfeld, F. C. (2002). Particle growth in the plumes of coal-fired power plants, J. Geophysical Research, 107(D12), 4155.
12. Byakov, V.M., & Stepanov, S.V. (2006). The mechanism for the primary biological effects of ionizing radiation. Physics – Uspekhi, 49, 469-487.
13. Chassaing, P., & Louchard, G. (2002). Phase transition for parking blocks, Brownian excursions and coalescence. Random Structures Algorithms, 21, 76-119.
14. Chen, W. Y. (1974). Energy Dissipation Rates of Free Atmospheric Turbulence. J. Atmospheric Science, 31, 2222–2225.
15. Cheng, Z., Redner, S., & Leyvraz, F. (1989). Coagulation with a steady point monomer source. Physical Review Letters, 62, 2321-2324.
16. Cohen, E.R., & Vaughan, E.U. (1971). Approximate solution of the equation for aerosol agglomeration. J. Colloid and Interface Science, 25, 612–623.
17. Crump, J. G., & Seinfeld, J. H. (1982). On existence of steady-state solutions to the coagulation equations, J. Colloid and Interface Science, 90-2, 469-476.
18. Dahneke, B. (1983). Simple kinetic theory of Brownian diffusion in vapors and aerosols. In: Meyer, R. (Ed.), Theory of Dispersed Multiphase Flow. Academic Press, New York, pp. 97–133.
19. Davies, S. C., King, J. R., & Wattis, J. A. D. (1999). The Smoluchowski coagulation equations with continuous injection, J. Phys. A: Math. Gen., 32, 7745-7763.
20. Du, H., & Yu, F. (2008). Nanoparticle formation in the exhaust of vehicles running on ultra-low sulfur fuel, Atmospheric Chemistry and Physics, 8, 4729-4739.

21. Ernst, F.O., & Pratsinis, S.E. (2006). Self-preservation and gelation during turbulence-induced coagulation, J. Aerosol Science, 37, 123-142.
22. Ernst, M. H. (1986). Kinetics of clustering in irreversible aggregation, in 'Fractals in Physics', Eds: L. Pietronero and E. Tossati, North-Holland, Amsterdam.
23. Fiebig, M., Stohl, A., Wendisch, M., Eckhardt, S., & Petzold, A. (2003). Dependence of solar radiative forcing of forest fire aerosol on ageing and state of mixture, Atmospheric Chemistry and Physics, 3, 881-891.
24. Friedlander, S. K. (2000). Smoke, Dust, and Haze: Fundamentals of Aerosol Dynamics, Second Edition, Oxford University Press, Oxford.
25. Friedlander, S.K., & Wang, C.S. (1966). The Self-Preserving Particle Size Distribution for Coagulation by Brownian Motion. Journal of Colloid and Interface Science, 22, 126-132.
26. Fuchs, N. A. (1964). The Mechanics of Aerosols, Pergamon, New York.
27. Ganguly, A.K., & Magee, J.L. (1956). Theory of radiation chemistry. III. Radical reaction mechanism in the tracks of ionizing radiations. Journal of Chemical Physics, 25, 129-134.
28. Garcıa-Nieto, P.J. (2006). Study of the evolution of aerosol emissions from coal-fired power plants due to coagulation, condensation, and gravitational settling and health impact. Journal of Environmental Management, 79, 372–382.
29. Gelbard, F., Tambour, Y., & Seinfeld, J.H. (1980). Sectional representations for simulating aerosol dynamics, J. Colloid and Interface Science, 76, 541-556.
30. Glasstone, S. (Ed), (1962). The Effects of Nuclear Weapons, rev. ed., pp. 68-86, U. S. Atomic Energy Commission, Washington, D. C.

31. Gramotneva, G., Brown, R., Ristovskia, Z., Hitchinsa, J., & Morawskaa, L. (2003). Determination of average emission factors for vehicles on a busy road. Atmospheric Environment, 37, 465–474.
32. Harper, F.T., Musolino, S.V., & Wente, W.B. (2007). Realistic radiological dispersal device hazard boundaries and ramifications for early consequence management decisions. Health Physics. 93(1), 1-16.
33. Herrero, M.A., & Rodrigo, M. (2005). A note on Smoluchowski's equations with diffusion. Applied Mathematics Letters, 18, 969-975.
34. Hidy, G.M., & Brock, J.R. (1972). Volume 3, Topics in Current Aerosol Research (Part 2). Pergamon Press: New York.
35. Hinze, J.O. (1975). Turbulence, Second Edition: McGraw-Hill: New York.
36. Hobbs, P. V., Sinha, P., Yokelson, R. J., Christian, T. J., Blake, D. R., Gao, S., Kirchstetter, T. W., Novakov, T., & Pilewskie, P. (2003). Evolution of gases and particles from a savanna fire in South Africa, J. Geophysical Research, 108, D13, 8485.
37. Holmes, N.S., & Morawska, L. (2006). A Review of Dispersion Modelling and its application to the dispersion of particles: An overview of different dispersion models available. Atmospheric Enivronment, 40(30): 5902-5928.
38. Huang, D.D., & Seinfeld, J.H. (1990). J. Colloid and Interface Science, 139, 238.
39. Hudischewskyj, A.B., & Seigneur, C. (1989). Mathematical Modeling of the Chemistry and Physics of Aerosols in Plumes. Environmental Science and Technology, 23, 413-421.
40. Hughes, L.S, Cass, G.R, Gone, J, Ames, M, & Olmez, I. (1998). Physical and chemical characterization of atmospheric ultrafine particles in the Los Angeles area, Environmental Science and Technology, 32, 1153–1161.

41. Ichoku, C., & Kaufman, Y.J. (2005). A method to derive smoke emission rates from MODIS fire radiative energy measurements. IEEE transactions on geosciences and remote sensing, 43 (11), .
42. Ichoku, C., Martins, J. V., Kaufman, Y. J., Wooster, M. J., Freeborn, P. H., Hao, W. M., Baker, S., Ryan, C. A., & Nordgren, B. L. (2008). Laboratory investigation of fire radiative energy and smoke aerosol emissions. Journal of Geophysical Research, 113, D14S09.
43. IPCC, 2007: Climate Change 2007: Synthesis Report. (2007). Contribution of working groups I, II and III to the fourth assessment report of the Intergovernmental Panel on Climate Change [Core Writing Team, Pachauri, R.K and Reisinger, A. (eds.)]. IPCC, Geneva, Switzerland, 104 pp.
44. Jacobson, M. Z. (2005). Chapter-15, Fundamentals of atmospheric modeling, Second Edition, Cambridge University Press.
45. Jacobson, M. Z., & Seinfeld, J. H. (2004). Evolution of nanoparticle size and mixing state near the point of emission. Atmospheric Environment, 38, 1839-1850.
46. Jaffe, G. (1913). Zur Theorie der Ionisation in Kolonnen. Ann. Physik. 42, 303.
47. Jaffe, G. (1940). The Theory of Recombination. Physical Review, 58, 968-976.
48. Janhall, S., Andreae, M. O., & Poschl, U. (2010). Biomass burning aerosol emissions from vegetation fires: particle number and mass emission factors and size distributions. Atmos. Chem. Phys., 10, 1427–1439.
49. Jeong, J. I., & Choi, M. (2003). A simple bimodal model for the evolution of non-spherical particles undergoing nucleation, coagulation, and coalescence, J. Aerosol Science, 34, 965-976.

50. Jones, H., & Miller, A. R. (1948). The Detonation of solid explosives: the equilibrium conditions in the detonation wave-front and the adiabatic expansion of the products of detonation, R. Soc. Lond. A, 194, 480-507.
51. Kasper, G. (1984). On the Coagulation Rate of Aerosols with Spatially Inhomogeneous Particle Concentrations, J. Colloid and Interface Science, 102-2 560-562.
52. Kerminen, V., & Wexler, A.S. (1995). The interdependence of aerosol processes and mixing in point source plumes, Atmospheric Environment, 29 (3), 361-375.
53. Kim, D. S., Park, S. H., Song, Y. M., Kim, D. H., & Lee, K. W. (2003). Brownian coagulation of polydisperse aerosols in the transition regime, Aerosol Science, 34, 859-868.
54. Kim, D., Kim, K., & Zhao, Q. (2003). Production of monodisperse nanoparticles and application of discrete-monodisperse model in plasma reactors, Journal of Nanoparticle Research, 5, 211-223.
55. Koch, W., & Friedlander, S. K. (1990). The effect of particle coalescence on the surface area of a coagulating aerosol, J. Colloid and Interface Science, 140(2), 419-427.
56. Koch, W., Pohlmann, G., & Schwarz, K. (2008). A reference number concentration generator for ultrafine aerosols based on Brownian coagulation, J. Aerosol Science, 39, 150-155.
57. Kramers, H.A. (1952). On a modification of Jaffe's theory of columnar-ionization. Physica, XVIII, 665-675.
58. Kruis, F.E., & Kusters, K.A. (1997). The collision rate of particles in turbulent flow. Chemical Engineering Communications, 158, 201-230.

59. Lai, F.S., Friedlander, S.K., Pich, J., & Hidy, G.M. (1972). The self-preserving particle size distribution for Brownian coagulation in the free-molecule regime. J. Colloid Interface Science, 39, 395–405.

60. Landgrebe, J. D., & Pratsinis, S. E. (1989). Gas-phase manufacture of particulates: Interplay of chemical reaction and aerosol coagulation in the free-molecular regime, Industrial Engineering Chemistry Research, 28, 1474-1481.

61. Landgrebe, J.D., & Pratsinis, S.E. (1990). A discrete-sectional model for powder production by gas phase chemical reaction and aerosol coagulation in the free-molecular regime. J. Colloid Interface Science, 139, 63–86.

62. Lee, K., McCormick, W.D., Pearson, J.E., & Swinney, H.L. (1994). Experimental observation of self-replicating spots in a reaction-diffusion system. Nature, 369, 215-218.

63. Lee, S.D., Snyder, E.G., Willis, R., Fischer, R., Gates-Anderson, D., Sutton, M., Viani, B., Drake, J., & MacKinney, J. (2010). Radiological dispersal device outdoor simulation test: Cesium chloride particle characteristics, Journal of Hazardous Materials, 176 (1–3), 56-63.

64. Lehtinen, K. E. J., & Zachariah, M. R. (2001). Self-Preserving Theory for the Volume Distribution of Particles Undergoing Brownian Coagulation. J. Colloid and Interface Science, 242, 314-318.

65. Li, C., Jenq, F., & Lin, W. (1992). Field characterization of submicron aerosols from indoor combustion sources. Journal of Aerosol Science, 23(1), 547-550.

66. Lighty, J. S., Veranth, J.M., & Sarofim, A. F. (2000). Combustion aerosols: factors governing their size and composition and implications to human health. Journal of the Air & Waste Management Association, 50, 1565-1618.

67. Lin, J.C. (1991). Symmetry between diffusion-limited coagulation and annihilation. Physical Review A, 43 (10), 5714-5716.
68. Liu, B. Y. H., Pui, D. Y. H., Hogan, A.W., & Rich, T.A. (1975). Calibration of the Pollak counter with monodisperse aerosols, J. Applied Meteorology, 14, 46-51.
69. Lushnikov, A. A. (2010). Introduction to Aerosols, in Aerosols - Science and Technology (Ed. I. Agranovski), Wiley-VCH Verlag GmbH & Co. KGaA, Weinheim, Germany.
70. Lushnikov, A.A. (2004). From Sol to Gel Exactly, Physical Review Letters, 93 (19), 198302 (1-4).
71. Lushnikov, A.A., & Kulmala, M. (2002). Singular self-preserving regimes of coagulation processes, Physical Review E, 65, 041604.
72. Lushnikov, A.A., Negin, A.E., & Pakhomov, A.V. (1990). Experimental observation of the aerosol-aerogel transition, Chemical Physics Letters, 175 (1,2), 138-142.
73. Mathematica, Wolfram Inc., 2005.
74. Matsoukas, T., & Friedlander, S. K. (1991). Dynamics of aerosol agglomerate formation, J. Colloid and Interface Science, 146(2), 495-506.
75. Mayya, Y.S., & Hollander, W. (1995). Ion Densities and Particle Charges for Alpha Ionization in an Aerosol Atmosphere: Columnar Recombination Corrections. Aerosol Science and Technology, 23, 628-640.
76. Mayya, Y.S., & Kotrappa. (1982). Modified ion balance equation for continuous columnar ionization in air. Radiation Research, 92, 19-29.
77. Monkkonen, P., Koponen, I.K., Lehtinen, K.E.J., Uma, R., Srinivasan, D., Hameri, K., & Kulmala, M. (2004). Death of nucleation and Aitken mode particles: observations at extreme atmospheric conditions and their theoretical explanation. J. Aerosol Science, 35, 781-787.

78. Mönkkönen, P., Uma, R., Srinivasan, D., Koponen, I. K., Lehtinen, K. E. J., Hämeria, K., Suresh, R., Sharma, V. P., & Kulmala, M. (2004). Relationship and variations of aerosol number and PM10 mass concentrations in a highly polluted urban environment—New Delhi, India. Atmospheric Environment, 38 (3), 425-433.

79. Mulholland, G. W., & Baum, H. R. (1980). Effect of initial size distribution on aerosol coagulation. Physical Review Letters, 45, 761-763.

80. Naito, S., Hirata, Y., Izumi, M., Sano, A., Miyamoto, Y., Aoyama, Y., & Yamaguchi, H. (2007). Ion current prediction model considering columnar recombination in alpha radioactivity measurement using ionized air transportation. Journal of Nuclear Science and Technology, 44, 121-128.

81. Narayanan, K.S.S., & Ramadurai, K.S. (1992). The numerical solution of inverse problems using Gaussian quadrature. European Journal of Physics, 13, 111-116.

82. Nathans, M.W., Thews, R., Holland, W.D., & Benson, P.A. (1970). Particle size distribution in clouds from nuclear airbursts. Journal of Geophysical Research, **75**, 7559-7572.

83. Oberdorster, G. (2000). Toxicology of ultrafine particles: in vivo studies, Philosophical Transactions of The Royal Society A, 358, 2719-2740.

84. Oberdörster, G., Oberdörster, E., & Oberdörster, J. (2005). Nanotoxicology: An emerging discipline evolving from studies of ultrafine particles. Environmental Health Perspectives, 113, 823-839.

85. Ott, S., & Mann, J. (2000). An experimental investigation of the relative diffusion of particle pairs in three-dimensional turbulent flow. Journal of Fluid Mechanics, 422, 207-223.

86. Otto, E., Fissan, H., Park, S. H., & Lee, K.W. (1999). The log-normal size distribution theory of Brownian aerosol coagulation for the entire particle size range: Part II - Analytical solution using Dahneke's coagulation kernel. Journal of Aerosol Science, 30 (1), 17–34.

87. Pandey, V. K., & Pandey, A.C. (2007). Turbulent kinetic energy and its dissipation rate of the Indonesian throughflow region via Lombok and Savu Straits, J. Ind. Geophys. Union, 11(2), 117-122.

88. Peliti, L. (1986). Renormalisation of fluctuation effects in the $A + A \rightarrow A$ reaction. Journal of Physics A: Mathematical and General, 19, L365-L367.

89. Pierce, J.R., Theodoritsi, G., Adams, P.J., & Pandis, S.N. (2009). Parameterization of the effect of sub-grid scale aerosol dynamics on aerosol number emission rates. Journal of Aerosol Science, 40, 385-393.

90. Prakash, A., Bapat, A.P., & Zachariah, M.R. (2003). A Simple numerical algorithm and software for solution of nucleation, surface growth, and coagulation problems. Aerosol Science and Technology, 37, 892–898.

91. Qiao, R.L., Li, Z., & Wen, C.S. (1998). Effect of weak Brownian motion on gravitational coagulation. J. Colloid and Interface Science, 202, 205-207.

92. Radke, L. F., Hegg, A. S., Hobbs, P. V., & Penner, J. E. (1995). Effects of aging on the smoke from a large forest fire. Atmospheric Research, 38, 315-322.

93. Ramachandran, S., & Rajesh, T.A. (2007). Black carbon aerosol mass concentrations over Ahmedabad, an urban location in western India: Comparison with urban sites in Asia, Europe, Canada, and the United States. Journal of Geophysical Research, 112, D06211.

94. Richardson, L.F. (1926). Atmospheric diffusion shown on a distance-neighbour graph. Proceedings of the Royal Society of London A, 110, 709-737.

95. Rodriguez, S., & Cuevas, E. (2007). The contributions of “minimum primary emissions” and “new particle formation enhancements” to the particle number concentration in urban air. Journal of Aerosol Science, 38, 1207-1219.

96. Rosen, G. (1984). Brownian-motion correspondence method for obtaining approximate solutions to nonlinear reaction-diffusion equations. Physical Review Letters, 53, 307-310.

97. Ruckenstein, E., & Chi, J.C. (1975). Conditions for the size spectrum of aerosols to be self-preserving. Journal of Colloid and Interface Science, *50*, 508–518.

98. Saffman, P.G., & Turner, J.S. (1956). On the collision of drops in turbulent clouds. J. Fluid Mechanics, 1, (1), 16-30.

99. Sahni, D. (1983a). Comment on exact Brownian coagulation. Journal of Colloid and Interface Science, 96 (2), 560–560.

100. Sahni, D. (1983b). An exact solution of Fokker-Planck equation and Brownian coagulation in the transition regime. Journal of Colloid and Interface Science, 91 (2), 418–429.

101. Schneider, T., & Jensen, K. A. (2009). Relevance of aerosol dynamics and dustiness for personal exposure to manufactured nanoparticles. J. Nanopart. Res, 11, 1637-1650.

102. Schneider, T., Brouwer, D. H., Koponen, I. K., Jensen, K. A., Fransman, W., Duuren-stuurman, B. V., Tongeren, M. V., & Tielemans, E. (2011). Conceptual model for assessment of inhalation exposure to manufactured nanoparticles. J. Exposure science and environmental epidemiology, 1-14, 2011.

103. Scott, W.T. (1968). Analytic Studies of Cloud Droplet Coalescence I. Journal of the atmospheric sciences, 25, 54–65.

104. Seinfeld J.H., & Pandis, S.N. (2006). Atmospheric Chemistry and Physics: From Air Pollution to Climate Change. Second Edition. John Wiley & Sons, Inc.

105. Seipenbusch, M., Binder, A., & Kasper, G. (2008). Temporal distribution of nanoparticle aerosols in workplace exposure. Annals of Occupation Hygiene, 52-8 707-716.

106. Shah, B.H., Ramakrishna, D., & Borwanker, J.D. (1977). Simulation of particulate systems using the concept of the interval of quiescence. AIChE Journal, 23, 897-904.

107. Sheih, C.M. (1977). Mathematical modeling of particulate thermal coagulation and transport downstream of an urban area source. Atmospheric Environment, 11, 1185–1190.

108. Sheth, R. K., & Pitman, J. (1997). Coagulation and branching process models of gravitational clustering. Monthly Notices of the Royal Astronomy Society, 289, 66–80.

109. Simons, S. (1987). The steady-state equation for Brownian diffusion in the presence of particle coagulation. Journal of Physics D: Applied Physics, 20, 75-81.

110. Simons, S. (1992). On the solution of the time independent equation for the diffusion of coagulating clusters. Physics Letters A, 171, 172-174.

111. Simons, S. (1996). On the steady-state equation for particles undergoing simultaneous Brownian diffusion and coagulation. Journal of Physics A: Mathematical and General, 29, 303–307.

112. Simons, S., & Simpson, D.R. (1988). The effect of particle coagulation on the diffusive relaxation of a spatially inhomogeneous aerosol. Journal of Physics A: Mathematical and General, 21, 3523-3536.

113. Simons, S., Williams, M. M. R., & Cassell, J. S. (1986). A kernel for combined Brownian and gravitational coagulation. J. Aerosol Science, 17(5). 789-793.

114. Slemrod, M. (1990). Coagulation-diffusion systems: Derivation and existence of solutions for the diffuse interface structure equations. Physica D, 46, 351-366.

115.Smoluchowski, M. V. (1916) Drei Vortrage uber Diffusion, Brownsche Bewegung und Koagulation von Kolloidteilchen, Physik. Zeit., vol. 17, p. 557-585.

116.Sreekanth, B. (2011). Modeling of aerosol particle size distribution from burst releases. M.Tech thesis, Homi Bhabha National Institute – Bhabha Atomic Research Centre, Mumbai.

117.Suresh Babu, S., & Krishna Moorthy, K. (2001). Anthropogenic impact on aerosol black carbon mass concentration at a tropical coastal station: A case study. Current Science, 81, 1208-1214.

118.Taylor, G.J. (1963). Analysis of the explosion of a long cylindrical bomb detonated at one end. The Scientific papers of Sir G. J. Taylor, Vol. III, p. 277, Cambridge University Press, London.

119.Thomas, J., & Imel, D.A. (1987). Recombination of electron-ion pairs in liquid argon and liquid xenon. Physical Review A, 36, 614-616.

120.Trueblood, M. B., Carter, M. A., Hagen, D. E., Whitefield, P. D., & Podzimek, J. (2000). Size distribution and critical supersaturation spectrum of the aerosol from an electrically heated nichrome wire. CP534, Nucleation and Atmospheric Aerosols: 15th International Conference, Edited by B. N. Hale and M. Kulamala, 873-876.

121.Turco, R.P, & Yu, F. (1997). Aerosol invariance in expanding coagulating plumes. Geophysical Research Letters, 24, 1223-1226.

122.Turco, R.P, & Yu, F. (1998). Aerosol size distribution in a coagulating plume: Analytical behavior and modeling applications. Geophysical Research Letters, 25, 927-930.

123.Turco, R.P, & Yu, F. (1999). Particle size distributions in an expanding plume undergoing simultaneous coagulation and condensation. Journal of Geophysical Research, 104, 19,227-19,241.

124.Vali, G., Rogers, D., Gordon, G., Saunders, C. P. R., Reischel, M., & Black, R. (1978). Aerosol and nucleation research in support of NASA cloud physics experiments in space, Report No.: NASA-CR-161115. Final Report Wyoming University, Laramie, Department of Atmospheric Science.

125.Van Dongen, P. G. J., & Ernst, M. H. (1985). Dynamic scaling in the kinetics of clustering. Physical Review Letters, 54, 1396-1399.

126.Vemury, S., Kusters, K.A., & Pratsinis, S.E. (1994). Time lag for attainment of the self-preserving particle size distribution by coagulation. J. Colloid Interface Sci., 165, 53–59.

127.Wang, C.S., & Friedlander, S.K. (1967). The self-preserving particle size distribution for coagulation by Brownian motion: II. Small particle slip correction and simultaneous shear flow. J. Colloid Interface Sci., 24, 170–179.

128.Wexler, A. S., Lurmann, F. W., & Seinfeld, J. H. (1994). Modeling urban and regional aerosols. I. Model development. Atmospheric Environment, 28, 531–546.

129.White, W. H., (1982). On the form of steady-state solutions to the coagulation equations. J. Colloid and Interface Science, 87-1, 204-208.

130.Wilhelm, H.E. (1967). Recombination in columns. Journal of Chemical Physics, 47, 4356-4366.

131.Williams, M.M.R., & Loyalka, S.K. (1991). Aerosol Science Theory and Practice. Pergamon Press: New York.

132.Wojcik, M., & Tachiya, M. (2004). Electron-ion recombination in dense gaseous and liquid argon: effects due to argon cation clusters allow to explain the experimental data. Chemical Physics Letters, 390, 475-480.

133.Xiong, Y., & Pratsinis, S.E. (1993). Formation of agglomerate particles by coagulation and sintering: part I. A two-dimensional solution of the population balance equation. J. Aerosol Science, 24, 283-300.

134.Zai, S., Zhen, H., & Jia-song, W. (2006). Studies on the size distribution, number and mass emission factors of candle particles characterized by modes of burning. Journal of Aerosol Science, 37, 1484-1496.

135.Zhang, K. M., & Wexler, A. S. (2004). Evolution of particle number distribution near roadways – Part I: analysis of aerosol dynamics and its implications for engine emission measurement. Atmospheric Environment, 38, 6643-6653.

136.Zhao, H., Maisels, A., Matsoukas, T., & Zheng, C. (2007). Analysis of four Monte Carlo methods for the solution of population balances in dispersed systems, Powder technology, 173, 38-50.

137.Zhu, Y., Hinds, W. C., Kim, S., Shen, S., & Sioutas, C. (2002). Study of ultrafine particles near a major highway with heavy-duty diesel traffic. Atmospheric Environment, 36, 4323-4335.

138.Ziff, R.M. (1980). Kinetics of polymerization. J. Statistical Physics, 23, 241-263.

139.Zukas, J.A., Walters, W.P. (1997). Explosive Effects and Applications, pp. 115-134, USA.

Appendix – A

Expressions for equation of state parameters of TNT explosion products

Many attempts were made in the past to estimate the volume expansion rate of explosive clouds. Glasstone (1962) obtained empirical relations/expressions for the volume expansion rate for high energetic explosions by fitting the measured values for various device yields (applicable for high yield devices in the range of kilo- and mega-tons). Turco and Yu (1997) used various functional forms of volume expansion rate for the aircraft and volcanic plumes in their model. However, the volume expansion rates mentioned above are either very general in nature or specific to a particular physical process, and they are not applicable to the low yield explosive systems involving materials like TNT in the present work. Although significant amount of literature is available about the equation of state parameters, i.e., puff volume, pressure and temperature, their time dependence has not been found particularly for low yield TNT explosions. In the present study, these state parameters as a function of time are obtained by combining the theories of Taylor (1963), and Jones and Miller (1948) for the equation of state variables (Sreekanth, 2011).

Consider a spherical gas cloud of radius *R*, mass *M*, temperature *T*, and pressure *P* expands adiabatically. Let *dR* be the increase in radius of the cloud, then the work done (*dW*) by the gas in expansion can be written as,

$$dW = pdV \tag{A1.1}$$

$$Ma.dR = p\,4\pi R^2 dR \tag{A1.2}$$

where, a is the acceleration. The pressure p is obtained from the JWL (Jones-Wilkins-Lee) equation as,

$$P = Ae^{-R_1 V/V_0} + Be^{-R_2 V/V_0} + C\left(\frac{V}{V_0}\right)^{-(1+\omega)} \tag{A1.3}$$

where, A = 371.2 GPa; B = 3.231 GPa; C = 1.045 GPa; R_1 = 4.15; R_2= 0.95; ω = 0.30 are all constants and their values are given for T.N.T of density 1.5 g/cm^3 (Zukas& Walters, 1997). Writing the acceleration a in terms of radial distance R as $a = \frac{d^2R}{dt^2}$, and substituting the Eq.(A1.3) in Eq.(A1.2),the volume of expanding spherical puff is given by,

$$V(t) = \frac{4}{3}\pi R_t{}^3 \tag{A1.4}$$

where, R_t, the radius of the expanding puff is obtained by numerically solving the Eq.(A1.5)given below:

$$\frac{dR}{dt} = \sqrt{\frac{2A_1}{3s_1}\left[\, e^{-s_1 R_0{}^3} - e^{-s_1 R^3}\right] + \frac{2B_1}{3s_2}\left[e^{-s_2 R_0{}^3} - e^{-s_2 R^3}\right] + \frac{2C_1}{(3\omega)}\left[R_0{}^{-3\omega} - R^{-3\omega}\right]} \tag{A1.5}$$

where, $A_1 = \frac{4\pi A}{M}$, $B_1 = \frac{4\pi B}{M}$, $C_1 = \frac{4\pi C}{M} R_0^{3(\omega+1)}$, $s_1 = \frac{R_1}{R_0^3}$, $s_2 = \frac{R_2}{R_0^3}$.

By substituting the Eq.(A1.4) in Eq.(A1.3), one can obtain the pressure in the expanding puff as,

$$p(t) = Ae^{-R_1\left(\frac{V(t)}{V_0}\right)} + Be^{-R_2\left(\frac{V(t)}{V_0}\right)} + C\left(\frac{V(t)}{V_0}\right)^{-(\omega+1)} \tag{A1.6}$$

Similarly, an expression for the temporal evolution of the temperature in the expanding puff can be obtained by using the following relation for the equation of state variables (Jones and Miller, 1948) given by,

$$p\frac{v\prime}{N\prime} = RT + b_1 p + c_1 p^2 + d_1 p^3 \tag{A1.7}$$

where,*v'* is the volume and *N'* the number of moles at temperature *T* and pressure *p* of the gaseous products of the detonation of 1 mole of explosive. The values of the coefficients for 1.5 g/cm^3 loading density of TNT are b_1 = 25.4, c_1 = -0.104, d_1= 2.33x10^{-4}. By rearranging the Eq.(A1.7) and writing the equation of state variables as a function of time, we get,

$$T(t) = \frac{1}{R}\left[p(t)\frac{V(t)}{N\prime} - b_1 p(t) - C_1 p(t)^2 - d_1 p(t)^3\right] \tag{A1.8}$$

Eq.(A1.8) can be applied to any amount of TNT explosive material with loading density 1.5 g/cm^3. Eqs. (A1.4), (A1.6) and (A1.8) provides the expressions for temporal evolution of the state parameters of the TNT explosive material.

Note:

The initial temperature and pressure of the cloud (at $t = 0$) is estimated to be 3400 K and 1.5 x 10^5 atm respectively, obtained from the equation of state prescribed in the literature for a loading density of 1.5 g/cm^3. The chemical reactions among the TNT detonation products (C, CH_4, N_2, CO_2, CO, etc.,) continue till the temperature of this cloud reaches to 1600 K. Since it is easier to calculate the transients for a fixed composition of detonation products and also the fact that the volume change to this stage (also the time to reach 1600 K) is negligible (Jones & Miller, 1948), the simulations are carried out by assuming the initial temperature as 1600 K. The initial cloud volume is considered to be equal to the unexploded device volume.

Appendix – B

Volume expansion rate of a diffusing puff

Turco and Yu's formula for the survival fraction is given by (Turco & Yu, 1997),

$$F(t) = \frac{1}{\left(1 + N_a / N_T\right)} \tag{A2.1}$$

where, $\frac{1}{N_T} = \frac{K}{2}\int_0^t \frac{1}{V(t)}dt$, and N_a is the total number of particles in the initial volume, K is the constant coagulation kernel and $V(t)$ is the volume of the aerosol puff at time t. Since the expansion of the puff is purely governed by the diffusion of aerosol particles contained in it, the volume expansion rate of this puff ($V(t)$) may be described as,

$$V(t) = \beta\left[{b_0}^2 + 4Dt\right]^{3/2} \tag{A2.2}$$

where, β is an unknown constant to be determined, b_0 is the initial puff width, and D is the diffusion coefficient of the particles.

Substituting Eq.(A2.2) in Eq.(A2.1) and rearranging,

$$F(\theta) = \frac{1}{\left(1 + \frac{KN_a\mu(\theta)}{8\beta Db_0}\right)} \tag{A2.3}$$

where, $\theta = \frac{4Dt}{b_0^2}$, and $\mu(\theta) = \int_0^\theta \frac{d\theta'}{(1+\theta')^{3/2}}$

The survival fraction formula derived using the diffusion approximation model is given by,

$$F(\theta) = \frac{1}{\left(1 + \frac{KN_a\mu(\theta)}{4(2\pi)^{3/2}Db_0}\right)} \tag{A2.4}$$

By comparing equations (A2.3) and (A2.4), we get,

$$\beta = \pi\sqrt{2\pi} \tag{A2.5}$$

Then, the volume expansion rate of the puff from Eq.(A2.2) is given by,

$$V(t) = \pi\left(\sqrt{2\pi}\right)\left[b_0^{\ 2} + 4Dt\right]^{3/2} \tag{A2.6}$$

At t = 0, the actual puff volume,

$$V(0) = \pi\left(\sqrt{2\pi}\right)b_0^{\ 3} \tag{A2.7}$$

Appendix – C

Similarity formulation of diffusion-coagulation equation

The coagulation-diffusion equation for a one-dimensional system is given by,

$$\frac{\partial n(u,r,t)}{\partial t}=D\frac{\partial^2 n(u,r,t)}{\partial r^2}+\frac{1}{2}\int_0^u K(u',u-u')\,n(u',r,t)\,n(u-u',r,t)\,du'-n(u,r,t)\int_0^\infty K(u,u')\,n(u',r,t)\,du' \tag{A3.1}$$

Assume a scaling solutions of self-preserving form,

$$n(u,r,t)=\frac{\phi(r,t)}{V^2(r,t)}g\left(\frac{u}{V(r,t)}\right) \tag{A3.2}$$

satisfying the constraints $\int_0^\infty g(w)dw=\int_0^\infty wg(w)dw=1$.

Substituting the Eq.(A3.2) in Eq.(A3.1),

$$\begin{aligned}\frac{\partial}{\partial t}\left\{\frac{\phi}{V^2}g\left(\frac{u}{V}\right)\right\}&=D\frac{\partial^2}{\partial r^2}\left\{\frac{\phi}{V^2}g\left(\frac{u}{V}\right)\right\}+\frac{\phi^2}{2V^4}\int_0^u K(u',u-u')\,g\left(\frac{u'}{V}\right)g\left(\frac{u-u'}{V}\right)du'\\&\quad-\frac{\phi^2}{V^4}g\left(\frac{u}{V}\right)\int_0^\infty K(u,u')\,g\left(\frac{u'}{V}\right)du'\end{aligned} \tag{A3.3}$$

Let $\frac{u'}{V}=w'$ and $\frac{u}{V}=w$, then $du'=Vdw'$ and $du=Vdw$. Substituting this in Eq.(A3.3), we get,

$$\begin{aligned}\frac{\partial}{\partial t}\left\{\frac{\phi}{V^2}g(w)\right\}&=D\frac{\partial^2}{\partial r^2}\left\{\frac{\phi}{V^2}g(w)\right\}+\frac{\phi^2}{2V^3}\int_0^u K(Vw',Vw-Vw')\,g(w')g(w-w')\,dw'\\&\quad-\frac{\phi^2}{V^3}g(w)\int_0^\infty K(Vw,Vw')\,g(w')\,dw'\end{aligned} \tag{A3.4}$$

For kernels of homogeneous type,

$$K(Vw,Vw')=V^\alpha K(w,w') \tag{A3.5}$$

Using this relation, Eq.(A3.4) is rewritten as,

$$\frac{\partial}{\partial t}\left\{\frac{\phi}{V^2}g(w)\right\} = D\frac{\partial^2}{\partial r^2}\left\{\frac{\phi}{V^2}g(w)\right\} + \frac{\phi^2}{2V^{3-\alpha}}\int_0^w K(w',w-w')\,g(w')g(w-w')\,dw'$$
$$-\frac{\phi^2}{V^{3-\alpha}}g(w)\int_0^\infty K(w,w')\,g(w')\,dw' \qquad \text{(A3.6)}$$

Multiply by $V^{\gamma+1}w^\gamma$ throughout the Eq.(A3.6), and integrating the entire equation from 0 to infinity with respect to *w*,

$$V^\gamma \frac{\partial}{\partial t}\left(\frac{\phi}{V}\right)C_\gamma = DV^{\gamma-1}\frac{\partial^2\phi}{\partial r^2}C_\gamma + \frac{\phi^2}{2V^{2-\alpha-\gamma}}\int_0^\infty\int_0^w w^\gamma K(w',w-w')\,g(w')g(w-w')\,dwdw'$$
$$-\frac{\phi^2}{V^{2-\alpha-\gamma}}\int_0^\infty\int_0^\infty w^\gamma K(w,w')\,g(w)g(w')\,dwdw' \qquad \text{(A3.7)}$$

where, $C_\gamma = \int_0^\infty w^\gamma g(w)dw$

The double integral in the second term of the RHS of the Eq.(A3.7) is shown below schematically:

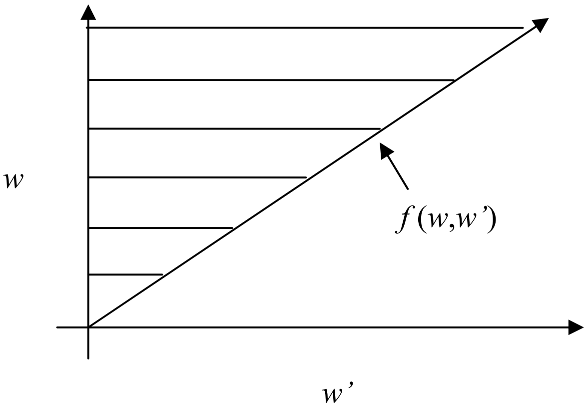

The first integral (innermost) with respect to *w'* is integrated from 0 to *w*, and then the second integral (outer one) is integrated with respect *w* from the limits 0 to infinity. This integration is equivalent to integrating first w.r.to *w* from *w'* to infinity, and then w.r.to *w'* from 0 to infinity. This is schematically shown below:

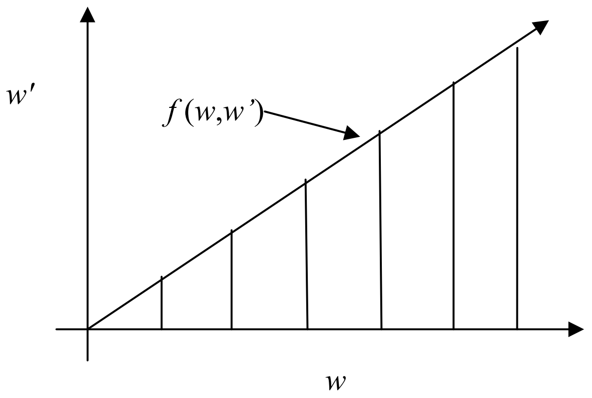

The integrals may be interchanged as,

$$\int_{w=0}^{\infty} w^{\gamma} dw \int_{w'=0}^{w} K(w', w-w')\, g(w')g(w-w')\, dw' = \int_{w'=0}^{\infty} dw' \int_{w=w'}^{\infty} w^{\gamma} K(w', w-w')\, g(w')g(w-w')\, dw$$

Let *w*-*w'* = *X*, then *dw* = *dX*, then the above integral becomes,

$$= \int_{w'=0}^{\infty} dw' \int_{X=0}^{\infty} (X+w')^{\gamma} K(w', X)\, g(w')g(X)\, dX$$

Replacing *X* by *w*,

$$= \int_{w'=0}^{\infty} dw' \int_{w=0}^{\infty} (w+w')^{\gamma} K(w', w)\, g(w')g(w)\, dw$$

Now, this integral is changed to the form that appears in the third term of the RHS by transformation of variables. Then the Eq.(A3.7) becomes,

$$V^{\gamma} \frac{\partial}{\partial t}\left(\frac{\phi}{V}\right) C_{\gamma} = DV^{\gamma-1} \frac{\partial^2 \phi}{\partial r^2} C_{\gamma} + \frac{\phi^2}{2V^{2-\alpha-\gamma}} \int_0^{\infty}\int_0^{\infty} (w+w')^{\gamma} K(w,w')\, g(w)g(w')\, dw dw'$$
$$- \frac{\phi^2}{V^{2-\alpha-\gamma}} \int_0^{\infty}\int_0^{\infty} w^{\gamma} K(w,w')\, g(w)g(w')\, dw dw' \qquad \text{(A3.8)}$$

Taking the zeroth moment w.r.to *w*, i.e., substituting $\gamma = 0$ in Eq.(A3.8), we get,

$$\frac{\partial}{\partial t}\left(\frac{\phi}{V}\right) = D \frac{\partial^2}{\partial r^2}\left(\frac{\phi}{V}\right) - \frac{\phi^2}{V^{2-\alpha}} R \qquad \text{(A3.9)}$$

where, $C_{\gamma=1} = \int_0^\infty w^\gamma g(w)dw = 1$, and $R = \frac{1}{2}\int_0^\infty\int_0^\infty K(w,w')\, g(w)g(w')\, dwdw'$

Since $\phi/V = N$, the Eq.(3.9) becomes,

$$\boxed{\frac{\partial N}{\partial t} = D\frac{\partial^2 N}{\partial r^2} - R\phi^\alpha N^{2-\alpha}} \tag{A3.10}$$

Taking the first moment w.r.to *w*, i.e., when γ = 1, Eq.(A3.8) becomes,

$$\frac{\partial \phi}{\partial t} = D\frac{\partial^2 \phi}{\partial r^2} + \frac{\phi^2}{2V^{1-\alpha}}\int_0^\infty\int_0^\infty w' K(w,w')\, g(w)g(w')\, dwdw' - \frac{\phi^2}{2V^{1-\alpha}}\int_0^\infty\int_0^\infty wK(w,w')\, g(w)g(w')\, dwdw'$$

(A3.11)

The second and third terms on the RHS of the Eq. (A3.11) are equal once it integrated, and hence,

$$\boxed{\frac{\partial \phi}{\partial t} = D\frac{\partial^2 \phi}{\partial r^2}} \tag{A3.12}$$

Appendix – D

Equation for total number concentration in the case of $K(u,v)=\alpha(u+v)$ kernel

The rate of change of aerosol concentration in a chamber with continuous source injection is given by,

$$\frac{\partial n(u,t)}{\partial t}=S(u,t)+\frac{1}{2}\int_0^u K(u',u-u')\,n(u',t)\,n(u-u',t)\,du'-n(u,t)\int_0^\infty K(u',u)\,n(u',t)\,du' \\ -\{\lambda_v+\lambda_d(u)\}\,n(u,t) \tag{A4.1}$$

Let us consider the additive kernel of the following type,

$$K(u,v)=\alpha(u+v) \tag{A4.2}$$

where, α is a constant. Substituting Eq.(A4.2) in Eq.(A4.1), and integrating the Eq.(A4.1) throughout with respect to the particle volume, we get,

$$\frac{\partial N(t)}{\partial t}=S(t)+\frac{\alpha}{2}\int_0^\infty\int_0^u (2u-u')\,n(u',t)\,n(u-u',t)du\,du'-\alpha\int_0^\infty\int_0^\infty (u+u')\,n(u,t)n(u',t)du\,du'-\lambda_v N(t) \tag{A4.3}$$

where, $N(t)=\int_0^\infty n(u,t)\,du$, $S(t)=\int_0^\infty S(u,t)\,du$, and the size dependent removal rate is neglected in this case. By noting from Appendix-C (transformation of Eq.(A3.7) to Eq.(A3.8)), Eq.(A4.3) can be transformed to,

$$\frac{\partial N(t)}{\partial t}=S(t)-\frac{\alpha}{2}\int_0^\infty\int_0^\infty u'n(u,t)\,n(u',t)du\,du'-\lambda_v N(t) \tag{A4.4}$$

Since $\phi(t)=\int_0^\infty u'\,n(u',t)\,du'$, Eq.(A4.4) can be rewritten as,

$$\frac{\partial N(t)}{\partial t}=S(t)-\frac{\alpha}{2}\phi(t)N(t)-\lambda_v N(t) \tag{A4.5}$$

The resultant equation after substituting the dimensionless variables defined in Eq.(5.17) in Eq.(A4.5) can be shown equivalent to that of Eq.(5.18) derived using two-group model.

Appendix - E

List of Publications

Publications in Refereed Journals

1. **S. Anand**, Y.S.Mayya, Coagulation in a diffusing Gaussian aerosol puff: Comparison of analytical approximations with numerical solutions, *Journal of Aerosol Science*, 40 (2009) 348-361.

2. **S. Anand**, Y.S.Mayya, A simplified approach for solving coagulation-diffusion equation to estimate atmospheric background particle number loading factors contributed by emissions from localized sources, *Atmospheric Environment*, 45 (26) (2011) 4488-4496.

3. **S. Anand**, Y.S. Mayya, M. Yu, M. Seipenbusch, G. Kasper, A numerical study of coagulation of nanoparticle aerosols injected continuously into a large, well stirred chamber, *Journal of Aerosol Science*, 52 (2012) 18-32.*

Presentations in Conferences and Workshops attended

1. **S. Anand**, Y.S.Mayya, A study on simultaneous coagulation and dispersion in a concentrated aerosol cloud, *Indian Aerosol Science and Technology Association (IASTA-2007) Conference on Emerging Trends in Aerosol Technology and Applications*, Nov 14-16, 2007 at NPL, New Delhi.

2. **S. Anand**, Y.S.Mayya, Modeling source strength modification due to coagulation in a diffusing aerosol puff, *European Aerosol Conference (EAC-2009)*, Sep 6-11, 2009 at University of Karlsruhe, Karlsruhe, Germany.

---

* Contributions – S.A., and Y.S.M. designed the study and developed the models. M.Y., M.S., and G.K. provided the experimental parameters for model comparisons.